TURN TO DESK
629.051
J82

JOURNAL OF THE AERONAUTICAL SCIENCES

VOLUME 14 APRIL, 1947 NUMBER 4

THE JOHN CRERAR LIBRARY
MAY 1947
LIBRARY

CONTENTS

Systematic Analysis of Thermal Turbojet Propulsion.....HANS REISSNER 197

Stresses in Cylindrical Semimonocoque Open Beams.....
.....HENRY L. LANGHAAR AND CLARENCE R. SMITH 211

The Use of Damping Screens for the Reduction of Wind-Tunnel Turbulence.....
.....HUGH L. DRYDEN AND G. B. SCHUBAUER 221

The Application of Basic Physiologic Data in the Design of Respiratory Equipment..
.....LOREN D. CARLSON AND VERNER J. WULFF 229

Numerical-Graphical Methods of Characteristics for Plane Potential Shock-Free Flow Problems.....LESTER L. CRONVICH 237

A Method of Airplane Performance Calculation Applicable to Any Polar.....
.....R. E. WENDT 243

Shear Distribution Due to Twist in a Cylindrical Fuselage with a Cutout.....
.....M. M. GOLOLOBOV 253

Letters to the Editor..... 236, 250

Published by the
INSTITUTE OF THE AERONAUTICAL SCIENCES, INC.

JOURNAL OF THE AERONAUTICAL SCIENCES

Editor: HUGH L. DRYDEN, *Associate Director, National Bureau of Standards*

Associate Editor: ROBERT R. DEXTER *Associate Editor:* BERNEICE H. JARCK

The Institute of the Aeronautical Sciences publishes monthly the JOURNAL OF THE AERONAUTICAL SCIENCES and the AERONAUTICAL ENGINEERING REVIEW.

The JOURNAL OF THE AERONAUTICAL SCIENCES prints papers of scientific and technical interest to Institute members and subscribers. In general, it provides an opportunity for specialists to publish articles disclosing new knowledge and new applications in the field of the aeronautical sciences. The JOURNAL restricts itself to the aeronautical aspects of advances in science and engineering, and papers printed have either been submitted directly to the JOURNAL or have been previously presented at a meeting of the Institute.

The AERONAUTICAL ENGINEERING REVIEW keeps members and subscribers informed regarding the contents of new books and current periodicals in the field of aeronautics. It reviews new developments in the aircraft industry and reports on progress from house organs and catalogs published by aircraft and engine manufacturers and other companies engaged in aeronautical activities. It publishes papers on applied engineering and aircraft production. News of Institute activities is published in the REVIEW.

Statements and opinions expressed in the JOURNAL are to be understood as individual expressions of the authors and not those of the Institute.

SUBSCRIPTION RATES

Journal of the Aeronautical Sciences
Published Monthly

United States and Possessions		Foreign Countries Including Canada (American Currency Rates)	
1 Year	$7.00	1 Year	$9.00
Single Copies	0.70	Single Copies	1.00

Aeronautical Engineering Review
Published Monthly

United States and Possessions		Foreign Countries Including Canada (American Currency Rates)	
1 Year	$3.00	1 Year	$3.50
Single Copies	0.30	Single Copies	0.35

Notices of change of address should be sent to the Institute at least 30 days prior to actual change of address.

Manuscripts for publication, proofs, and all correspondence should be addressed to the Editorial Office of the JOURNAL.

Correspondence regarding subscriptions may be addressed to Publication Office, 20th and Northampton Sts., Easton, Pa., or to the Editorial Office of the JOURNAL OF THE AERONAUTICAL SCIENCES, 2 East 64th Street, New York 21, New York.

Copyright, 1947, by the Institute of the Aeronautical Sciences, Inc.

Entered as Second-Class Matter at the Post Office, Easton, Pa., May 1, 1937. Acceptance for mailing at a special rate of Postage provided for in the Act of August 24, 1912. Authorized April 29, 1937.

INSTITUTE of the AERONAUTICAL SCIENCES

President

P. R. BASSETT

Vice-Presidents

WELLWOOD E. BEALL
REX B. BEISEL
LUIS DE FLOREZ
JOHN K. NORTHROP

Director

S. PAUL JOHNSTON

Executive Vice-President

BENNETT H. HORCHLER

Past-Presidents

J. C. HUNSAKER
CHARLES L. LAWRANCE
DONALD W. DOUGLAS
GLENN L. MARTIN
CLARK B. MILLIKAN
T. P. WRIGHT
GEORGE W. LEWIS
JAMES H. DOOLITTLE
FRANK W. CALDWELL
HALL L. HIBBARD
HUGH L. DRYDEN
R. H. FLEET
CHARLES H. COLVIN
ARTHUR E. RAYMOND

Secretary

ROBERT R. DEXTER

Treasurer

BURDETTE S. WRIGHT

Controller

JOSEPH J. MAITAN

Counsel

ALLAN D. EMIL

COUNCIL

E. E. ALDRIN
LAWRENCE D. BELL
GEORGE W. BRADY
W. A. M. BURDEN
VICTOR E. CARBONARA
CARL DE GANAHL
JAMES H. DOOLITTLE
WILLIAM K. EBEL
SHERMAN M. FAIRCHILD
C. C. FURNAS
J. A. HERLIHY
WILLSON H. HUNTER
JEROME LEDERER
JOHN C. LESLIE
A. ELLIOTT MERRILL
EARL D. OSBORN
ELMER A. SPERRY, JR.
JOHN C. SQUIRES
M. F. STOUGHTON
ERNEST G. STOUT
C. FAYETTE TAYLOR

ADVISORY COMMITTEE

Chairman: CHARLES H. COLVIN

WALTER BEECH
FRANK W. CALDWELL
RALPH S. DAMON
KENNETH S. M. DAVIDSON
R. H. FLEET
R. PAUL HARRINGTON
R. M. HAZEN
HALL L. HIBBARD
J. C. HUNSAKER
TH. VON KÁRMÁN
THOMAS A. KNOWLES
I. M. LADDON
GROVER LOENING
GLENN L. MARTIN
CLARK B. MILLIKAN
THOMAS A. MORGAN
R. C. MUIR
ARTHUR E. RAYMOND
F. W. REICHELDERFER
L. B. RICHARDSON
RUSSELL G. ROBINSON
LAURANCE S. ROCKEFELLER
T. CLAUDE RYAN
EDWARD P. WARNER

HONORARY MEMBERS

JOHN C. ADAMS
GRIFFITH BREWER
JOHN N. BROWN
W. A. M. BURDEN
E. U. CONDON
L. C. CRAIGIE
IRA C. EAKER
HARRY F. GUGGENHEIM
HENRY G. HOUGHTON
GEORGE C. KENNEY
CURTIS E. LE MAY
GEORGE B. PEGRAM
B. M. POWERS
J. LAURENCE PRITCHARD
ARTHUR W. RADFORD
F. W. REICHELDERFER
H. B. SALLADA
CARL SPAATZ
L. C. STEVENS
NATHAN F. TWINING

HONORARY FELLOWS

H. H. ARNOLD
FRANK W. CALDWELL
SIR GEOFFREY DE HAVILLAND
DONALD W. DOUGLAS
HUGH L. DRYDEN
W. F. DURAND
SIR RICHARD FAIREY
SIR ROY FEDDEN
J. C. HUNSAKER
SIR MELVILL JONES
GEORGE W. LEWIS
GLENN L. MARTIN
GEORGE J. MEAD
SIR FREDERICK HANDLEY PAGE
D. R. PYE
IGOR I. SIKORSKY
SIR GEOFFREY I. TAYLOR
TH. VON KÁRMÁN
EDWARD P. WARNER
ORVILLE WRIGHT
T. P. WRIGHT

BENEFACTORS

E. E. ALDRIN
HART O. BERG (Deceased)
W. A. M. BURDEN
E. L. CORD
DONALD W. DOUGLAS
SHERMAN M. FAIRCHILD
SIR RICHARD FAIREY
R. H. FLEET
FLORENCE GUGGENHEIM (Deceased)
C. D. HANSCOM
JOHN P. V. HEINMULLER
ALEXANDER KLEMIN
PAUL KOLLSMAN
BELLA C. LANDAUER
WILLIAM LANDAUER
GROVER LOENING
EDMUND C. LYNCH (Deceased)
F. W. MAGIN
GLENN L. MARTIN
GEORGE J. MEAD
S. A. REED (Deceased)
LAURANCE S. ROCKEFELLER
EDWARD P. WARNER

AMERICAN FELLOWS

JOHN D. AKERMAN
E. E. ALDRIN
HARRY G. ARMSTRONG
KARL ARNSTEIN
J. L. ATWOOD
PAUL S. BAKER
RALPH S. BARNABY
P. R. BASSETT
WELLWOOD E. BEALL
REX B. BEISEL
G. M. BELLANCA
DON R. BERLIN
HENRY A. BERLINER
WILLIAM BOLLAY
B. C. BOULTON
GEORGE W. BRADY
LYMAN J. BRIGGS
W. G. BROMBACHER
WILLIAM G. BROWN
CHARLES P. BURGESS
KENNETH CAMPBELL
CHARLES H. CHATFIELD
ALLAN CHILTON
V. E. CLARK
FRANKLIN R. COLLBOHM
CHARLES H. COLVIN
KARL T. COMPTON
EMERSON W. CONLON
JOHN W. CROWLEY, JR.
RALPH S. DAMON
LUIS DE FLOREZ
SMITH J. DE FRANCE
J. P. DEN HARTOG
WALTER S. DIEHL
JAMES H. DOOLITTLE
C. S. DRAPER
IVAN H. DRIGGS
WILLIAM K. EBEL
C. L. EGTVEDT
FREDERIC FLADER
CHARLES FROESCH
JACK FRYE
GARLAND FULTON
LESTER D. GARDNER
RICHARD C. GAZLEY
MICHAEL E. GLUHAREFF
MELVIN N. GOUGH
LEROY R. GRUMMAN
HAROLD R. HARRIS
R. M. HAZEN
ALBERT F. HEGENBERGER
EDWARD H. HEINEMANN
S. D. HERON
HALL L. HIBBARD
L. S. HOBBS
PAUL R. HOVGAARD
WILLIAM HOVGAARD
ROBERT INSLEY
EASTMAN N. JACOBS
CLARENCE L. JOHNSON
S. PAUL JOHNSTON
ALEXANDER KARTVELI
PAUL H. KEMMER
J. H. KINDELBERGER
OTTO E. KIRCHNER
ARTHUR L. KLEIN
ALEXANDER KLEMIN
W. B. KLEMPERER
PAUL KOLLSMAN
OTTO C. KOPPEN
B. V. KORVIN-KROUKOVSKY
S. M. KRAUS
I. M. LADDON
E. S. LAND
CHARLES L. LAWRANCE
JEROME LEDERER
JOHN G. LEE
JOHN C. LESLIE
CHARLES A. LINDBERGH
WILLIAM LITTLEWOOD
GROVER LOENING
ALBERT E. LOMBARD
W. RANDOLPH LOVELACE, II
EUGENE E. LUNDQUIST
R. D. MACCART
JOHN R. MARKHAM
ERLE MARTIN
WM. H. MCAVOY
C. J. MCCARTHY
CLARK B. MILLIKAN
ROBERT J. MINSHALL
JOSEPH S. NEWELL
ALFRED S. NILES
JOHN K. NORTHROP
ARTHUR NUTT
SHATSWELL OBER
ROBERT R. OSBORN
W. BAILEY OSWALD
GEORGE A. PAGE, JR.
F. W. PAWLOWSKI
F. W. PENNOYER, JR.
A. A. PRIBSTER
ARTHUR E. RAYMOND
F. W. REICHELDERFER
ELLIOTT G. REID
H. J. E. REID
H. C. RICHARDSON
RUSSELL G. ROBINSON
LEONARD E. ROOT
C. E. ROSENDAHL
ADDISON M. ROTHROCK
WILLIAM T. SCHWENDLER
FRANCIS R. SHANLEY
JAMES M. SHOEMAKER
MAC SHORT
IGOR ALEXIS SIKORSKY
ABE SILVERSTEIN
SHELDEN B. SPANGLER
ELMER A. SPERRY, JR.
JOHN STACK
WILLIAM B. STOUT
HARRY A. SUTTON
C. FAYETTE TAYLOR
EDWARD S. TAYLOR
PHILIP B. TAYLOR
TH. THEODORSEN
T. E. TILLINGHAST
S. TIMOSHENKO
L. B. TUCKERMAN
RALPH H. UPSON
J. PARKER VAN ZANDT
J. G. VINCENT
RICHARD VON MISES
FRANK L. WATTENDORF
P. V. H. WEEMS
FRED E. WEICK
R. D. WEYERBACHER
JOHN B. WHEATLEY
ANDREW V. WILLGOOS
DONALD H. WOOD
ROBERT J. WOODS
JOHN E. YOUNGER
ALBERT F. ZAHM
STEPHEN J. ZAND

An Appreciation
To Corporate Members of the Institute of the Aeronautical Sciences

Listed below are the leading aeronautical and industrial companies that make possible the publication of the *Journal of the Aeronautical Sciences*.

They enable the Institute to publish scientific and technical papers in the *Journal* and to devote its pages exclusively to editorial material.

Dues from individual members which would normally be used to publish this scientific and engineering monthly are thus released for additional services to the profession and industry.

The *Aeronautical Engineering Review* and the *Aeronautical Engineering Catalog*, together with the *Journal*, provide a comprehensive technical information service for the benefit of the aircraft and related industries.

Academy of Aeronautics, Inc.
Casey Jones School of Aeronautics
Aero Insurance Underwriters
Aerojet Engineering Corporation
Aeronca Aircraft Corporation
Aeroproducts Division, General Motors Corporation
Aeroquip Corporation
Agawam Aircraft Products, Inc.
Airborne Instruments Laboratory, Inc.
Airchox Company Division, Joyce Aviation, Inc.
Aircraft Radio Corporation
AiResearch Manufacturing Company
AiResearch Manufacturing Company of Arizona, Inc.
Allis-Chalmers Manufacturing Company
Allison Division, General Motors Corporation
Aluminum Company of America
American Airlines System
American Overseas Airlines, Inc.
American Bosch Corporation
American Phenolic Corporation
Associated Aviation Underwriters
Associated Foundries & Manufacturers, Inc.
Atlas Supply Company
Baker Steel & Tube Company
Beech Aircraft Corporation
Bell Aircraft Corporation
Bendix Aviation Corporation
Bendix Products Division
Bendix Radio Corporation
Eclipse-Pioneer Division
Export Division
Friez Instrument Division
Pacific Division
Scintilla Magneto Company
The BG Corporation
Boeing Aircraft Company
Breeze Corporations, Inc.
Essex Tool & Die Company
Federal Laboratories, Inc.
Cal-Aero Technical Institute, A Division of Grand Central Airport Company
Carrier Corporation
Cessna Aircraft Company
Chandler-Evans Division, Niles-Bement-Pond Company
Chase National Bank of the City of New York
The Cleveland Graphite Bronze Company
The Cleveland Pneumatic Tool Company
Automotive-Aircraft Division
Clifford Manufacturing Company
Consolidated Vultee Aircraft Corporation
Nashville Division
Stinson Aircraft Division
Continental Motors Corporation
Cox and Stevens Aircraft Corporation
Culver Aircraft Corporation
Curtiss-Wright Corporation
Airplane Division
Development Division
Propeller Division
Wright Aeronautical Corporation
Doak Aircraft Company, Inc.
Douglas Aircraft Company, Inc.
El Segundo Plant
Long Beach Plant
The Dow Chemical Company
Dzus Fastener Company, Inc.
Eastern Air Lines, Inc.
Eaton Manufacturing Company
Thomas A. Edison, Incorporated, Instrument Division
Edo Aircraft Corporation

The Electric Auto-Lite Company
Electrol Incorporated
Engineering and Research Corporation
Ethyl Corporation
Fairchild Camera & Instrument Corporation
  Fairchild Aerial Surveys, Inc.
Fairchild Engine and Airplane Corporation
  Duramold Division
  Fairchild Aircraft Division
  Ranger Aircraft Engines Division
Federal Telephone and Radio Corporation
Firestone Aircraft Company
General Aviation Equipment Company, Inc.
General Electric Company
The B. F. Goodrich Company
The Goodyear Tire & Rubber Company
Grumman Aircraft Engineering Corporation
W. & L. E. Gurley
The Hilliard Corporation
The International Nickel Company
Irving Air Chute Company, Inc.
Jack & Heintz, Inc.
Johns-Manville Sales Corporation
Kaiser Fleetwings, Inc.
Walter Kidde & Company, Inc.
Kollsman Instrument Division, Square D Company
Lavelle Aircraft Corporation
Lear Incorporated
Link Aviation Devices, Inc.
The Liquidometer Corporation
Lockheed Aircraft Corporation
Longines-Wittnauer Watch Company, Inc.
The Glenn L. Martin Company
The W. L. Maxson Corporation
Warren McArthur Corporation
McDonnell Aircraft Corporation
Menasco Manufacturing Company
Micromatic Hone Corporation
Minneapolis-Honeywell Regulator Company
Moore Drop Forging Company
National City Bank of New York
National Credit Office, Inc.
North American Aviation, Inc.
  North American Aviation, Inc., of Texas
Northrop Aircraft, Inc.
Northwest Airlines, Inc.
Owens-Corning Fiberglas Corporation
Pan American World Airways System
The Parker Appliance Company
Pesco Products Company Division, Borg-Warner Corporation
Phillips Petroleum Company
Pioneer Parachute Company, Inc.
Piper Aircraft Corporation
Pure Oil Co.
Radioplane Company
Republic Aviation Corporation
A. V. Roe Canada Limited
John A. Roebling's Sons Company
Rohr Aircraft Corporation
The Ryan Aeronautical Company
Scott Aviation Corporation
Shell Oil Company, Inc.
Simmonds Aerocessories, Inc.
Skydyne, Inc.
Socony-Vacuum Oil Company
Solar Aircraft Company
Sperry Gyroscope Company, Inc.
Square D Company
Standard Oil Company of California
Standard Oil Company (Indiana)
Standard Oil Company of New Jersey
The Texas Company
Thompson Products, Inc.
Tinnerman Products, Inc.
Transcontinental & Western Air, Inc.
Union Carbide and Carbon Corporation
  Bakelite Corporation
  Haynes Stellite Company
  Linde Air Products Company
  National Carbon Company
United Aircraft Corporation
  Chance Vought Aircraft Division
  Hamilton Standard Propellers Division
  Pratt & Whitney Aircraft Division
  Pratt & Whitney Aircraft Corporation of Missouri
  Sikorsky Aircraft Division
United Air Lines, Inc.
United States Aviation Underwriters, Inc.
United States Rubber Company
  Dominion Rubber Company, Ltd.
Vickers, Inc.
The Waco Aircraft Company
Warner Aircraft Corporation
The Weatherhead Company
Western Air Lines, Inc.
Westinghouse Electric Corporation
Weston Electrical Instrument Corporation
Willys-Overland Motors, Inc., Aircraft Research and Development Division
Wyman-Gordon Company
Young Radiator Company

EDITORIAL COMMITTEE

HUGH L. DRYDEN, *Chairman*

Aerodynamics

Francis Clauser
Howard Emmons
R. Paul Harrington
R. T. Jones
W. B. Klemperer
Otto C. Koppen
John G. Lee
H. P. Liepmann
John R. Markham
Clark B. Millikan
Shatswell Ober
W. Bailey Oswald
Allen E. Puckett
Elliott G. Reid
H. J. E. Reid
Russell Robinson
L. E. Root
G. B. Schubauer
W. R. Sears
John Stack
Th. von Kármán
Richard von Mises

Air Transport

A. W. Dallas
Charles Froesch
J. A. Herlihy
Otto E. Kirchner
John C. Leslie

Aircraft Design

W. E. Beall
Rex B. Beisel
W. K. Ebel
Hall L. Hibbard
C. L. Johnson
I. M. Laddon
C. J. McCarthy
Fred E. Weick
Robert J. Woods

Physiologic Problems

H. G. Armstrong
Louis H. Bauer
Eugene Du Bois
W. Randolph Lovelace II
Ross A. McFarland
A. D. Tuttle

Aircraft Propulsion

George W. Brady
Frank W. Caldwell
L. S. Hobbs
E. E. Johnson
Joseph Keenan
R. P. Kroon
Arthur Nutt
Hans Reissner
Abe Silverstein
C. Fayette Taylor
E. S. Taylor
P. Taylor

Structures and Materials

W. B. Bleakney
E. W. Conlon
J. P. Den Hartog
L. H. Donnell
E. C. Hartmann
N. J. Hoff
H. L. Langhaar
E. E. Lundquist
C. F. Nagel, Jr.
J. S. Newell
Alfred S. Niles
W. Ramberg
E. Reissner
F. R. Shanley
H. W. Sibert
C. R. Strang
S. Timoshenko
H. S. Tsien

Meteorology

C. F. Brooks
D. M. Little
E. J. Minser
F. W. Reichelderfer
H. C. Willett

Fuels and Oils

A. L. Beall
J. H. Doolittle
Graham Edgar
R. T. Goodwin
S. D. Heron
A. M. Rothrock

Instruments

Allan G. Binnie
W. G. Brombacher
J. Callahan
Charles H. Colvin
C. S. Draper
O. E. Esval
David W. Moore
W. A. Reichel
C. F. Savage
O. Hugo Schuck
R. Sylvander

Rotating Wing Aircraft

Robert Coleman
M. L. Deutsch
G. Horvay
Alexander Klemin
Ralph McClarren
R. H. Prewitt
Igor I. Sikorsky
Robert A. Wolf

Vibration and Flutter

Lee Arnold
M. A. Biot
William Bollay
J. P. Den Hartog
Manfred Rauscher

Flight Testing

William K. Ebel
R. R. Gilruth
Melvin N. Gough
Robert Stanley
E. A. Stout

I.A.S. REPRESENTATIVES TO OTHER ORGANIZATIONS

Aircraft Industries Association of America, Inc.—CHARLES MARCUS

American Association for the Advancement of Science—J. C. HUNSAKER

American Society of Mechanical Engineers—CHARLES H. COLVIN

American Standards Association—P. R. BASSETT

Engineering Society of Detroit—DONALD C. HUNT, GEORGE TWENEY

Greater New York Safety Council—WILLIAM LITTLEWOOD

Daniel Guggenheim Medal Board of Award—CHARLES H. COLVIN, GROVER LOENING, LESTER D. GARDNER

Institute of Radio Engineers—L. M. HULL

Manufacturers Aircraft Association—ARTHUR E. RAYMOND

National Aeronautic Association—WILLIAM R. ENYART

National Fire Protection Association—E. E. ALDRIN

National Research Council Engineering Division—HUGH L. DRYDEN

National Safety Council—JEROME LEDERER

New York Museum of Science and Industry—LESTER D. GARDNER

Society of Automotive Engineers—STEPHEN J. ZAND

JOURNAL OF THE AERONAUTICAL SCIENCES

VOLUME 14 APRIL, 1947 NUMBER 4

Systematic Analysis of Thermal Turbojet Propulsion

HANS REISSNER*

Polytechnic Institute of Brooklyn

SUMMARY

The propulsion unit is divisible into six sections: free inflow, intake, compressor, heat chamber, turbine, and exit nozzle. It is treated uniformly by the quintuple system of dynamic and thermodynamic flow equations with their power or heat inputs, the conditions of change of state (cycle), the continuity equations, and the thrust equation. These equations also comprise in each section the retarding forces and the heat creation of turbulent flow and the loss of mechanical power and of heat leakage. They form successive sets of equations, and their solution is derived in terms of the required data of altitude, flying speed, thrust, pressures in front and at the exit of the compressor, permissible entrance temperature at the turbine, and permissible ratio of power of compressor and turbine to heat input.

This procedure, to illustrate the basic ideas, is, at first, worked out for a perfect unit (that is, without losses), and is afterwards completed for the percentual losses of heat and work in each section.

The necessary heat input, the propulsion effectiveness, the distribution of temperatures, pressures, velocities and cross sections, the best cycle conditions, and the most efficient pressure-velocity relations at the exit are then determined by those data.

INTRODUCTION

THE THERMAL JET PROPULSION UNIT treated in this paper is given by a schematic representation of Fig. 1. It shows the five sections of intake, compressor, heat chamber with flame holders, turbine, and nozzle. The unit is supposed to move at an altitude (a_ρ) defined by the density (ρ_0) and the pressure (p_0) with the constant, not necessarily horizontal velocity (V_0), and is required to produce a thrust (Th.) sufficient to overcome the total drag of the airplane at a steady, horizontal, climbing, or gliding velocity (V_0).

Presented at the Aerodynamics Session, Fourteenth Annual Meeting, I.A.S., New York, January 29–31, 1946. Revised and received December 16, 1946.

* Professor of Aerodynamics and Aero Structures.

The theoretical treatment of this paper was started in 1945 and presented at the Annual Meeting of the Institute of the Aeronautical Sciences in January, 1946. Other work meanwhile has delayed the publication, and this delay has been used to make some slight changes and additions.

In view of the great number of valuable literary contributions in this field,† it may be appropriate to indicate the different approach and analysis of this paper.

It is more elementary insofar as it starts from the Bernoulli equation of steady compressible flow, combined with the transformation first given by Zeuner, which expresses the influence of heat input and of dissipation of mechanic energy on the equation of flow.

On the other hand, it attempts a more general analysis by incorporating in the integration of the flow equations the friction and leakage losses, the relations between change of state (cycle) and the changes of cross sections and the excess of turbine over compressor power. A further difference appears in the evaluation of the thrust of the jet in terms of pressure ratio, velocity ratio, and temperature ratio at the exit and in a discussion of a pertinent maximum condition.

Compressor and turbine are represented by a force field, helical in each stage, which represents the actually

† See Bibliography at the end of this paper.

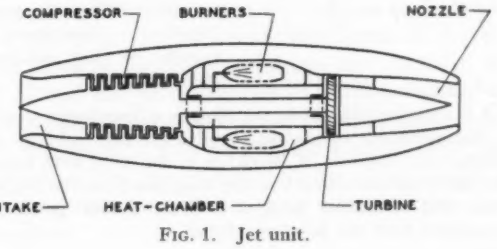

FIG. 1. Jet unit.

finite number of pressure-discontinuity surfaces of the blades by a continuous distribution of helical surfaces of infinitesimal discontinuity. This concept has the advantage that all duct sections can be treated by one and the same general flow equation and by its general integral and that they differ only in the values of the heat and mechanical work input or loss and the change of state characteristic. It can be proved that the actual compressor or turbine with its rotating blades and countervanes can be designed so as to accomplish the same effect as the force field.*

The solution proceeds in successive steps from one section to the next in such a way that the requirements of compression ratio of the compressor, the temperature requirement in the heat chamber, and the thrust requirement determine the total heat input and the compressor and turbine power.

The representation uses as much as possible dimensionless variables and the energy and power values, including heat in mechanical units (ft.lb. per lb.) and (ft.lb. per lb.sec.) which unifies and simplifies the equations but can easily be changed into the language of B.t.u. or kg.cal. if so desired.

An assumption of the analysis is that the approach of the relative flow velocity toward the velocity of sound does not give rise to noticeable shock waves in the inside of the duct. The velocity of sound being proportional to the square root of the temperature and the temperature ratio being between two and four everywhere, except at the intake, gives a velocity of sound between 987 and 1,520 m.p.h. so that the approach to a local Mach Number 1 is not imminent if increases of local velocity in corners and bends are avoided. Only the intake temperatures will be smaller unless the intake is also heated by heat conduction from the compressor. In order to take into account the case of turbulent friction in the duct section in a not too complicated manner, the cross sections are assumed to be annular in such a measure as to enable a one-dimensional treatment with an average velocity (superposed by turbulence fluctuation), an average temperature, and an average pressure in every cross section.

Symbols

p, ρ, T, V, A	= pressure, density, absolute temperature, velocity relative to the propulsion duct, and area of a cross section, respectively
$q \equiv \frac{p}{p_0}, \sigma \equiv \frac{\rho}{\rho_0}$ $\tau \equiv \frac{T}{T_0}, \varphi \equiv \frac{V}{V_0}$	= the dimensionless pressure density, temperature, and velocity variables referred to the undisturbed atmosphere (V_0 velocity of duct relative to atmosphere)
h	$\equiv V_0^2/2g$
$H \equiv p_0/{}^1/_2\rho_0 V_0^2$	= static over dynamic pressure
Hh	$= p_0/\rho_0 g = p_0 v_0$
l_4, l_c, l_h, l_t, l_r	= lengths of the duct sections
ds	= element of length of a streamline
ds'	$\equiv ds/l$
$D_h \equiv$ area/circumference	= hydraulic diameter along a section
$\zeta\varphi^2/4D_h$	= relative loss of head per unit of length
dQ/ds	= heat input (if negative loss of heat) or heat created by dissipation of energy, per unit of length of travel and per unit of weight of a fluid element, in mechanical units (ft.lb per ft.lb.)
$Q = \int_i^e dQ$	= heat input in mechanical units per unit of weight of fluid for the total length of travel along a duct section
dW/ds	= work input (if negative output) per unit of weight of fluid and per unit of length of travel (of a fluid element)
$W = \int_i^e dW$	= work input per unit of weight of fluid for the total length of travel (along a duct section)
Th.	= thrust of jet propulsion unit
Th.* $=$ Th.$/\rho_0 V_0 A_e$	= thrust coefficient
$m' = \rho VA$	= mass passing duct per unit of time
$Q_e m' g$	= total external heat-power input per second ft.lb. per sec.)
$\eta =$ Th. $V_0/Q_e m' g$	= propulsive efficiency
γ	= ratio of specific heats of the gas in its actual state
n	= polytropic exponent
μ	$= \gamma/(\gamma - 1)$
λ	$= n/(n - 1)$
c_μ	$= \mu/(\mu - \lambda)$
c_λ	$= \lambda/(\mu - \lambda)$
z	$= \zeta l/4D_h$
a	$= e^{-c_\mu \int_0^1 z ds'}$
W^*	$= Wh^{-1}$
Q^*	$= Qh^{-1}$
b	$= a(W^* - c_\lambda Q^*)^{-1} \int_0^1 d \times (W^* - c_\lambda Q^*) e^{+c_\mu \int_0^{s'} z ds'}$
e	$= -W_t/W_e$
δ	= coefficient indicating the percentual loss of heat in a section, with the subscript pertinent to it
β_e	$= b_e(1 + c_\lambda \delta_e)$
β_h	$= c_{\lambda h} b_h (1 - \delta_h)$
β_t	$= b_t(1 - c_{\lambda t}\delta_t)$
γ_e	$= (1 - \delta_e - \beta_e)/H\mu$
γ_h	$= (1 - \delta_h + \beta_h)/H\mu$
γ_t	$= (1 - \delta_t - \beta_t)/H\mu$
γ_n	$= \delta n(1 + c_{\lambda a} b n)/H\mu$
α	$= (1 - a)/H\mu$, with a subscript indicating the section

Subscripts

0	= undisturbed atmosphere at flying altitude
i	= duct section of intake and in general inlet of any section
c	= duct section of compressor

* The author has elaborated this streamline design method in a (hectographed) course on compressors and turbines at the Polytechnic Institute of Brooklyn in the 1945–1946 term. It was shown in this course how the transition from the continuous force and streamline field to a discontinuous pressure and streamline field can be accomplished.

h = duct section of heat chamber
t = duct section of turbine
n = duct section of nozzle
e = exit of a section and particularly of nozzle

The Continuity Equation

The continuity equation can be written in terms of the density ρ, the velocity V averaged over a cross section, and the cross section area A as functions of the distance s from the entrance of a duct-section.

$$\rho V A = \text{const.} \tag{1}$$

Introducing the ratios of ρ and V relative to the values ρ_0, V_0 in the undisturbed (ambient) atmosphere, viz.,

$$\rho/\rho_0 = \sigma, \quad V/V_0 = \varphi$$

one can express Eq. (1) by

$$\sigma\varphi A = A_0 \tag{1a}$$

where A_0 is the cross section of the relative inflow far in front, where $\sigma = 1$ ($\rho = \rho_0$) and $\varphi = 1$ ($V = V_0$).

In case the equation of state and the change of state is given, it will often be of advantage to express σ in this Eq. (1a) either by the temperature ratios $T_0/T = \tau$ or by the pressure ratio $p/p_0 = q$.

Furthermore, if the flow is rotating so that the axial velocities are $V_{\text{axial}} = V \cos\theta$ (θ pitch angle), Eq. (1a) changes to $\sigma\varphi \cos\theta\, A = A_0$.

The Thrust and Efficiency Equations

Thrust and body drag of the propulsion unit are linked to each other by their influence on the surrounding atmosphere.

To express the performance of jet propulsion, one needs the separation of these two forces. This may be done in the following way:

Consider a cylindrical fluid volume surrounding the propulsion unit and axially coinciding with the axis of the unit. The front section of this surrounding gas-fluid cylinder may be so far in front that on it one can assume undisturbed pressure p_0 and undisturbed relative velocity V_0. Its rear cross section may coincide with the exit cross section of the unit but may radially continue to the cylindrical (generator) surface of the fluid cylinder, so far outside that only undisturbed pressures and velocities on this cylinder surface are encountered.

However, the radially outside part of the rear cross section of said fluid cylinder, surrounding the duct unit, will have pressures and velocities disturbed by the outside drag of the duct body. This drag will be the drag of the outside of this body, while the drag of the entrance and the exit edges of it will have no effect, since they are streamlines by the incoming and outgoing jet. On the other hand, this consideration will also cover the eventual shock waves starting from the outside or the front edges of the duct, since they only contribute to the pressure and velocity distribution of the outside and the outside fluid cross section at the rear.

Observing now the time rate of momentum of flow relative to the momentum of the undisturbed flow and the pressure at the exit section relative to the undisturbed pressure of the atmosphere, it is possible to evaluate the thrust (Th.) of the jet propulsion duct, while for the evaluation of the body drag the observation of momentum and pressure difference on the outside rear cross section of the surrounding fluid cylinder would be necessary. The thrust of the jet proper (subscript e for exit) is therefore given by:

$$\text{Th.} = \rho_e V_e A_e (V_e - V_0) + A_e(p_e - p_0) \tag{2}$$

or in the dimensionless variables defined above, by a thrust coefficient

$$\text{Th.}^* = \frac{\text{Th.}}{\rho_0 V_0^2 A_e} = \sigma_e\varphi_e(\varphi_e - 1) + \frac{p_0}{\rho_0 V_0^2}(q_e - 1) \tag{2a}$$

By observing that by the equation of state of the gas ($p/p_0 = Rg\rho T/Rg\rho_0 T_0$ or $q = \sigma\tau$), $\sigma_e = q_e\tau_e^{-1}$, and with the abbreviation $H = p_0/{}^1\!/_2\,\rho_0 V_0^2$, the above equation is changed to:

$$\text{Th.}^* = q_e\tau_e^{-1}\varphi_e(\varphi_e - 1) + {}^1\!/_2 H(q_e - 1) \tag{2b}$$

Dividing the work per unit of time of the thrust, Eq. (2a), by the total heat input Q per unit of time and per unit of weight of the fluid times the weight of flow per unit of time, one arrives at an expression for the value of the propulsion efficiency (η)

$$\eta = \frac{\text{Th.}\ V_0}{Q\rho_e g V_e A_e} = \frac{h}{Q}\left[2(\varphi_e - 1) + H(1 - q_e^{-1})\tau_e\varphi_e^{-1}\right] \tag{3}$$

where $h = V_0^2/2g$ is the velocity head and Q ft.lb. per lb. the heat input per unit of fluid weight in mechanical units.

Eqs. (2), (2b), and (3) leave the question open as to how much velocity $V_e(\varphi_e)$ and how much pressure $p_e(q_e)$ should contribute to attain the maximum of thrust. The answer will depend on the obtainable pressure excess $p_e - p_0$ and on the cross-section distribution along the duct, and it will be given in one of the following sections.

Another remark on the nature of the thrust may be clarifying. It was necessary to determine the thrust value by the indirect, somewhat abstract method of using a cylindrical air volume surrounding the propulsion duct. The direct (concrete) method would derive the thrust as the axial component of the resultant force of all inside pressures and frictions on walls, blades, etc., of the duct unit. It is evident that such an evaluation, though correct in principle, is practically impossible. This justifies the application of the somewhat indirect method used above of the excess of the leaving over the entering momentum and pressure components.

The separate determination of net thrust and external drag, as explained above, is based on the premise that the outside surface of the duct does not contribute to the thrust. The author owes to J. V. Foa the interesting remark that a small contribution to the thrust may be produced if the inflow is partly spilling over the rounded intake edge and producing a suction, in case the intake is built such that a stagnation line appears on the inside near the edge. However, nothing seems to be gained because of the corresponding loss of inside mass flow, and at any rate not for compressor driven units.

The Fuel-Air, Thrust-Air Ratio

In contrast to other propulsion devices the compressor-turbine propulsion relies very little on the momentum of the stoichiometric (saturated) fuel-air mixture but preponderantly on the much greater total mass of air flowing through the duct.

Assuming, to show this, a work output of 1.5×10^7 ft.lbs. for each pound of gasoline fuel and a minimum requirement of 16 lbs. per sec. air for 1 lb. per sec. gasoline, one obtains for the power input $Qm'g(m'g = \rho_e V_e A_e g$, total weight of air traversing the duct per second).

$$Q(m'g)_{\text{total}} = (1.5 \times 10^7/16)(m'g)_{\text{combustion}}$$

where $(m'g)_{\text{combustion}}$ is the minimum weight of air per second necessary for combustion.

Hence,

$$\frac{(m'g)_{\text{combustion}}}{(m'g)_{\text{total}}} = Q \times 0.939 \times 10^{-6} \qquad (4)$$

The numerical significance of this result can be estimated by means of the efficiency formula, Eq. (3), as follows.

The exit pressure ratio q_e can be assumed of the order of magnitude 1, the efficiency η of the order of magnitude 0.2, the velocity head can be estimated to

$$h = \frac{V_0^2}{2g} = \frac{750^2}{64.4} = 0.875 \times 10^4 \text{ ft.}$$

the exit velocity ratio, to $\varphi_e \approx 2.6$. This furnishes (see Eq. (3))

$$Q = 2(h/\eta)(\varphi_e - 1) = 14 \times 10^4 \text{ ft.lbs. per lb.}$$

Eq. (4) above gives then

$$(m'g)_{\text{combustion}}/m'g_{\text{total}} = 14 \times 10^4 \times 0.939 \times 10^{-6} = 0.131$$

and

$$(m')_{\text{fuel}}/(m')_{\text{total}} = 0.131/16 = 0.0082$$

At any rate, this high dilution (except in the flame holder) makes the change of the equivalent molecular weight, and with it of the gas constant R, negligible. However, the ratio γ of the specific heats may change noticeably with increasing temperature.

The General Flow Equations

The *Bernoulli equation* of steady flow for a streamline filament may be written in the form

$$d(V^2/2g) + vdp = fvds = (f_a - f_r)vds \qquad (5)$$

where

v = $1/\rho g$ the specific (per unit of weight) volume
f = the force intensity (per unit volume)
f_a = the accelerating part of f
f_r = the retarding part of f
ds = an element of length of the filament of flow

From the Bernoulli equation, Zeuner has derived a second equation by the introduction of the thermodynamic relations, taking into account the heat added, the heat created by the loss of head, and the physical properties of gases—that is, the specific heats and the equation of state (gas constant, molecular weight, etc.).

This *Zeuner equation*, as shown below, also contains and establishes the function of the concepts of entropy and enthalpy (heat content).

The Zeuner equation may now be developed as follows: The first term on the right side of Eq. (5) can be expressed by

$$f_a vds = dW \qquad (5a)$$

where dW is the mechanical work per unit of time and per unit of weight on the length ds of travel along the streamline.

For the second term $f_r\, vds$ it may be assumed that it is the negative work of friction forces (loss of head) and that it is entirely transformed into heat dQ_r, so that

$$f_r vds = dQ_r \qquad (5b)$$

where dQ_r is the heat energy in mechanical units (ft.lbs. per lb.) created on the length ds of travel along the streamline.

If the external heat-input dQ_e is added to the heat dQ_r due to the loss of head, the total heat input will increase the internal energy dU and may do work pdv so that

$$dQ_e + dQ_r = dU + pdv \qquad (6)$$

It may now be assumed that the fluid is a gas in which the energy-increase dU depends only on the temperature increase dT but not on the volume, since this is exactly the case in perfect gases and sufficiently exact in the actual gases considered here. It follows then that

$$dU = dT\frac{c_v}{A} = d(pv)\frac{c_v}{AR} = d(pv)\frac{c_v}{c_p - c_v} \qquad (6')$$

where

A = 1/778.26 (B.t.u./ft.lb.) = 1/426.9 (kg.cal.÷ kg.m.) the reciprocal of the mechanical quivalent of heat

R = $R_0\Sigma(g_n/M_n)$, the gas constant of a gas mixture

R_0 = 1,544 ft.lbs. per °F. = 848 kg.m. per °C., the general gas constant

g_n = the percentage portion of one gas in a mixture of gases

M_n = the molecular weight of one gas in a mixture of gases

c_p/c_v = γ, the ratio of specific heats

The value of γ changes somewhat with the temperature—namely, from 1.4 to 1.38 between the temperatures $T = 490°$ and 2,300°F. absolute, while it is practically independent of the pressures used in jet propulsion. In the later formulas the expression $\gamma/(\gamma - 1) = \mu$ appears. Its value varies between the same temperature limits from 3.5 to 3.67.

With the high dilutions of the fuel in the combustion chamber, the resultant reciprocal molecular weight $\Sigma g_n/M_n$ due to the combustion differs so little from the molecular weight of the air alone that the gas constant can be treated as constant in the case of turbojet propulsion.

Inserting the value of dU of Eq. (6′) into Eq. (6) one obtains

$$d(Q_e + Q_r) = d(pv)[c_v/(c_p - c_v)] + pdv \qquad (6a)$$

Now if Eqs. (6a), (5a), and (5b) are introduced into Eq. (5), and it is observed that $vdp \equiv d(pv) - pdv$, Eq. (5) assumes the form

$$d\left(\frac{V^2}{2g}\right) + d(pv)\,\frac{c_p}{c_p - c_v} = d(W + Q_e) \qquad (7)$$

It is convenient to bring this equation into a nondimensional form and use an abbreviation for the factor $d(pv)$, appearing often, by using the following definitions and abbreviations:

V/V_0 = φ, velocity ratio

p/p_0 = q, pressure ratio

ρ/ρ_0 = σ, density ratio

T/T_0 = τ, temperature ratio

$p_0/{}^1\!/_2\rho_0 V_0^2$ = H, static over dynamic pressure at the flying altitude

The subscript 0 in the expressions above denotes the values in the undisturbed atmosphere at the flying altitude.

$$c_p/(c_p - c_v) = \gamma/(\gamma - 1) = \mu$$

As the change of the gas constant after entering the duct can be neglected, the equation of state of the gas in nondimensional form becomes

$$q = \tau\sigma \qquad (8)$$

Eq. (7) changes then to

$$d(\varphi^2 + H\mu\tau) = h^{-1}d(W + Q_e) \qquad (7a)$$

The retarding (negative) work of the friction forces has been expressed thermodynamically in the Zeuner Eq. (Eqs. (7) and (7a)). It may, in the Bernoulli equation, be expressed as the loss of head caused by viscous (Poiseuille) and turbulent, momentum exchange-shear (Reynolds) stresses. In order to do that, one may content oneself with the integration of Eq. (5) over the cross sections of a duct section since the proposition to express the turbulent and viscous friction for an individual streamline filament is prohibitively complicated.

With this simplification of taking the average over a cross section, one can write the well-known relation:

$$f_r\,vds = dQ_r = \frac{\zeta h}{4D_h}\,\varphi^2 ds \qquad (5c)$$

where ζ is a coefficient depending on the Reynolds Number and D_h is the hydraulic diameter of the cross section. This one-dimensional proposition can be justified if annular, not too wide cross sections are used.

For the value of the coefficient ζ of turbulent friction see Jacob and Erk, Stanton and Pannell, and Moody, where ζ is given in function of the Reynolds Number. For example, if $T = 1{,}000°$F., $D_h = 1$ in., $V = 750$ ft. per sec., and the kinematic viscosity $\nu = 0.13$ sq.in. per sec., then the Reynolds Number $R_e = 300{,}000$ and the value of $\zeta = 0.015$.

The Bernoulli equation, Eq. (5), and the Zeuner equation, Eq. (7), with the ratios and abbreviations given above, assume the form (l length of a duct section $ds' = ds/l$)

$$d(\varphi^2 - h^{-1}W) + H\tau d(\log q) + (\zeta l/4D_h)\varphi^2 ds' = 0 \qquad (5d)$$

$$d(\varphi^2 - h^{-1}W + H\mu\tau - h^{-1}Q_e) = 0 \qquad (7d)$$

Observing that $(\zeta l/4D_h)ds' = h^{-1}dQ_r$ (according to Eqs. (5b) and (5c)) and subtracting Eq. (7d) from Eq. (5d) one obtains an equation for the entropy S, viz.:

$$\left.\begin{aligned}[d(Q_e + Q_r)]/T = dS = Rd\,\log\,(\tau^\mu q^{-1})\\ S = R\,\log\,(\tau^\mu q^{-1}) + C\end{aligned}\right\} \qquad (9)$$

This functional value of S is valid for any change of state—that is, for any condition of $\rho = F(p)$[or $\tau = F(q)$]. To make Eq. (9) dimensionless, one has to introduce a pure number that may be called "entropy number" Σ

$$\Sigma = S/R = \log\,(\tau^\mu q^{-1}) + C_0 \qquad (9a)$$

The enthalpy (heat content) is defined by

$$dI = d\,(U + pv)$$

and using Eq. (6′), which implies the property of a perfect gas

$$dI = p_0 v_0 \mu d\tau = RT_0\mu d\tau \qquad (10)$$

so that a pure number can be introduced, which may be called *enthalpy-number* J.

$$J = I/p_0v_0\mu = I/RT_0\mu = \tau \qquad (10a)$$

S and I (also Σ and J) are the entropy and the enthalpy functions for any change of state [$p = p(\rho)$] of perfect gases.

For any change of state [e.g., $\tau = F(q)$], the enthalpy is expressed by the entropy, so that in the equations of flow, Eqs. (5d) and (7d), pressure and temperature ratios can be replaced either by the entropy number (Σ) or by the enthalpy number (J) with the result that then either entropy number or enthalpy number would appear with the velocity ratio φ as the only variables of state. This representation, however, is not chosen for the analysis in this paper.* One reason is that in case of leakage or bleeding of heat (dQ negative) the flow system is not thermodynamically complete and the local entropy value is no measure of efficiency.

Change of State and Cross Sections

The change of state in a flow, in which the influence of transverse conduction and radiation of heat is either balanced by opposite transverse momentum exchange or very small, is expressed by an equation of change of state—that is, a relation between two of the variables appearing in the equation of state of the fluid.

The usual expression of a change of state is given by $\rho = F(p)$ so that the integral $\int dp/\rho$ or the differential vdp appearing in the Bernoulli Eq. (5) can be evaluated. The change of state in a flow is governed by external and internal heat input or loss dQ_e and dQ_r, respectively, and by the variation of cross sections along the duct. This can be seen from the fact that, after the change of state $\rho = F(p)$ has been assumed and also after the heat and work input have been given, velocity and density along a duct follow immediately from Bernoulli and Zeuner equations. On the other hand, velocity and density along a duct determine the variation of cross section by the continuity equation.

Conversely, the choice of the cross sections, together with the heat and work input, determines the corresponding change of state condition (which at supersonic velocity can be confined to a shock-wave layer).

These relations are expressed by the continuity condition $A\rho V = \text{const.}$ or

$$A\sigma\varphi = Aq\tau^{-1}\varphi = \text{const.} \qquad (1c)$$

If the change of state $\sigma = F(q)$ is prescribed, σ, q, τ, and φ follow from the solution of the Bernoulli and Zeuner Eqs. (5d) and (7d), and $A = A(s)$ (s abscissa along duct) follows then from Eq. (1c).

If, on the other hand, $A(s)$ is prescribed, a relation between the velocity ratio φ, the pressure ratio q, and the temperature ratio τ follows from the continuity Eq. (1c), and Bernoulli and Zeuner Eqs. (5d) and (7d) then determine their functional values in terms of the abscissa s along the duct.

The flow Eqs. (5d) and (7d) are incomplete as long as no condition of change of state is introduced.

For the case where no heat is put in, generated, or lost, the condition of adiabatic change of state has to be applied—i.e., $pv^\gamma = \text{const.}$, or

$$q\tau^{-\mu} = \text{const.}, \qquad \mu = \gamma/(\gamma - 1) \qquad (10')$$

For the case with heat added, generated, or lost, a condition mathematically convenient and covering a wide range of physically appropriate changes is the polytropic change of state, $pv^n = \text{const.}$, or

$$q\tau^{-\lambda} = \text{const.}, \qquad \lambda = n/(n - 1) \qquad (11)$$

The cases of adiabatic, isothermal, constant pressure, and constant density (or constant specific volume) change of state can be envisaged as special or limiting cases of the polytropic change.

However, it is simpler to treat them by inserting these special change-of-state conditions directly into the equations of flow, Eqs. (5d) and (7d), as will be seen in the case of the "perfect" jet engine treated as the simplest example.

The "Perfect" Jet Engine

The analysis of jet engines may be first applied to an engine idealized by the assumption that it is perfectly insulated, that the flow is frictionless, and that the power of the compressor is equal and opposite to the power of the turbine and can be represented by the work per unit of time of a force field (f_a) acting on the streamlines in the duct section of the compressor and respectively of the turbine.

Moreover, here, as well as in the analysis of the actual jet engine, the gas constant R and the value of $\mu = \gamma/(\gamma - 1) = 3.5$ shall be assumed not to vary, since in fact for a temperature range from 500 to 2,000°F. the value of R changes less than 0.3 per cent and the value of μ changes from 3.5 to 3.67, as indicated in the derivation of Eq. (7).

Following from the "ideal" conditions, the flow through intake and compressor and through turbine

---

* In terms of entropy and enthalpy the Bernoulli and Zeuner equations appear in the form

$$d[\varphi^2 - h^{-1}(W - Q_r)] + H[dJ - \frac{J}{\mu}d\Sigma] = 0 \qquad (5e)$$

$$d[\varphi^2 - h^{-1}(W - Q_e)] + HdJ = 0 \qquad (7e)$$

The polytropic change of state [see Eq. (11)] below is in these terms given by

$$\Sigma_1 + (\lambda - \mu)\log J_1 = \Sigma_2 + (\lambda - \mu)\log J_2 \qquad (11a)$$

Here again the conditions of adiabatic, isothermal, constant pressure, and constant density are represented by special values of $\lambda = n/(n - 1)$.

$n = \gamma$, $\lambda = \mu$, adiabatic; $n = 1$, $\lambda^{-1} = 0$, isothermal; $n = 0$, $\lambda = 0$, constant pressure; $n^{-1} = 0$, $\lambda = 1$, constant specific volume (constant density).

and nozzle will be adiabatic, while in the combustion chamber a certain freedom is left by the assumption of a polytropic change of state that for steady combustion will be near a constant pressure condition—i.e., $n \ll 1$, $\lambda \ll 1$. The value of λ, together with the amount of heat input, determines the cross-section change along the combustion chamber, and its effect on the propulsion efficiency will also be discussed

The analysis will give velocities, pressures, temperatures, and densities everywhere in the unit in terms of the data characteristics.

These data are:

The static to dynamic pressure ratio

$$H = p_0/{}^1\!/_2\,\rho_0 V_0^2$$

The velocity head

$$h = V_0^2/2g$$

both in the undisturbed atmosphere and for the velocity V_0 relative to the unit.

The compression ratio of intake and compressor

$$q_{ec} \equiv q_{ih} \equiv q^*$$

The temperature ratio at the transition from the combustion (heat) chamber to the turbine

$$\tau_{eh} \equiv \tau_{it} \equiv \tau^*$$

The (specific) heat input in the heat chamber per unit of time divided by the weight of gas passing a cross section per unit of time:

$$Q_h \text{ ft.lbs. per lb.}$$

The flow Eqs. (5d) and (7d) in the case of adiabatic flow (see Eq. (10′)) and for a specific work input W (for intake and compressor) are:

$$\left.\begin{aligned} \varphi_e^2 - \varphi_i^2 + H\mu(\tau_e - \tau_i) &= h^{-1}W \equiv W^* \\ \tau_e/\tau_i &= (q_e/q_i)^{1/\mu} \end{aligned}\right\} \quad (5 \text{ adiab.})$$

Eqs. (5d) and (7d) become, for polytropic flow (in the combustion chamber) with specific heat input Q_h but no work input,

$$\varphi_e^2 - \varphi_i^2 + H\lambda(\tau_e - \tau_i) = 0 \quad (5 \text{ polytr.})$$

$$\varphi_e^2 - \varphi_i^2 + H\mu(\tau_e - \tau_i) = h^{-1}Q_h \equiv Q^*_h \quad (7 \text{ polytr.})$$

so that

$$H(\mu - \lambda)(\tau_e - \tau_i) = Q^*_h$$

$$\varphi_e^2 - \varphi_i^2 = -Q^*_h[\lambda/(\mu - \lambda)]$$

Applying these equations for intake and compressor, from infinity in front to the entrance to the exit of the compressor:

(*a*) *Intake and Compressor (Adiabatic)*:

$$q_{ec} \equiv q^* = \tau_{ec}{}^{\mu} \quad (12a)$$

$$\varphi_e^2 = 1 + H\mu(1 - q^{*1/\mu}) + W^*_e \quad (13a)$$

where

$$q^{*1/\mu} = \tau_{ec},\ W^*_e \equiv h^{-1}W_e \quad (14a)$$

(*b*) *Combustion (Heat) Chamber:*

$$q_{ih} \equiv q_{ec} \equiv q^*,\quad Q_h h^{-1} \equiv Q^*_h$$

$$\tau_{eh} \equiv \tau^* = \tau_{ec} + \frac{Q^*_h}{H(\mu - \lambda)} = q^{*1/\mu} + \frac{Q^*_h}{H(\mu - \lambda)} \quad (15b)$$

with the abbreviations $c_\lambda \equiv \lambda/(\mu - \lambda)$ and $c_\mu \equiv \mu/(\mu - \lambda)$,

$$\varphi_{eh}^2 \equiv \varphi_{it}^2 = \varphi_{ec}^2 - Q^*_h c_\lambda = 1 + H\mu(1 - q^{*1/\mu}) + W^*_e - Q^*_h c_\lambda \quad (16b)$$

$$q_{eh} \equiv q_{it} = q_{ih}\tau_{ih}{}^{-\lambda}\tau_{eh}{}^{\lambda} = q^{*1/c_\mu}\,\tau^{*\lambda} \quad (17b)$$

From Eq. (14b) it can be seen that the requirement of the temperature ratio τ^* in front of the turbine, the compression ratio q^* at the entrance of the heat chamber, and the amount of heat input Q^*_h into the heat chamber determines the polytropic exponent $n = \lambda/(\lambda - 1)$ and with it, by means of the continuity equation, also the cross section change along the heat chamber. Eq. (14b) also confirms the experience that a higher compression ratio q^* and a higher specific heat input Q^*_h creates a higher turbine temperature τ^* and so, because of the limit of heat resistance of the turbine material, enforces a limit of compression ratio and heat input—that is, a limit of the performance of the jet engine.

(*c*) *Turbine Plus Nozzle (Adiabatic)*:

$$\left.\begin{aligned} &q_{en} \equiv q_e,\ \tau_{en} \equiv \tau_e,\ W^*_t = -W^*_c \equiv -W^*,\ \varphi_{en} \equiv \varphi_e \\ &q_e\tau_e{}^{-\mu} = q_{it}\tau_{it}{}^{-\mu} = q^{*1/c_\mu}\tau^{*\lambda-\mu} \\ &\varphi_e^2 = \varphi_{eh}^2 - W^* - H\mu(\tau_e - \tau) = \\ &\quad 1 + H\mu(1 - q^{*1/\mu}) - Q^*_h c_\lambda - H\mu(\tau_e - \tau^*) \end{aligned}\right\} \quad (18c)$$

and by Eq. (15b)

$$\varphi_e^2 = 1 + H\mu(1 - \tau_e) + Q^*_h \quad (19c)$$

The stepwise analysis of the entire unit applied above, shows that the exit velocity ratio φ_e by Eq. (19c) and the product of exit pressure ratio q_e, and exit temperature ratio τ_e (i.e., $q_e\tau_e{}^{-\mu}$) by Eq. (18c) is determined by prescribing the heat input Q^*_h, the compression ratio q^*, and the turbine temperature ratio τ^*. However, the choice of the separate values of q_e and τ_e remains at first arbitrary. It is sometimes assumed that the jet acquires at the exit the pressure of the undisturbed outside atmosphere. But this is not necessarily so, since a pressure excess at the exit will outside set itself in equilibrium with the ambient atmosphere by momentum transfer (friction) and by converging for subsonic and by diverging for supersonic jet velocity.

From Eq. (19c) and the thrust Eqs. (2a) and (2b), it can be seen that the exit velocity ratio φ_e increases with the specific heat input Q^*_h and decreases with the exit temperature ratio τ_e, while the thrust also increases

with φ_e and decreases with τ_e. Moreover, Eq. (18c) shows that τ_e decreases with an increase of q^*.

In agreement with engineering practice, this proves quantitatively that, with fixed turbine temperature ratio τ^* and with fixed specific heat input Q^*_h, a higher compression ratio produces a higher thrust.

The Cross-Section Distribution of the "Perfect" Jet Engine

After the velocity ratios φ and the pressure ratios q are determined, the cross-section areas A or their ratios A/A_e with the exit area are found by means of the continuity Eq. (1a). As said before, only the axial components of φ must be used if there is rotation of the flow, but in the case treated here, it is assumed that in each duct section the rotation is eliminated by countervanes so that the tangential components of φ are zero at each end of a section.

Eq. (1a) can, for adiabatic flow in a section, be written in the form

$$A_i = A_e(\varphi_e/\varphi_i)(q_e/q_i)^\gamma \tag{1c}$$

and for polytropic flow

$$A_i = A_e(\varphi_e/\varphi_i)(q_e/q_i)^n \tag{1d}$$

which for constant pressure ($n = 0$) becomes

$$A_i = A_e(\varphi_e/\varphi_i) \tag{1e}$$

and if in this case mechanical work input or friction is excluded (see Eq. (5d))

$$\varphi_e = \varphi_i,\ A_e = A_i \tag{1f}$$

In this way the results of Eqs. (12a) to (19c) of the performance of the unit can be used to determine along the unit those area ratios without which the performance values of pressures, densities, temperatures, and velocities would not be accomplished.

One obtains from Eqs. (1c) and (1d) the successive area values as follows:

The flow from infinity to the compressor exit being assumed adiabatic, one has:

$$A_{ec}^2 = A_e^2\frac{[1 + H\mu(1-\tau_e) + Q^*]q_e^{2/\gamma}(q^{1/\mu}\tau^{*-1})^{2/c_\mu}}{[1 + H\mu(1 - q^{1/\mu}) + W^*]q^{2/\gamma}} \tag{20a}$$

where A_e, q_e, φ_e are the nozzle exit values. This equation determines either A_e/A_{ec} from a required specific work nput W^* of the compressor or, vice versa, the specific compressor work input from this area ratio and, of course, also from the required compression ratio q^*.

Analogously, the area ratio A_{ec}/A_{eh} of entrance and exit section of the combustion (heat) chamber is given by

$$A_{ch}^2 = A_{ec}^2(q^{*-1/\mu}\tau^*)^{2(1-\lambda)}\left[\frac{1 + H\mu(1 - q^{*1/\mu}) + W^*}{1+H\mu(1-q^{1/\mu})+W^*-Q^*c_\lambda}\right] \tag{20b}$$

Finally, the area ratio A_{eh}/A_e of entrance to turbine and exit of nozzle becomes

$$A_{eh}^2 = A_e^2(q_e q^{-1/c_\mu}\tau^{*-\lambda})^{2/\gamma} \times \left[\frac{1 + H\mu(1 - \tau_e) + Q^*}{1 + H\mu(1 - q^{*1/\mu}) + W^* - Q^*c_\lambda}\right] \tag{20c}$$

Eqs. (20a), (20b), and (20c) show that all areas (A) are determined by one of them, preferably by the exit area A_e and by the value $W\rho_e g V_e A_e = P_c$ of the compressor power, prescribed so that it gives feasible dimensions and weight of compressor and turbine. It seems appropriate to measure W^* in terms of Q^* (say $W^* = kQ^*$, k of the order of magnitude 1).

Relations Between Thrust, Power, Speed, Altitude, and Exit Area of the "Perfect" Jet Engine

The thrust of a jet engine is not uniquely determined by the data of performance. Eqs. (18c) and (19c), in fact, show that of the three exit variables of temperature ratio τ_e, pressure ratio q_e, and velocity ratio φ_e one remains arbitrary—that is, only expressible in terms of the other two exit variables. It is possible, however, to complete the conditions by choosing in the continuity Eq. (20c) an appropriate area ratio $A_{eh}/A_e \equiv A_{tt}/A_e$ between the exit areas of heat chamber and nozzle.

The choice of this area ratio or what amounts to the same of exit pressure q_e or temperature ratio τ_e must obviously, all other data unchanged, depend on their effect on the magnitude of thrust.

Different ways to estimate the effectiveness of jet propulsion are possible. One method uses the efficiency η—that is, the ratio of useful to total work of Eq. (3):

$$\eta = Q^{*-1}[2(\varphi_e - 1) + H(1 - q_e^{-1})\tau_e\varphi_e^{-1}] \tag{3}$$

expresses by means of Eqs. (18c) and (19c) two of the variables φ_e, q_e, τ_e by one of them, for instance, φ_e and q_e by τ_e and by means of $d\eta/d\tau_e = 0$ determines the value of τ_e (and φ_e and q_e), which gives the maximum of η.

This method leads to a mathematically involved relation between τ_e and Q^*, which, as in the case of the screw propeller, may give the trivial result that the highest efficiency appears at lowest power input.

A second method taken from the theory of the screw propeller requires the maximum of thrust Th. if, with the other data of speed and altitude, the heat power is assumed as prescribed. This method may be represented as follows:

The thrust expression taken from Eq. (2b) is:

$$\text{Th.} = \rho_0 V_0^2 A_e[q_e\tau_e^{-1}\varphi_e(\varphi_e - 1) + {}^1/_2H(q_e - 1)] \tag{2b}$$

The heat-power input P, or better its dimensionless parameter II,

$$\Pi = P/{}^1\!/_2\,\rho_0 V_0^3 A_e, \quad P = Q^* h g \rho_e V_e A_e \qquad (21a)$$

becomes

$$\Pi = Q^* q_e \varphi_e \tau_e^{-1} \qquad (21b)$$

One has then to determine the maximum of thrust for a prescribed power by requiring the value zero for the differential coefficient after q_e and φ_e are expressed by τ_e:

$$\frac{d}{d\tau_e}\,[\text{Th.} + L\Pi] = 0 \qquad (22)$$

where L is the Lagrange multiplicator to be determined by the above Eq. (21b) for Π and after q_e and φ_e have been expressed by τ_e by means of Eqs. (18c) and (19c).

The author has not yet succeeded in deriving from this second proposition sufficiently simple conclusions.

A third proposition requires the thrust coefficient Th.* (that is, the thrust per unit of nozzle exit area A_e and of ambient dynamic pressure ${}^1\!/_2\,\rho_0 V_0^2$) to become a maximum for a prescribed specific heat input $Q^* = Qh^{-1}$—that is, for a heat power input per unit of weight flow $\rho_e g V_e A_e$ and per unit of head $h = V_0^2/2g$ of the ambient atmosphere. Both quantities Th.* and Q^* are dimensionless parameters.

This last proposition, which leads to fairly simple results, is in detail illustrated by an example.

A thrust coefficient Th.* = Th./$\rho_0 V_0^2 A_e$ was given in Eq. (2a) in the form

$$\text{Th.}^* = q_e \tau_e^{-1} \varphi_e (\varphi_e - 1) + {}^1\!/_2 H (q_e - 1) \qquad (2a)$$

The results of the performance Eqs. (12a) to (19c) serve to express the exit temperature ratio τ_e and the exit jet-velocity ratio φ_e by the exit pressure ratio q_e. In these expressions the coefficients depend on the prescribed values of V_0, p_0, ρ_0, T_0; on the prescribed compression ratio q^*; on the prescribed turbine temperature ratio τ^*, and on the specific heat-input Q^*.

The relations between q_e, φ_e, and τ_e may be repeated in the form

$$q_e = \tau_e^{\mu}\, l^{-\mu} \qquad (18c)$$

where

$$l \equiv (q^{*-1/\mu_c} \tau^*)^{1/c_\mu}, \quad c_\mu = \mu/(\mu - \lambda) \qquad (18'c)$$

$$\varphi_e^2 = k - H\mu\tau_e \qquad (19c)$$

where (see Eq. (19))

$$k \equiv Q^* + 1 + H\mu \qquad (19'c)$$

Eq. (2a) can then be expressed in a form that contains as the only variable τ_e—namely,

$$\text{Th.}^* = l^{-\mu}\tau_e^{\mu-1}[k - H\mu\tau_e - (k - H\mu\tau_e)^{1/2}] + {}^1\!/_2 H(l^{-\mu}\tau_e^{\mu} - 1) \qquad (2b)$$

To obtain an extremum value for Th.* one must make vanish the differential coefficient with respect to τ_e, which leads to:

$$\frac{d\text{Th.}^*}{d\tau_e} = (\mu - 1)\tau_e^{\mu-2}[k - H\mu\tau_e - (k - H\mu\tau_e)^{1/2}] + {}^1\!/_2 H\mu\tau_e^{\mu-1} + \tau_e^{\mu-1}[-H\mu + {}^1\!/_2 H\mu(k - H\mu\tau_e)^{-1/2}] = 0$$

Canceling the factor $\tau_e^{\mu-1}$, which is certainly different from zero, and multiplying by $(k - H\mu\tau_e)^{1/2}$, which, according to Eq. (19'c), is also not equal to zero but is greater than 1, one obtains the equation

$$(k - H\mu\tau_e - 1)[H\mu(2\mu - 1)\tau_e - 2k(\mu - 1)]^2 = 0$$

or, since the first factor (see Eq. (18c)) has the value $\varphi_e^2 - 1 > 0$,

$$(\tau_e)_{max.} = k\,\frac{2(\mu - 1)}{H\mu(2\mu - 1)} = (Q^* + 1 + H\mu)\left[\frac{2(\mu - 1)}{H\mu(2\mu - 1)}\right] \qquad (23)$$

From Eq. (19c) the exit velocity ratio φ_e is then given by

$$\varphi_e^2 = (Q^* + 1 + H\mu)[(\gamma - 1)/(\gamma + 1)] \qquad (24)$$

and from Eq. (18c) the exit pressure ratio by

$$q_e = [2\varphi_e^2(1/\gamma HL)]^{\mu} \qquad (25)$$

The maximum thrust coefficient then becomes

$$(\text{Th.}^*)_{max.} = \frac{H}{2}\left([q^{*}\tau^{*-\mu}]^{1/c_\mu}\left[\left(\frac{2k}{H\gamma}\right)\left(\frac{\gamma - 1}{\gamma + 1}\right)\right]^{\mu} \times \{1 - \gamma[k(\gamma - 1)]^{-1/2}\} - 1\right) \qquad (2c)$$

However, since the expressions for the exit values of temperature, relative jet velocity, and pressure ratio are given by Eqs. (23), (24), and (25), it seems to be more convenient to use, as will be done below, the form of Eq. (2b) instead of Eq. (2c) for the thrust coefficient.

The value of the polytropic characteristic $\lambda \equiv n/(n - 1)$ (n polytropic exponent) in the combustion chamber is in general assumed as zero, which means constant pressure change of state. The question is whether this value of n is the best one for the thrust maximum. Looking at the expression for τ_e, φ_e, and q_e to find an answer to this question, one sees that only q_e is dependent on the value of λ (see Eq. (25)) because of the term $l \equiv (q^{*-1/\mu}\tau^*)^{1-(\lambda/\mu)}$. One also sees that $\lambda > 0$, $n < 0$ gives a smaller value of $l^{-\mu}$ and therefore a smaller value of Th.*, so that Eq. (2b) (and also Eq. (2c)) give smaller thrust values if λ is positive—that is, tending toward $\rho = \text{const}$.

On the other hand, a doubt about the allowable value of excess of exit pressure ratio q_e does arise, since it must not be higher than the pressure excess realizable by an equilibrium between free jet and ambient air arising from friction (i.e., momentum transfer) and from convergence of a subsonic or divergence of a supersonic free jet.

The case $\lambda < 0$, $n > 0$, which deviates from constant pressure toward isothermal change of state, seems to give increase of thrust but has not yet been evaluated.

The thrust itself is obtained from Eq. (2b), which may be repeated here

$$(\text{Th.})_{max.} \equiv (\text{Th.}^*)_{max.}\rho_0 V_0^2 A_e \qquad (2a)$$

Numerical values of thrust coefficient and thrust are now ready for calculation from the data. Using for instance the data given below, one has to proceed as follows:

Compression ratio and turbine temperature ratio may be required to be $q^* = 4$ and $\tau^* = 4$. The change of state in the heat chamber may be required to be of constant pressure—that is, $n = 0$, $\lambda = 0$. With a velocity $V_0 = 750$ ft. per sec. and an altitude of 22,000 ft.,

$$H = \frac{p_0}{{}^1/_2\rho_0 V_0^2} = 2.82, \qquad h = \frac{V_0^2}{2g} = 0.875 \times 10^4$$

$$H\mu = 2.82 \times 3.5 = 9.87, \; (l)_{\lambda=0} = q^{*-1/\mu}\,\tau^* = 4^{0.714} = 2.7$$

For the specific heat input (see Eq. (15b))

$$Q^* = H(\mu - \lambda)(\tau^* - q^{*1/\mu}) = 9.87(4 - 4^{0.286}) = 24.8$$

It follows then

$$k = Q^* + 1 + H\mu = 35.67$$

$$\varphi_e^2 = k\left(\frac{\gamma - 1}{\gamma + 1}\right) = 35.67\left(\frac{0.4}{2.4}\right) = 5.945$$

$$\tau_e = \frac{2k}{H}\left(\frac{\gamma - 1}{\gamma(\gamma + 1)}\right) = \frac{71.34}{2.82}\left(\frac{0.4}{1.4 \times 2.4}\right) = 3.01$$

$$q_e = \left(\frac{2\varphi_e^2}{\gamma H l}\right)^{\mu} = \left(\frac{1.890}{1.4 \times 2.82 \times 2.7}\right)^{3.5} = 1.558$$

The thrust coefficient with these values (see Eq. (2b)) becomes

$$(\text{Th.}^*)_{max.} = \frac{1.558 \times (5.945 - 2.435)}{3.01} + (1.41 \times 0.558) = 1.811 + 0.786 = 2.597$$

Assuming a nozzle exit-area $A_e = 1.5$ sq.ft., the thrust will have the value

$$\text{Th.} = 2.597\rho_0 V_0^2 A_e = 2.597 \times 0.0012 \times 750^2 \times 1.5 = 2{,}620 \text{ lbs.}$$

If now the thrust value corresponding to the exit pressure ratio $q_e = 1$ ($p_e = p_0$) shall be determined, in order to compare it for the same data with the maximal value calculated above, one has to proceed as follows:

The equation for the thrust coefficient is simplified to

$$(\text{Th.}^*)_{q_e=1} = \tau_e^{-1}(\varphi_e^2 - \varphi_e)$$

From Eq. (18c) can be seen

$$\tau_e = l = 2.7$$

From Eq. (19c)

$$\varphi_e^2 = Q^* + 1 + H(1 - \tau_e) = 9.01$$

so that

$$(\text{Th.}^*)_{q_e=1} = (1/2.7)6.01 = 2.225$$

$(\text{Th.})_{q_e=1} = 2.225 \times 0.0012 \times 750^2 \times 1.5 = 2{,}245$ lbs. The gain in thrust is for the specific heat input of

$$Q^* = 24.8$$

$$(\text{Th.}^*)_{max.}/(\text{Th.}^*)_{q_e=1} = (\text{Th.})_{max.}/(\text{Th.})_{q_e=1} = 1.168$$

From Eq. (2b) and (3) the efficiency formula can be stated in the form

$$\eta = \text{Th.}^* 2Q^{*-1}\tau_e\varphi_e^{-1}q_e^{-1} \qquad (3a)$$

With the values computed above one obtains: for $q_e > 1$, $\eta = 16.65$ per cent; for $q_e = 1$, $\eta = 16.15$ per cent.

The comparison of the efficiencies η for the case of equal specific heat input Q^* but for different exit pressure ratios q_e shows the peculiar result of smaller efficiency at smaller exit pressure but at still smaller thrust.

The reason is that in the efficiency expression (see Eq. (21b)) the value $Q^* q_e\varphi_e\tau_e^{-1}$ of the total heat-input power appears in the denominator. This may cause, with increasing exit pressure ratio q_e, the factor $q_e\varphi_e\tau_e^{-1}$, denoting the mass flow, to increase more than the thrust-power value in the numerator.

This observation, together with the consideration of the feasible values of exit pressure augmentation by friction, transverse momentum transfer, and transverse centrifugal force of the converging streamlines of the jet emerging into the ambient atmosphere, indicates a certain advantage for maximum method 2 because it introduces the total heat power input (see Eq. (22)).

Analysis of Losses in the Jet Engine

The Nonadiabatic Bernoulli-Zeuner Equations of Flow

The perfect (or ideal) jet engine was analyzed by means of Eqs. (5d) and (7d) with the simplification of omitting the turbulent loss of head ($\zeta\varphi^2/4D_h$) per unit of streamline length, the actual excess of power of turbine over the power of compressor, and the losses of heat due to imperfect insulation.

These facts, making the flow in all sections of the duct unit nonadiabatic, necessitate an assumption for the changes of state in the different sections of the unit, which afterwards must be justified by the energy balance and the choice of the cross sections along the duct.

Following this reasoning, a polytropic change of state

$$q\tau^{-\lambda} = \text{const.} \qquad (11)$$

with λ possibly different in each section of the unit, may be introduced.

Eq. (10) is equivalent to

$$q_2\tau_2^{-\lambda} = q_1\tau_1^{-\lambda} \qquad (11b)$$

where the subscripts 2 and 1 denote two cross sections of one section of the unit.

It is also well known that all of these relations have the same structure as the adiabatic relations inasmuch as the difference between them consists only in changing γ into n or $\mu = \gamma/(\gamma - 1)$ into $\lambda = n/(n - 1)$.

Using Eq. (10b) to eliminate q from Eq. (5d), one obtains the equations

$$\frac{d}{ds'}(\varphi^2 + H\lambda\tau) + z\varphi^2 = \frac{dW^*}{ds'} \tag{5e}$$

$$\frac{d}{ds'}(\varphi^2 + H\mu\tau) = \frac{d}{ds'}(W^* + Q^*_e) \tag{7e}$$

where, for abbreviation (see Eq. (5c)), $z = \zeta l/4D_h$.

The Integration of the Bernoulli-Zeuner Equation

The mechanical (positive or negative) specific work input W^*, heat input Q^*, and coefficient $z(s')$ may be assumed to be prescribed. Then Eqs. (5e) and (7e) appear as two equations with the two unknown variables τ and φ. The temperature ratio function $\tau(s')$, eliminated from the two flow equations above, leaves, for the square of the velocity ratio φ, the differential equation

$$\frac{d\varphi^2}{ds'} + c_\mu z\varphi^2 = \frac{d}{ds'}(W^* - c_\lambda Q^*_e) \tag{5f}$$

With the abbreviations

$$c_\mu \equiv \mu/(\mu - \lambda),\ c_\mu = \lambda/(\mu - \lambda)$$

the integral will be

$$\varphi^2 = e^{-c_\mu \int_i^{s'} z\,ds'}\left[\varphi_i^2 + \int_i^{s'} ds' e^{+c_\mu \int_i^{s'} \zeta\,ds'} \times (d/ds')(W^* - c_\lambda Q^*_e)\right] \tag{5g}$$

where the subscript i denotes the entrance station of the duct section in consideration. If one is content with the determination of the state at the entrance and exit of each duct section, the integral functions become constants. It is convenient to introduce the following abbreviations:

$$a \equiv e^{-c_\mu \int_0^1 z\,ds'} \tag{26}$$

$$b \equiv ((W^* - c_\lambda Q^*)_0^1)^{-1} a \int_0^1 e^{+c_\mu \int_0^{s'} \zeta\,ds'}\, d(W^* - Q^* c_\lambda) \tag{27}$$

Eq. (5g) specialized for the values at the entrance (i) and the exit (e) station of any duct section then assumes the form

$$\varphi_e^2 = \varphi_i^2\, a + (W^* - c_\lambda Q^*)_0^1 b \tag{5h}$$

Eqs. (5e) and (7e), after subtraction and in consequence of Eq. (5h), furnish

$$H\mu\tau_e = H\mu\tau_i + \varphi_i^2(1 - a) + [W^*(1 - b) + Q^*(1 + c_\lambda b)]_0^1 \tag{7h}$$

In the following development W^* and Q^* may denote, respectively, the total specific (positive or negative) work and heat input of a section of the unit, whereby the different sections may be indicated by the subscripts i for intake, c for compressor, h for heat chamber, t for turbine, and n for nozzle.

The analysis can now be performed step by step analogously to the analysis of the perfect jet engine. Only the number of steps will be higher, since for nonadiabatic flow neither intake and compressor nor turbine and nozzle can be treated as one step. To be quite exact the heat chamber should also be treated in the two sections of flame holder and heat flow, but this must be left for a special investigation. However, if only the states at the exit and entrance are to be considered, the treatment of the heat chamber in one step, with an average change of state, may be justified as a first approximation.

To the two last flow equations, Eqs. (5h) and (7h), the change of state condition between the entrance and the exit stations of each duct section must be added as the third equation—namely,

$$q_e = q_i(\tau_e/\tau_i)^\lambda \tag{11b}$$

The continuity Eq. (1c), combined with the preceding equation, provides a fourth relation between the entrance and exit cross-section ratio and the pressure and temperature ratios at these same cross sections—namely,

$$q_e(\varphi_e A_e)^n = q_i(\varphi_i A_i)^n \tag{1d}$$

where the polytropic exponent n for adiabatic change of state becomes γ, for constant pressure $n = 0$, for constant temperature $n = 1$.

SUCCESSIVE ANALYSIS OF A "NONPERFECT" JET ENGINE

The four equations, Eqs. (5h), (7h), (11b), and (1d), are consistently arranged in such a manner that the significant variables at the exit (e) of a duct section follow immediately from their values at the entrance (i). The exit values then serve as the entrance values for the adjoining duct section.

Thus, the analysis is as follows:

(*1*) *The Intake.*—First subscript i. Since the flow arrives from the undisturbed atmosphere (i.e., $q_\infty = 1$, $\tau_\infty = 1$, $\varphi_\infty = 1$) and since no mechanical work or external heat W and Q is put in, Eq. (5h) furnishes (first subscript c for compressor)

$$\left.\begin{aligned} &\varphi_{ie}^2 \equiv \varphi_{ic}^2 = a_i \\ &a_i \equiv e^{-c_\mu i \int_0^1 z\,ds'} \text{ (Eq. (26))} \end{aligned}\right\} \tag{28}$$

$$H\mu\tau_{ie} \equiv H\mu\tau_{ci} = H\mu + 1 - a_i \tag{29}$$

$$q_{ie} \equiv q_{ci} = \tau_{ie}^{\lambda_i} \equiv \tau_{ci}^{\lambda_i} = [(H\mu + 1 - a_i)/H\mu]^{\lambda_i} \tag{30}$$

$$A_{ii}/A_{ci} = \varphi_{ie} q_{ie}^{1/n_i} = \varphi_{ci}\, q_{ci}^{1/n_i} = a_i^{1/2}[(H\mu + 1 - a_i)/H\mu^*]^{1/n_i - 1} \tag{31}$$

There is a certain interest in providing, at the entrance of the compressor, a high pressure ratio $q_{ie} \equiv q_{ci}$. In order to investigate this possibility, a numerical example is given.

Assume again $H\mu = 9.87$, $V_0 = 750$ ft. per sec., $\rho_0 = 0.0012$, $\zeta = 0.015$, $l/D_h = 10$. Then one obtains

$$a_i = e^{-2 \cdot 5 c_f \mu i}$$

Some preliminary estimates show that appropriate values of the polytropic exponent are

$$n_i = 3,\ \lambda_i = 1.5$$

$$n_i = 5,\ \lambda_i = 1.25$$

The table below shows the consequences of these assumptions.

n_i	λ_i	c_{ui}	a_i	φ_{ie}	τ_{ie}	A_{ie}/A_{ii}	q_{ie}
3	1.5	1.75	0.013	0.114	1.10	8.4	1.153
5	1.25	1.556	0.02	0.1414	1.0995	6.9	1.126

The result of the last column of the table above following from the equation of continuity, can be interpreted either envisaging A_{ii} as the cross section in front of the intake or as the cross section of the incoming free column of air far in front, where the disturbance of the atmosphere by the jet engine is negligible.

The first interpretation, if required with appreciable pressure increases, would lead to flow separation and backflow caused by the corresponding diameter increase at feasible intake length.

At the front station of the intake in the latter interpretation, there is already a partial stagnation so that the increase of areas along the intake proper is smaller than appearing in this last column of the table. With this interpretation the front area at infinity may be called A_0.

It is evident that by prescribing the ratio of diameter increase to intake length one can calculate velocity ratio φ_{ii} and pressure ratio q_{ii} at the front section of the intake.

However, for a given exit area of the intake (i.e., entrance section of the compressor) the resultant mass flow of air, which is important for the attainment of thrust, becomes smaller if the intake and the counterpressure of the compressor is designed for higher stagnation (ram) pressure.

(2) *The Compressor.*—The heat that the compressor produces by compression and by friction leaves again partly through the inner and outer walls. It is plausible to assume for the loss of heat a percentage of the specific work (per pound weight and per unit of length of a streamline) of the compressor, which, with the sign definition of this paper, is positive. This loss, therefore, is expressed by

$$Q^*_c = -\delta_c W^*_c$$

so that

$$(W^*_c - c_{\lambda c} Q^*_c) b_c = W^* b_c (1 + c_\lambda \delta_c)$$

and

$$W^*_c(1 - b_c) + Q^*_c(1 + c_{\lambda c} b_c) = W_c[1 - \delta_c(1 + c_{\lambda c}\delta_c)]$$

If now for convenient writing one introduces the abbreviations

$$(1 - a_c)/H\mu_c = \alpha_c, \qquad q_c(1 + c_{\lambda c}\delta_c) = \beta_c$$

and

$$(1 - \delta_c - \beta_c)/H\mu = \gamma_c$$

Eqs. (5h) and (7h) become

$$\varphi_{ce}^2 = \varphi_{ci}^2 a_c + W^*_c \beta_c \tag{32}$$

$$\tau_{ce} = \tau_{ci} + \varphi_{ci}^2 \alpha_c + W^*_c \gamma_c \tag{33}$$

The change of state Eq. (10b) gives

$$\tau_{ce}^{-\lambda_c} q_{ce} = \tau_{ci}^{-\lambda_c} q_{ci} \tag{34}$$

and the continuity equation

$$q_{ce}^{1/n_c} \varphi_{ce} A_{ce} = q_{ci}^{1/n_c} \varphi_{ci} A_{ci} \tag{35}$$

Using now the values of q_{ci}, φ_{ci}, τ_{ci}, and A_{ci} found for the intake, one obtains by means of Eqs. (32) to (35) the exit values of velocity, temperature, pressure, and either area ratio A_{ce}/A_{ci} by the polytropic exponent n_c or the polytropic exponent n_c by a chosen area ratio A_{ce}/A_{ci} and the specific work-input W^*_c of a value limited by permissible weight and length.

If, however, as was done for the "perfect" jet engine, the compression ratio q^* is prescribed, then all four variables φ_{ce}, τ_{ce}, A_{ce}, and n_c are expressed in terms of A_{ci}.

(3) *The Heat Chamber.*—In the heat chamber no work is performed ($W^*_h = 0$), but the heat input $Q_h h^{-1} = Q^*_h$ may be diminished by insulation losses proportional to it of value $-\delta_h Q^*_h$ so that

$$c_{\lambda h} b_h (Q^*_h)_{\text{effect.}} = c_{\lambda h} b_h (1 - \delta_h) Q^*_h = Q^*_h \beta_h$$

where Q^*_h is the original heat input and

$$\beta_h = c_{\lambda h}(1 - \delta_h)$$

Furthermore

$$Q^*_{h\,\text{effect.}}(1 + c_{\lambda h} q_h) = Q^*_h (1 - \delta_h)(1 + c_{\lambda h} q_h) \equiv Q^*_h \gamma_h H\mu$$

where

$$\gamma_h = (1 - \delta_h + \beta_h)/H\mu$$

and

$$\alpha_h = (1 - a_h)/H\mu$$

The flow equations then become

$$\varphi_{he}^2 = \varphi_{hi}^2 a_h - Q^*_h \beta_h \tag{36}$$

$$\tau^* \equiv \tau_{he} = \tau_{hi} + \varphi_{hi}^2 \alpha_h + Q^*_h \gamma_h \tag{37}$$

$$\tau_{he}^{-\lambda_h} q_{he} = \tau_{hi}^{-\lambda_h} q_{hi} \quad \text{or} \quad \tau^{*-\lambda_h} q_{he} = \tau_{hi}^{-\lambda_h} q \tag{38}$$

$$q_{he}^{1/n_h} \varphi_{he} A_{he} = q_c^{\prime\,1/n_h} \varphi_{ce} A_{ce} = q^{*1/n_h} \varphi_{ci} A_{ce} \tag{39}$$

These equations again determine velocity, temperature, and pressure ratios and either polytropic exponent or area ratio in terms of the corresponding determined values of the preceding section. If, moreover, as for the "perfect" jet engine, the temperature ratio $\tau_{he} = \tau^*$ at the exit of the heat chamber is prescribed, all four variables have fixed values only depending on one of the areas. Eq. (37) analogously to Eq. (15b) determines again the heat input in terms of compression ratio and turbine temperature.

(4) *The Turbine.*—In the turbine no heat is added, but heat of amount proportional to work produced (W_t negative) expressed by $Q^*_t = W^*_t\delta_t$ may leave. If, then, for abbreviation one introduces

$$b_t(1 - c_{\lambda t}\delta_t) = \beta_t$$

and

$$(1 + \delta_t - \beta_t)/H\mu = \gamma_t$$

$$\alpha_t = (1 - a_t)/H\mu$$

the flow equations assume the form:

$$\varphi_{te}^2 = \varphi_{he}^2 a_t + W^*_t\beta_t \tag{40}$$

$$\tau_{te} = \tau_{he} + \varphi_{he}^2\alpha_t + W^*_t\gamma_t \tag{41}$$

$$q_{te}\tau_{te}^{-\lambda_t} = q_{he}\tau_{he}^{-\lambda_t} \tag{42}$$

$$q_{te}^{1/n_t}\varphi_{te}A_{te} = q_{he}^{1/n_t}\varphi_{he}A_{he} \tag{43}$$

One has again five new quantities [i.e., φ_{te}, τ_{te}, q_{te}, A_{te} or $\lambda_t = n_t/(n_t - 1)$, and W^*_t] but only four equations. However, there is one more relation between the specific work input W^*_c of the compressor and the work output W^*_t of the turbine—namely,

$$W^*_t = -W^*_c\,\epsilon \tag{44}$$

where $\epsilon > 1$ expresses the additional work of the turbine to be performed for accessory motors or generators, for the covering of friction losses in bearings and gears, and, eventually, for a screw propeller.

With this relation the turbine variables are all expressed in terms of the corresponding values of the preceding (heat chamber) section and of the specific compressor work.

(5) *The Nozzle.*—In this section neither work nor heat is put in. Only a heat loss may appear, which here may be assumed proportional to the exit temperature-ratio τ_{te} of the turbine expressed by

$$Q^*_n = -\tau_{te}\delta_n$$

The flow equations are now

$$\varphi_{ne}^2 \equiv \varphi_e^2 = \varphi_{te}^2 a_n + \tau_{te}\delta_n c_{\lambda n} b_n \tag{45}$$

$$\tau_{ne} \equiv \tau_e = \tau_{te} + \varphi_{te}^2\alpha_n - \tau_{te}\gamma_n \tag{46}$$

where $\gamma_n = \delta_n(1 + b_n c_{\lambda n})/H\mu$ and $\alpha_n = (1 - a_n)/H\mu_n$.

$$\tau_e^{-\lambda_n} q_e = \tau_{te}^{-\lambda_n} q_{te} \tag{47}$$

$$q_e^{1/n_h}\varphi_e A_e = q_{te}^{1/n_h}\varphi_{te}A_{te} \tag{48}$$

One has again here the five unknown quantities φ_e, τ_e, q_e, $\lambda_n = n_n/(n_n - 1)$, and A_e and only four equations to determine them.

However, as in the analysis of the "perfect" jet engine, an additional relation between q_e and τ_e must be prescribed. This must be done either by a maximum condition for the thrust at prescribed total heat input or by the condition of the exit pressure equal to the undisturbed atmospheric pressure—that is, by the condition $q_e = 1$.

If this is done, then all state variables (velocity, temperature, pressure, and area ratios and polytropic exponents) are expressed in terms of either the intake entrance A_∞ or the nozzle exit area A_e; the specific compressor work W^*_c; the specific heat input Q^*_h in the heat chamber; the compression ratio $q^* \equiv q_{ce}$; the turbine temperature ratio $\tau^* \equiv \tau_{te}$; also the data H, h, R, and γ and the section-wise loss coefficients a, b, δ, and ϵ; the gas constant, R; the adiabatic exponent $\gamma = c_p/c_v$; and the losses due to leakage and internal drag expressed by the coefficients β, δ, and γ_{tchtn}.

Acknowledgments

The analysis given above is based on the achievements of the pioneers (Campini, Whittle, and Junkers) in the field of turbojet propulsion and on the information available in the publications named in the Bibliography.

The author also takes pleasure in acknowledging the discussions, suggestions, and criticisms of the colleagues at the Polytechnic Institute of Brooklyn and of the staff of the National Advisory Committee for Aeronautics.

Bibliography

Whittle, Frank, *Systems of Jet Propulsion*, Automotive & Aviation Industry, January 15, 1944.

Smith, G. Geoffrey, *Gas Turbines and Jet Propulsion for Aircraft.*

Eksergian, R., *On the Reaction of Fluids and Fluid Jets*, Journal of the Franklin Institute, May, 1944, p. 385.

Sawyer, Tom, *The Modern Gas Turbine*, Prentice-Hall, Inc., 1945.

Flagle, C. O., and Godsey, F. W., *How the Gasturbine Flies*, July 7, 1945, p. 465.

Warner, D. F., and Auyer, E. L., *Gas Turbines for Aircraft*, Mechanical Engineering, November, 1945, p. 707.

Puffer, S. R., and Alford, J. S., *The Gas Turbine in Aviation*, Mechanical Engineering, December, 1945, p. 803.

Hawthorne, W. R., *Factors Affecting the Design of Jet-Turbines*, Preprint, S.A.E. Meeting, January, 1946.

Campbell, K., and Talbert, T. E., *Some Advantages and Limitations of Centrifugal and Axial Aircraft Compressors*, S.A.E. Journal, October, 1945.

Mayers, M. A., and Carter, W. W., *The Elbow Combustion Chamber*, Annual Meeting, A.S.M.E., November, 1945.

Mock, Fr. C., *Engineering Development of the Jet Engine and Gas Turbine Burner*, S.A.E. Meeting, January, 1946.

(*Continued on page 210*)

(*Continued from page 209*)

Sawyer, J. G., *Design and Application of High-Pressure Coefficient Axial-Flow Fans*, Journal of the Aeronautical Sciences, Vol. 12, No. 3, July, 1945, p. 281.

Jacob and Erk, V.D.I. Forschungsarbeiten, Vol. 267, 1914.

Stanton and Pannell, Phil. Transact., 1914, p. 199.

Moody, L. F., *Friction Factors for Pipe Flow*, Transactions, A.S.M.E., November, 1944, p. 671.

Keenan and Kaye, *Thermodynamic Properties of Air;* John Wiley & Sons, Inc., New York, 1945.

Services of the Libraries of the Institute of the Aeronautical Sciences

The services of the Libraries are available to all members of the Institute, to Corporate Members, to advertisers in the AERONAUTICAL ENGINEERING REVIEW and AERONAUTICAL ENGINEERING CATALOG, and, under usual library limitations, to the public. Four specialized services are available.

The Paul Kollsman Lending Library

This lending library service makes available, *without charge*, the latest and more important aeronautical books.

Members may request the loan of any aeronautical or technical book they wish to borrow. Through an exchange agreement with the Engineering Societies Library, any book on general engineering may be borrowed from its great collection of over 160,000 volumes.

A photostating service is available at usual library rates.

Applications for membership in the library and further information will be sent on request.

The W. A. M. Burden Reference Library

This reference library contains over 12,000 aeronautical books, magazines, pamphlets, and reports gathered from world-wide sources and is one of the most complete aeronautical libraries in the world. Material from this library is not available for loan but may be used for reference purposes.

The Pacific Aeronautical Library

6715 Hollywood Boulevard
Los Angeles 28, California

Established in cooperation with the aircraft companies the library serves. The leading aircraft companies in or near Los Angeles participate in its support and operation.

This service library for aeronautical research is available to the public for reading privileges. Source material includes aerodynamic and structural research reports, as well as books on drafting, production methods, history, and allied sciences. It furnishes books, periodicals, and pamphlet material to the participating aircraft companies to supplement their engineering libraries.

Technical Information Service

This service has experienced personnel under the supervision of trained aeronautical engineers to compile any information desired. The services range from listing specialized reference books to the preparation of exhaustive bibliographies, digesting of reports, and general surveys of any aeronautical subject. Some of the available services are:

Bibliographies on any aeronautical subject.
Reports on any aeronautical subject.
Digests of aeronautical books, papers, periodicals, and references.
Translations.
Engineering investigations of special aeronautical subjects.
Biographies of individuals engaged in aeronautics.
Photostats of any aeronautical or general engineering material.
Microfilms made on special order.
Photographs made from the Institute's photographic collection.
Drawings and tracings made.

In addition to the services mentioned any commission which comes within the scope of the Service will be accepted. Special arrangements may be made for work requiring several weeks or months.

Translators are available for accurate transcriptions of all foreign language data. Translations are carefully edited by trained engineers.

Reproductions of any material in the collections of the Institute may be ordered at standard photostat rates.

INSTITUTE OF THE AERONAUTICAL SCIENCES, INC.

2 EAST 64TH STREET, NEW YORK 21, N.Y.

Stresses in Cylindrical Semimonocoque Open Beams

HENRY L. LANGHAAR* AND CLARENCE R. SMITH†

Consolidated Vultee Aircraft Corporation

SUMMARY

The theory of open, symmetrical, semimonocoque beams of circular-cylindrical shape is developed by direct minimizing of the strain energy in a length of open beam whose ends are acted upon by specified resultant forces and moments. Simple explicit formulas are obtained for the stresses. The theory exhibits exponential stress gradients near the longerons—an effect that has not heretofore been incorporated in the analyses of open beams. This phenomenon may cause high axial stresses at the corners of a cutout in a cylindrical beam and high shearing stresses near the longerons. Experimental data are presented which tend to confirm these conclusions.

INTRODUCTION

THE THEORY of open semimonocoque beams is of interest to aircraft designers because it affords a basis for the stress analysis of structures such as the portion of a fuselage in the interval of a cargo door. The experimental data presented in conjunction with the following theory of open beams indicate that this theory is satisfactory for these applications, even though the cutout is short. The transition from the open-beam distribution to the closed-beam distribution has not been theoretically investigated in this study. However, the test data indicate that the transition length is fairly short, even if the beltframes are extremely flexible. This suggests that hoop stresses are active agents for effecting redistribution in the region beyond the cutout.

NOTATIONS

Consider a symmetrical open beam of circular cross section, as shown in Fig. 1. Let the x, y, z axes form a right-handed system (positive z-axis directed toward the reader). (Fig. 1.) Let the plane $z = 0$ lie at the mid-section of the open beam. Let the beam be subjected to a vertical shear V through the geometric axis of the cylinder and a torque M (Fig. 1). Let the resultant x- and z-components of the force and the resultant y-component of the bending moment be zero. Let the resultant forces, bending moment, and torque at any station z_1 be the resultants of the actions of the portion of the beam in the region $z > z_1$ upon the section at z_1. The x-component of the bending moment at station z_1 then has the value $(M_{x0} + Vz_1)$.

The following nomenclature is employed:

t = skin thickness (assumed to be constant)

t_e = equivalent thickness of the plate-stringer combination (assumed to be constant). The equivalent thickness may be defined by the formula $t_e = t + (A_s/b)$ in which A_s/b is the ratio of the cross-section area of a stringer to the stringer spacing

a = cross-section area of either bar (longeron) reinforcing the free edge (Fig. 1)

$2L$ = length of the open beam

r = radius of the cylinder

2β = central angle included by the cross section of the beam (Fig. 1)

θ = polar coordinate (Fig. 1)

N = axial load per unit length of the plate-stringer cross-sectional periphery (tension positive)

q = shear load per unit length of the plate-stringer cross-sectional periphery (positive counterclockwise, Fig. 1)

$\sigma = N/t_e$ = axial stress in the skin and stringers

$\tau = q/t$ = shearing stress in the skin

M_{x0} = bending moment about the x-axis at the station $z = 0$ (positive when it tends to rotate the section in the sense of a right-hand screw advancing along the x-axis)

V = shear load in the direction of the positive y-axis (Fig. 1)

M = torque with reference to the geometric axis of the beam (positive counterclockwise, Fig. 1)

N_0 = value of N at the station $z = 0$

T = tension in the lower longeron

ν = Poisson's ratio

E = Young's modulus

$G = 0.5E/(1 + \nu)$ = shear modulus

U = strain energy in the open beam

$\lambda = a/rt_e$ = a dimensionless parameter

$k^2 = 6r^2t_e(1 + \nu)/L^2t$ = a dimensionless parameter

$I_{xx} = r^3t_e(\beta - \sin\beta\cos\beta + 2\lambda\sin^2\beta)$ = moment of inertia of the beam cross section about the x-axis

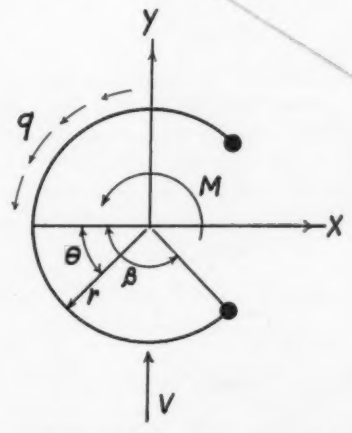

FIG. 1. Cross section of open beam showing nomenclature.

Received July 1, 1946. Revised and received November 4, 1946.

* Structural Engineer.

† Research Engineer.

Statical Conditions

It is assumed, as is usual in open-beam theory (see references 1 and 2) that hoop stresses in the skin are negligible. The differential conditions of equilibrium for a rectangular element then show that the shear q is independent of the axial coordinate z and that the axial force N is a linear function of z; specifically

$$N = (-zq'/r) + N_0 \tag{1}$$

in which the prime denotes a derivative with respect to the angular coordinate θ.

The differential condition of equilibrium for the lower longeron (Fig. 1) is $dT/dz = q$, in which T is the tension in the longeron and q is the shear in the adjacent skin. Also, continuity requires the relationship

$$\sigma = T/a = N/t_e \tag{2}$$

in which N is the axial load intensity in the plate-stringer combination adjacent to the longeron. Hence, by Eq. (1),

$$dT/dz = -aq'/rt_e = -\lambda q'$$

in which

$$\lambda = a/rt_e \tag{3}$$

Thus, the boundary condition at the lower longeron is

$$q + \lambda q' = 0 \tag{4}$$

The corresponding condition for the upper longeron is

$$q - \lambda q' = 0 \tag{4'}$$

In addition to the preceding differential conditions of statical equilibrium, there are six integral relationships of statics. The first three of these relationships pertain to the shears, and, since shear loads in the longerons may be assumed to be negligible, the equations do not involve the longeron forces. Hence, the equations are:

$$\begin{gathered} \int_{-\beta}^{\beta} q \cos\theta \, d\theta = -V/r \\ \int_{-\beta}^{\beta} q \sin\theta \, d\theta = 0 \\ \int_{-\beta}^{\beta} q \, d\theta = M/r^2 \end{gathered} \tag{5}$$

In setting up the equilibrium conditions for the axial forces, the tensions in the upper and lower longerons at the mid-section are respectively designated by $-T_0$ and T_0. This is in conformity with an anti-symmetry of the plate-stringer stresses which is subsequently confirmed. It follows:

$$\begin{gathered} \int_{-\beta}^{\beta} N_0 \, d\theta = 0 \\ 2(T_0/r)\sin\beta + \int_{-\beta}^{\beta} N_0 \sin\theta \, d\theta = -M_{x0}/r^2 \\ \int_{-\beta}^{\beta} N_0 \cos\theta \, d\theta = 0 \end{gathered} \tag{6}$$

Strain Energy in an Open Beam

The strain energy in the beam is represented by the equation

$$U = r\int_{-L}^{L} dz \int_{-\beta}^{\beta} \left(\frac{N^2}{2Et_e} + \frac{q^2}{2Gt}\right) d\theta + U_{\text{longerons}}$$

With Eq. (1), this may be expressed

$$U = \int_{-L}^{L} dz \int_{-\beta}^{\beta} \left[\left(-\frac{zq'}{r} + N_0\right)^2 + 2(1+\nu)(t_e q^2/t)\right] \times d\theta + K\,U_{\text{longerons}}$$

in which an irrelevant constant factor is discarded. This may be integrated with respect to z, and there results

$$U = \int_{-\beta}^{\beta} [(L^2 q'^2/3r^2) + N_0^2 + 2(1+\nu)(t_e q^2/t)]\, d\theta + KU_{\text{longerons}} \tag{7}$$

in which the factor $2L$ is discarded.

Minimizing of Strain Energy

If the strain-energy expression, Eq. (7) is minimized with respect to N_0, under the restrictions imposed by the auxiliary equations, Eq. (6), the elementary flexure formula results;* i.e., the axial stresses at the mid-section of the open beam (i.e., the section $z = 0$) are expressed by the ratio of the bending moment to the section modulus. This result may be expressed analytically as follows

$$N_0 = -(M_{x0} r t_e / I_{zz}) \sin\theta \tag{8}$$

It is convenient to introduce a constant ψ, defined by the equation

$$\psi = M_{x0}/[r^2(\beta - \sin\beta\cos\beta + 2\lambda\sin^2\beta)] \tag{9}$$

Then

$$N_0 = -\psi \sin\theta \tag{10}$$

To minimize the strain energy with respect to q, an undetermined linear combination of the integrals of Eq. (5) is added to the strain-energy expression, Eq. (7). This is a common adaptation of Lagrange's method[3] of undetermined multipliers for the treatment of variational problems of this type. The modified strain-energy expression is

$$\bar{U} = \int_{-\beta}^{\beta} [(L^2 q'^2/3r^2) + 2(1+\nu)(t_e q^2/t) + \phi_1 q\cos\theta + \phi_2 q \sin\theta + \phi_3 q + N_0^2] d\theta + KU_{\text{longerons}} \tag{11}$$

in which ϕ_1, ϕ_2, ϕ_3 are constants.

The minimizing of $\bar{U}$ is a variable end-point problem in the calculus of variations. According to Eqs. (4) and (4'), variations of q are restricted by the end conditions.

$$\delta q|^{\beta} + \lambda \delta q'|^{\beta} = \delta q|^{-\beta} - \lambda \delta q'|^{-\beta} = 0$$

However, it may be shown that these conditions are necessary for a relative minimum of $\bar{U}$ when q is freely varied. This result might have been anticipated; it merely verifies that Eqs. (4) and (4') could have

* See Appendix.

been derived as natural boundary conditions of the variational problem.

Irrespective of the end conditions, the Euler equation for q must be satisfied. This equation is

$$2L^2q''/3r^2 - 4(1 + \nu)(t_eq/t) - \phi_1 \cos\theta - \phi_2 \sin\theta - \phi_3 = 0 \quad (12)$$

Let

$$k^2 = 6r^2t_e[(1 + v)/L^2t] \quad (13)$$

Then, with a modification of the ϕ's, Eq. (12) may be expressed:

$$q'' - k^2q = \phi_1 \cos\theta + \phi_2 \sin\theta + \phi_3 \quad (14)$$

The general solution of Eq. (14) is

$$q = B_1 \cosh k\theta + B_2 \sinh k\theta + A_2 \cos\theta + A_3 + A_4 \sin\theta \quad (15)$$

in which the A's and B's are constants.

The second of Eqs. (5) is automatically satisfied if q is an even function of θ. Also, this condition satisfies the boundary condition for the upper longeron when Eq. (4) is satisfied. Therefore, a solution will be sought with the assumption that q is an even function. Then $B_2 = A_4 = 0$, and Eq. (15) reduces to

$$q = B_1 \cosh k\theta + A_2 \cos\theta + A_3 \quad (16)$$

The first and the third of Eqs. (5) then yield

$$\left.\begin{aligned} 2(1 + k^2)^{-1}(\sin\beta \cosh k\beta + k \cos\beta \sinh k\beta)B_1 + \\ (\beta + \sin\beta \cos\beta)A_2 + 2A_3 \sin\beta = -V/r \\ B_1k^{-1} \sinh k\beta + A_2 \sin\beta + A_3\beta = M/2r^2 \end{aligned}\right\} \quad (17)$$

The boundary condition Eq. (4) yields

$$\left.\begin{aligned} B_1(\cosh k\beta + \lambda k \sinh k\beta) + A_2(\cos\beta - \lambda \sin\beta) + \\ A_3 = 0 \end{aligned}\right. \quad (18)$$

Now $\sinh k\beta \approx \cosh k\beta \approx 0.5 \exp k\beta$. It is therefore convenient to introduce a new constant defined by $A_1 = 05B_1 \exp k\beta$. Then Eqs. (17) and (18) become

$$\left.\begin{aligned} 2(1 + k^2)^{-1}(\sin\beta + k \cos\beta)A_1 + (\beta + \\ \sin\beta \cos\beta)A_2 + 2A_3 \sin\beta = -V/r \\ A_1k^{-1} + A_2 \sin\beta + A_3\beta = M/2r^2 \\ A_1(1 + \lambda k) + A_2(\cos\beta\lambda \sin\beta) + A_3 = 0 \end{aligned}\right\} \quad (19)$$

The first term in Eq. (16) is negligible when θ is small. Hence, it is permissible to make the approximation

$$\cosh k\theta = 0.5 \exp k|\theta|$$

in which the symbol $|\theta|$ denotes the absolute value of θ. Then, Eq. (16) becomes

$$q = A_1e^{k(|\theta| - \beta)} + A_2 \cos\theta + A_3 \quad (20)$$

in which e is the base of natural logarithms. Hence, with the aid of Eqs. (1) and (10), the axial load N may be expressed by the equation

$$N = (\mp 1)kzr^{-1}A_1e^{k(|\theta| - \beta)} + (zr^{-1}A_2 - \psi) \sin\theta \quad (21)$$

in which the factor (∓ 1) is opposite to the sign of θ.

Eqs. (19), (20), and (21) are a solution of the problem. The A's are determined by the linear algebraic equations, Eq. (19). These constants are to be substituted in Eqs. (20) and (21), to furnish the shears and the

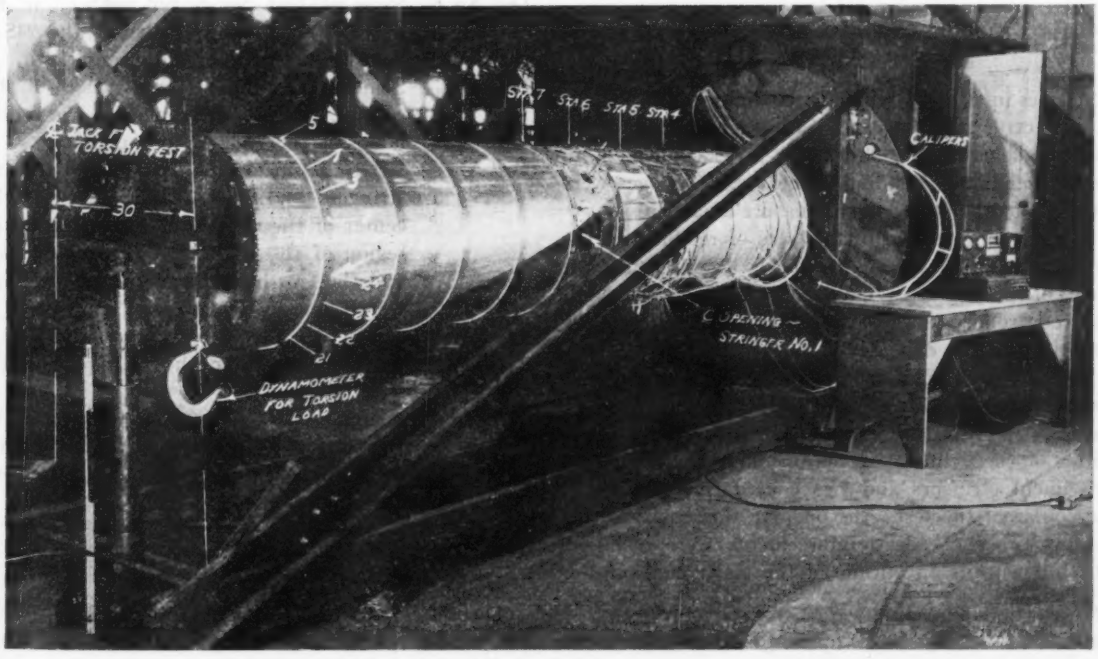

FIG. 2. Photograph of test setup.

axial loads. The stresses are determined by the equations $\tau = q/t$ and $\sigma = N/t_e$.

Test Specimen and Procedure

In order to test the foregoing theory, a 24S-T Alclad cylinder 30 in. in diameter and 168 in. long was constructed. The skin was 0.027 in. thick. The cylinder was reinforced by internal extruded angle-type stringers of cross-section area 0.087 sq.in. spaced at 15°, and external strap-type $^1/_4$ in. by $1^5/_8$ in. hoops spaced at 14 in.

The cylinder was set up as a cantilever beam. Shear loads were applied by means of a calibrated hydraulic ram. Fig. 2 shows the test setup for the cantilever tests. An adaptation for making torsion tests was also installed. This was accomplished by radially displacing the loading ram 15 in. and reacting the applied load by a symmetrically located turnbuckle in series with a spring dynamometer. (Fig. 2.) Thus, a couple with a 30-in. moment arm was applied to the cylinder. Fig. 3 is an elevation view of the cylinder showing station locations and the point of application of the shear load.

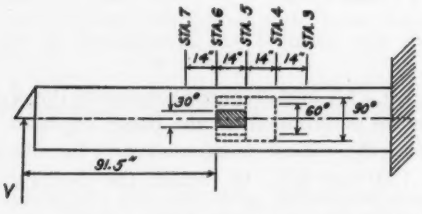

Fig. 3. Elevation drawing of cylinder, showing 30° by 14-in. opening. Dotted lines indicate subsequent enlargements of opening to 60° by 14-in., 90° by 14-in., and 90° by 28-in.

Stresses in the test cylinder were determined by 120-ohm electric strain gages. Strain gage rosettes on opposite sides of the skin were series-connected, in order to eliminate bending effects. Single gages were attached to the stringers to measure axial stresses.

A test run consisted of two sets of readings of the strain gages. These readings served to determine the slopes of the load-stress curves. In all cases, the loads were controlled so that the proportional limit of the material was not exceeded.

In the first test, the cylinder had no opening. This test served as a calibration of the strain gages. After the first test, a 30° by 14-in. opening was cut near the center of the cylinder. This opening was framed by two uncut stringers and two consecutive hoops. In the course of the tests, the opening was enlarged and various types of edge-reinforcements were installed. The following is an outline of the test conditions:

Test No. 1—No opening.

Test No. 2—30° by 14-in. opening bordered by uncut stringers and hoops.

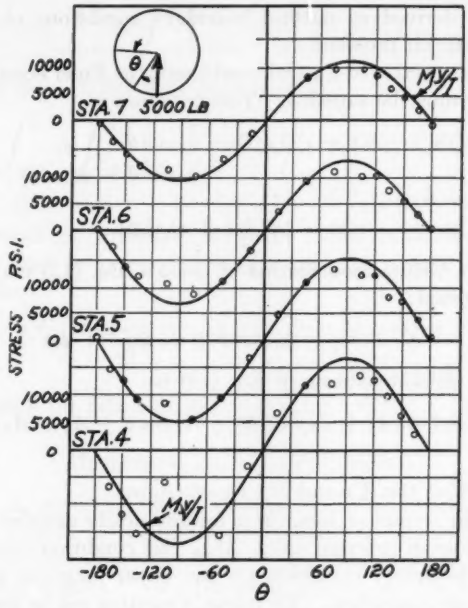

Fig. 4. Stringer stresses for Test No. 1 with cantilever loading. Curves are derived from the elementary beam formula, $\sigma = My/I$.

Test No. 3—60° by 14-in. opening bordered by uncut stringers and hoops.

Test No. 4—90° by 14-in. opening bordered by uncut stringers and hoops.

Test No. 5—Same as Test No. 4, but with $^1/_4$ in. by $^3/_4$ in. 24S-T edge-reinforcing strips (longerons) extending one bay beyond each end of the cutout.

Test No. 6—Same as Test No. 5, but with $^1/_4$ in. by $1^5/_8$ in. steel hoops replacing the 24S-T hoops at the ends of the opening.

Test No. 7—Same as Test No. 4, but with $^1/_4$ in. by $1^5/_8$ in. steel hoops replacing the 24S-T hoops at the ends of the opening.

Test No. 8—90° by 28-in. opening bordered by uncut stringers and hoops. The hoop at the center of the opening was cut out in the region of the opening. The center hoop and the two hoops bordering the opening were $^1/_4$ in. by $1^5/_8$ in. steel straps.

Test No. 9—Same as Test No. 8, but with 24S-T $^1/_4$ in. by $1^5/_8$ in. hoops replacing the steel hoops.

Test No. 10—Same as Test No. 9, but with $^1/_4$ in. by $^3/_4$ in. 24S-T edge-reinforcing strips (longerons) extending one bay beyond each end of the opening.

Discussion of Results

Theoretical stress curves, determined by Eqs. (19), (20), and (21) are shown in Figs. 4 to 17. Test points are plotted on these figures. Test points for the bays

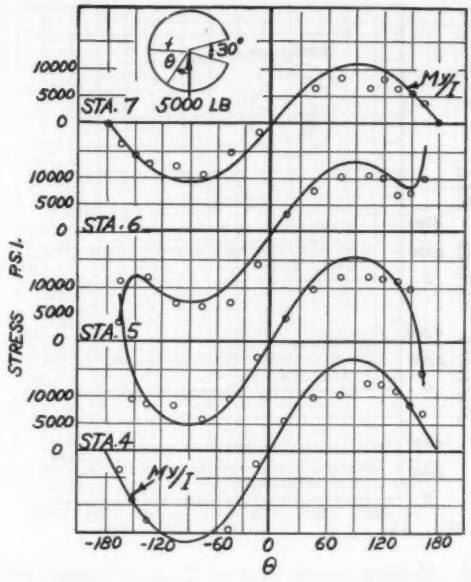

FIG. 5. Stringer stresses for Test No. 2 with cantilever loading. Curves for Stations 5 and 6 are derived from Eq. (21).

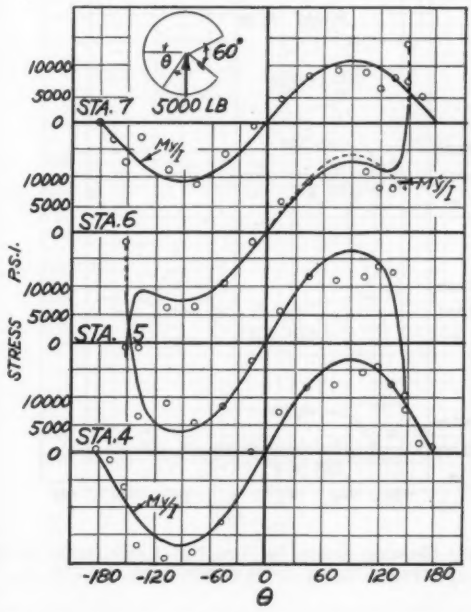

FIG. 6. Stringer stresses for Test No. 3 with cantilever loading. Curves for Stations 5 and 6 are derived from Eq. (21). For comparison, a curve derived from the formula $\sigma = My/I$ is also shown for Station 6.

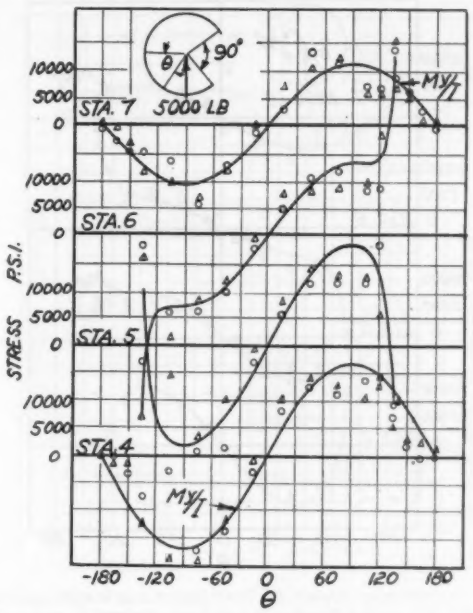

FIG. 7. Stringer stresses for Test Nos. 4 and 7 with cantilever loading. Curves for Stations 5 and 6 are derived from Eq. (21). Circles and triangles show data from Test Nos. 4 and 7, respectively.

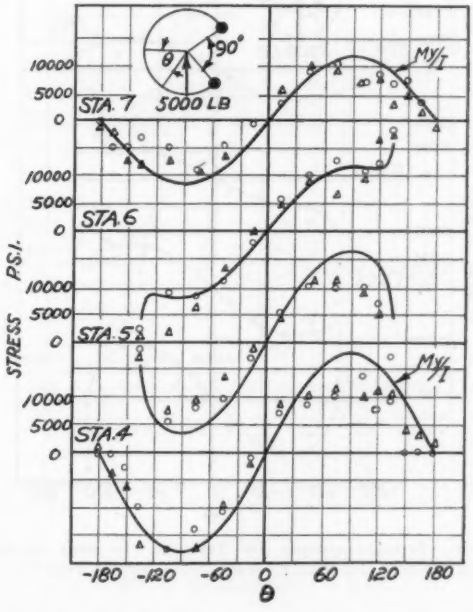

FIG. 8. Stringer stresses for Test Nos. 5 and 6 with cantilever loading. Curves for Stations 5 and 6 are derived from Eq. (21). Circles and triangles show data from Test Nos. 5 and 6, respectively.

beyond the cutout are also shown, and the theoretical stress curves for the closed beam with no opening are plotted for these bays in order to indicate the rate of transition to the undistorted stress pattern.

The test points exhibit considerable scatter. This may be partly attributable to incomplete elimination of local bending stresses. The fact that Fig. 4 shows two stringers that gave consistently low stresses at four stations indicates that these stringers were bowing under the application of the load, and that the bending stresses were detracting from the average stresses.

Despite the test scatter, the data show a marked trend to follow the theoretical curves. It is especially

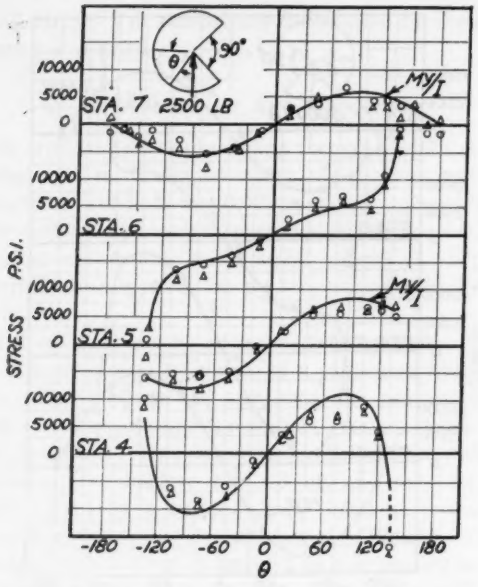

FIG. 9. Stringer stresses for Test Nos. 8 and 9 with cantilever loading. Curves for Stations 4 and 6 are derived from Eq. (21). Circles and triangles show data for Test Nos. 8 and 9, respectively.

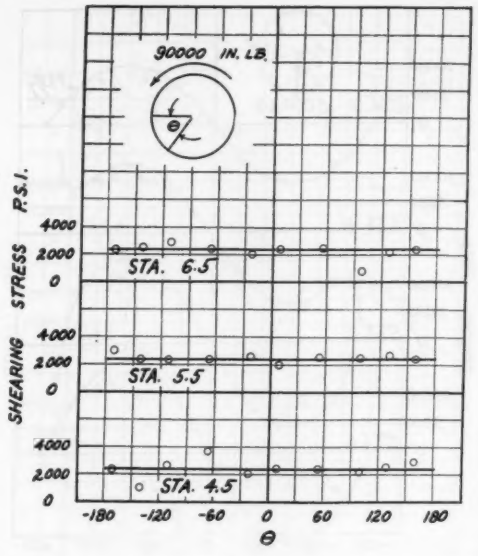

FIG. 11. Shearing stresses for Test No. 1 with torque loading. Curves are derived from the Prandtl torsion formula, $\tau = M/2At$.

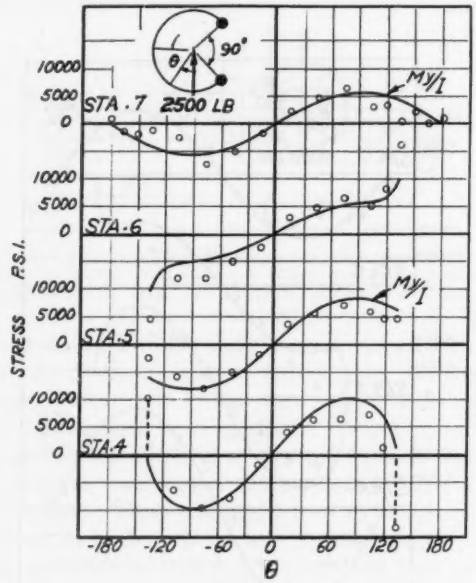

FIG. 10. Stringer stresses for Test No. 10 with cantilever loading. Curves for Stations 4 and 6 are derived from Eq. (21).

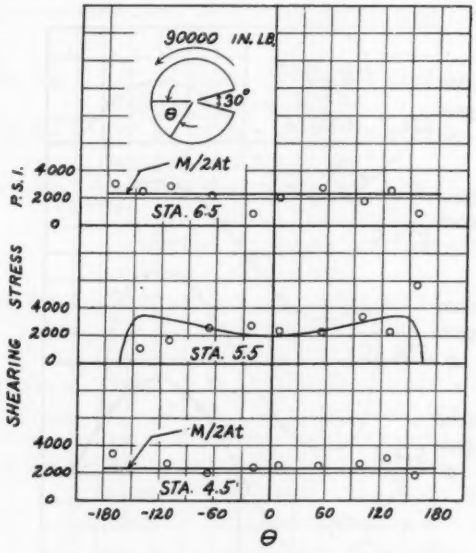

FIG. 12. Shearing stresses for Test No. 2 with torque loading. Curve for Station 5.5 is derived from Eq. (20).

noteworthy that the tests exhibit extremely high stringer stresses at the corners of the opening and high shearing stresses near the longitudinal edges of the opening. This is in agreement with the exponential stress gradients that the theory predicts.

Fig. 18 shows test points for a run in which the beam was subjected to a symmetrical cantilever load that produced equal tensions in the two stringers bordering the opening. The curves on this figure represent the theoretical stringer stresses as determined by the elementary flexure formula; i.e., the ratio of the bending moment to the section modulus. It is apparent that the stresses at stations numbers 4 and 7 are not fully developed in the sector of the opening. However, for calculating stringer stresses in the longitudinal interval of the opening, the elementary flexure formula appears to be adequate if the bending is symmetrical. This is an important result because stresses due to symmetrical bending must frequently be superposed on stresses due to antisymmetrical bending. Such is the case if a fuselage that sustains a vertical tail load

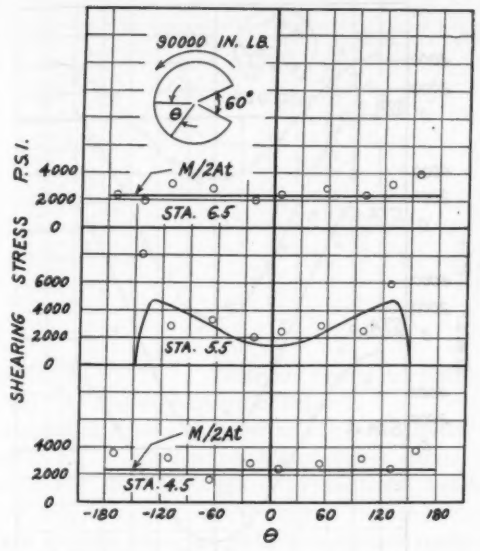

FIG. 13. Shearing stresses for Test No. 3 with torque loading. Curve for Station 5.5 is derived from Eq. (20).

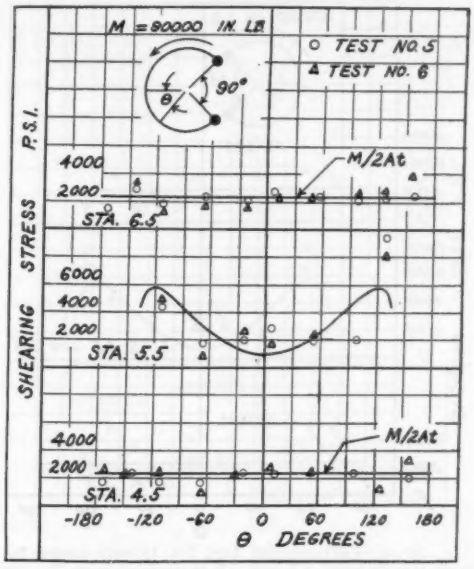

FIG. 15. Shearing stresses for Test Nos. 5 and 6 with torque loading. Curve for Station 5.5 is derived from Eq. (20).

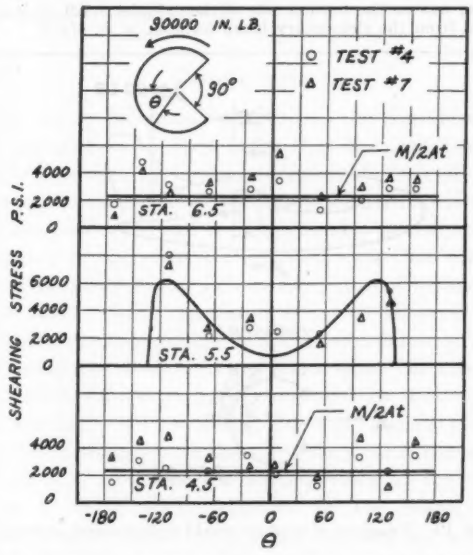

FIG. 14. Shearing stresses for Test Nos. 4 and 7 with torque loading. Curve for Station 5.5 is derived from Eq. (20).

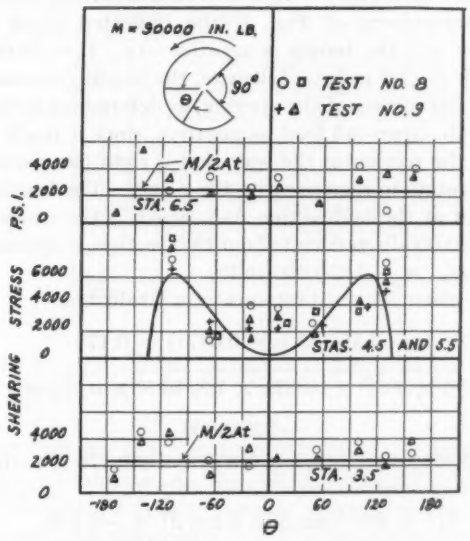

FIG. 16. Shearing stresses for Test Nos. 8 and 9 with torque loading. Curve for Stations 4.5 and 5.5 is derived from Eq. (20).

has a rectangular opening that is not centered on a horizontal or vertical radius of the cross section.

Example

To illustrate the application of the results of the foregoing investigation, a typical stress-analysis problem is presented. An airplane is subjected to a tail load which creates torsion and shear on cross sections in the region of a door in the port side of the fuselage (Fig. 19). The skin thickness is 0.025 in. The stringers are zee-sections having 0.0676-sq.in. cross-section area and spacing of 5.6 in. Hence:

$$t_e = 0.025 + (0.0676/5.6) = 0.0371 \text{ in.}$$

The opening includes an angle of 62°, and therefore $\beta = 149° = 2.60$ rad. The radius of the fuselage at the mid-section of the cutout is $r = 53.4$ in. The cross-section area of either longeron is $a = 0.35$ sq.in. The length of the opening is $2L = 33$ in.

As in Fig. 1, the positive x-direction is taken to be in the direction of the opening. The ordinate y and the angle θ must then be measured as shown in Section A-A, Fig. 19, in order to conform with Fig. 1. The agreement between these figures may be seen by the fact

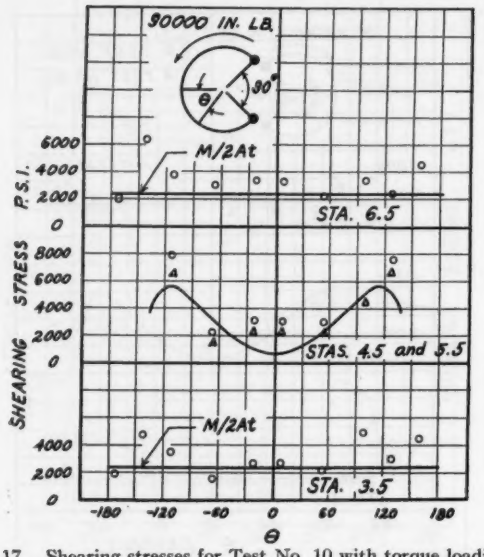

FIG. 17. Shearing stresses for Test No. 10 with torque loading. Curve for Stations 4.5 and 5.5 is derived from Eq. (20).

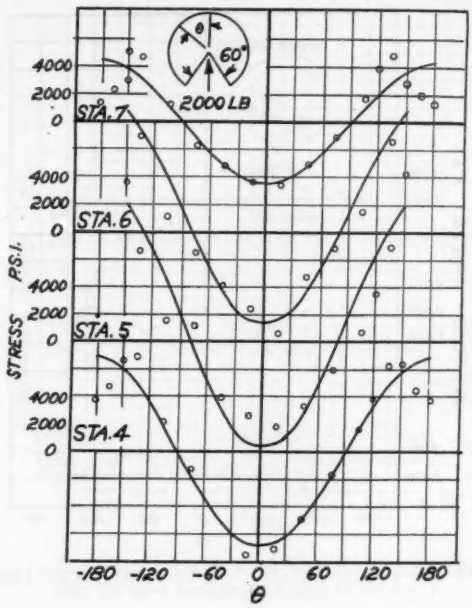

FIG. 18. Stringer stresses for cantilever test in which the opening was on the tension side of the cylinder. All curves are derived from the elementary beam formula, $\sigma = My/I$.

that Section A-A, Fig. 19, may be rotated into coincidence with Fig. 1. It is seen that according to the sign conventions of Fig. 1, the indicated shear is positive and the torque is negative—i.e., $V = 30{,}000$ lbs., $M = -10^6$ in.lbs. Likewise, the bending moment at the mid-section of the opening, as determined by the 30,000-lb. down-tail load, is negative, since it tends to rotate the section in the way that a right-hand screw would rotate in regressing on the x-axis. The bending moment at the mid-section A-A, which is the moment of the 30,000-lb. tail load about that section, is specified to be $M_{x_0} = -2{,}250{,}000$ in.lbs.

The essential constants are now evaluated.

$$\lambda = 0.35/(53.4 \times 0.0371) = 0.176$$

$$k = \sqrt{6 \times 53.4^2 \times 0.0371 \times 1.3/16.5^2 \times 0.025} = 11.0$$

$$\psi = \frac{-2{,}250{,}000}{53.4^2\,(2.60 + 0.515 \times 0.857 + 2 \times 0.176 \times 0.515^2)} = -252$$

$$2(1 + k^2)^{-1}(\sin\beta + k\cos\beta) = -0.146$$

$$\beta + \sin\beta\cos\beta = 2.16$$

$$2\sin\beta = 1.03, \quad 1/k = 0.091, \quad 1 + \lambda k = 2.94$$

$$\cos\beta - \lambda\sin\beta = -0.948$$

$$-V/r = -562, \quad M/2r^2 = -175.4.$$

With these numerical values, Eq. (19) becomes

$$-0.146A_1 + 2.16A_2 + 1.03A_3 = -562$$
$$0.091A_1 + 0.515A_2 + 2.60A_3 = -175.4$$
$$2.94A_1 - 0.948A_2 + A_3 = 0$$

The solutions of these equations are

$$A_1 = -79.0, \quad A_2 = -260, \quad A_3 = -13.4$$

Then, for $\theta > 0$, Eqs. (20) and (21) yield

$$q = -79e^{11(\theta - \beta)} - 260\cos\theta - 13.4$$
$$N = 16.26ze^{11(\theta - \beta)} + (-4.86z + 252)\sin\theta$$

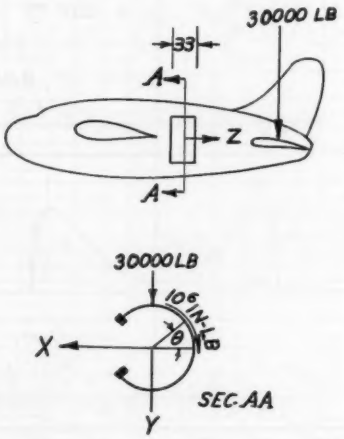

FIG. 19. Diagram of airplane used for illustrative example.

It follows

$$\tau = q/t = -3{,}160e^{11(\theta - \beta)} - 10{,}400\cos\theta - 540 \quad \text{(A)}$$
$$\sigma = N/t_s = 438ze^{11(\theta - \beta)} + (-131z + 6{,}800)\sin\theta \quad \text{(B)}$$

At the forward and aft ends of the cutout, z takes the respective values -16.5 in. and $+16.5$ in. Hence,

$$\sigma_{\text{aft}} = 7{,}240e^{11(\theta - \beta)} + 4{,}640\sin\theta \quad \text{(C)}$$
$$\sigma_{\text{fwd.}} = -7{,}240e^{11(\theta - \beta)} + 8{,}960\sin\theta$$

For negative values of θ, the signs of the first terms of Eq. (C) are reversed, as is indicated by the factor (∓ 1) in Eq. (21).

Stress curves may be plotted from Eqs. (A) and (C). Standard tables of the function e^{-x} determine values

TABLE 1

θ	$\beta - \theta$	$11(\theta - \beta)$ (Rad.)	$e^{11(\theta - \beta)}$	$-3{,}160e^{11(\theta - \beta)}$	$-10{,}400 \cos \theta$	τ (by Eq. (A))
0	149°	−28.6	0	0	−10,400	−10,940
15°	134°	−25.7	0	0	−10,040	−10,580
30°	119°	−22.8	0	0	−9,000	−9,540
45°	104°	−20.0	0	0	−7,360	−7,900
60°	89°	−17.1	0	0	−5,200	−5,740
75°	74°	−14.2	0	0	−2,700	−3,240
90°	59°	−11.3	0	0	0	−540
105°	44°	− 8.4	0	0	2,700	2,160
120°	29°	− 5.6	0.0037	−10	5,200	4,650
135°	14°	− 2.68	0.0684	−220	7,360	6,600
140°	9°	− 1.73	0.178	−560	7,960	6,860
145°	4°	− 0.77	0.463	−1,460	8,520	6,520
149°	0	0	1.000	−3,160	8,900	5,200

of the factor $e^{11(\theta - \beta)}$. Tabular values are obtained from Eq. (A) and are shown in Table 1.

The axial stresses σ may be similarly tabulated by means of Eq. (C). The calculated stress curves are shown in Fig. 20. Although a symmetrical bending moment due to a load on the fin and rudder was not included in this example, such a condition could be incorporated in the calculations by superposing an ordinary flexural stress distribution (ratio of bending moment to section modulus) on the stringer stresses that are plotted in Fig. 20.

CONCLUSIONS

The theory has been restricted to the consideration of a segment of an open beam that is in equilibrium under the action of forces and moments that are applied at the ends. The traction on either end is such that the resultant force is perpendicular to the axis of symmetry of the cross section, and such that the resultant moment vector lies in the plane of symmetry of the beam. With the assumption that hoop stresses in the skin are negligible, it has then been demonstrated that minimum strain energy results when the stresses throughout the beam are determined by Eqs. (19), (20), and (21). In particular, Eqs. (20) and (21) show that the shearing stress does not vary with the axial coordinate z, and that the axial stresses at the mid-section ($z = 0$) are determined by the elementary flexure formula (ratio of bending moment to section modulus).

Tests that were conducted for the purpose of estimating the applicability of these results to the stress analyses of cylinders with cutouts have furnished the following conclusions:

(1) In the cutout interval the shearing stress does not vary appreciably with the axial coordinate z. (See Figs. 16 and 17.)

(2) Pure torsion creates no axial stress at the mid-section of the cutout interval.

(3) In the case of lateral bending which produces a symmetrical axial-stress distribution about the x-axis, the elementary flexure formula (ratio of bending moment to section modulus) applies accurately for the cutout interval. (See Fig. 18.)

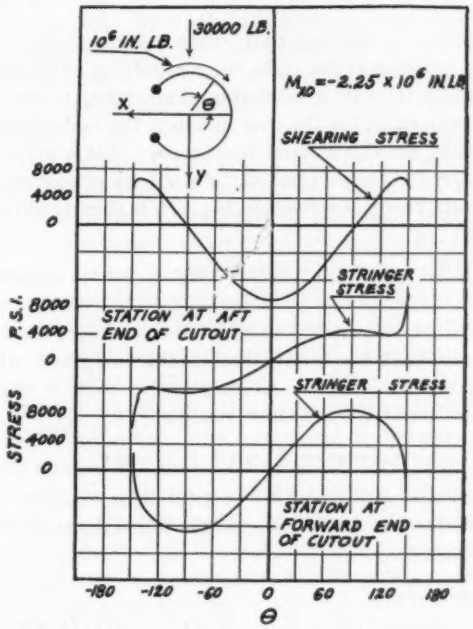

FIG. 20. Stress curves for portion of fuselage in interval of the cargo door (see Fig. 19). Curves are derived from Eqs. (20) and (21).

(4) In the case of bending which produces an antisymmetrical stress distribution about the x-axis, the elementary flexure formula determines the axial stresses at the mid-section ($z = 0$) of the cutout interval. (See Figs. 9 and 10.)

(5) In the case of bending which produces an antisymmetrical stress distribution about the x-axis, the stresses in the region opposite to the cutout are determined accurately by the elementary flexure formula. However, this formula is inapplicable for large values of the angular coordinate θ; i.e., for values of $|\theta|$ approaching β. (See Fig. 6.)

(6) When the beam cross section is symmetrical about the x-axis, the axial stresses and the shearing stresses due to combined torsion and antisymmetrical shear and bending are respectively odd and even functions of the angular coordinate θ.

(7) The stress distribution varies rapidly in the cutout interval as the longerons are approached. High axial stresses usually occur at the longerons near the corners of the opening. (See Figs. 5 to 17.)

(8) Eqs. (20) and (21) are fairly accurate for determining the stresses in the cutout interval of a symmetrical cylindrical beam of constant skin thickness and constant equivalent plate-stringer thickness. (See Figs. 5 to 17.) Although the case of variable thickness was not investigated, a reasonable approximation procedure is to calculate N and q with average thicknesses. The stresses may then be calculated by the formulas $\sigma = N/t_e$ and $\tau = q/t$, in which t and t_e are local values of the skin thickness and the equivalent thickness.

(9) Some persistence of the stress distribution in the region of the opening is observed in the bays adjacent to the opening. (See Figs. 5 to 18.) However, the data indicate that the transition to the undistorted stress pattern is fairly rapid, and therefore hoop stresses must be significant in the bays beyond the cutout.

Appendix

It has been remarked that, when a segment of an open cylindrical beam is loaded by self-equilibrating forces that are applied at the ends, the minimizing of the strain energy furnishes the result that the axial stresses at the mid-section ($z = 0$) are distributed according to the elementary flexure formula. This appendix supplies a proof of this statement for the case in which the beam loading is antisymmetrical. The case of symmetrical loading is covered by the elementary beam theory that is given in texts on mechanics of materials.

In order to take account of the auxiliary conditions, Eq. (6), the Lagrange multiplier method is again employed. The strain energy expression, Eq. (7), is then modified by the addition of a linear combination of the integrals of Eq. (6); i.e.,

$$\bar{U} = \int_{-\beta}^{\beta} [(L^2q'^2/3r^2)N_0^2 + 2(1+\nu)(t_eq^2/t) + \phi_1 N_0 + \phi_2 N_0 \sin\theta + \phi_3 N_0 \cos\theta]d\theta + KU_{\text{longerons}}$$

The Euler equation, in this case, reduces to the statement that the derivative of the integrand with respect to N_0 is zero. Consequently, with a slight modification of the ϕ's there results

$$N_0 = \phi_1 + \phi_2 \sin\theta + \phi_3 \cos\theta \qquad (A)$$

When this expression is substituted in Eq. (6), the integrals may be evaluated, and the following equations are obtained:

$$\phi_1\beta + \phi_3 \sin\beta = 0$$
$$\phi_2\beta - \phi_2 \sin\beta\cos\beta = (-M_{x0}/r^2) - 2(T_0/r)\sin\beta$$
$$2\phi_1 \sin\beta + \phi_3\beta + \phi_3 \sin\beta\cos\beta = 0$$

It follows

$$\phi_1 = \phi_3 = 0$$
$$\phi_2 = \frac{-M_{x0} - 2rT_0 \sin\beta}{r^2(\beta - \sin\beta\cos\beta)}$$

Consequently, Eq. (A) yields

$$N_0 = -\frac{(M_{x0} + 2rT_0\sin\beta)\sin\theta}{r^2(\beta - \sin\beta\cos\beta)} \qquad (B)$$

Now, by Eq. (2),

$$T_0 = \lambda r N_0|^{\beta} \qquad (C)$$

Consequently, Eq. (B) yields

$$T_0 = -\frac{\lambda(M_{x0} + 2rT_0\sin\beta)\sin\beta}{r(\beta - \sin\beta\cos\beta)}$$

Solving for T_0 gives

$$T_0 = \frac{-\lambda M_{x0}\sin\beta}{r(\beta - \sin\beta\cos\beta + 2\lambda\sin^2\beta)}$$

Hence, by Eq. (C)

$$N_0|^{\beta} = \frac{-M_{x0}\sin\beta}{r^2(\beta - \sin\beta\cos\beta + 2\lambda\sin^2\beta)} \qquad (D)$$

Now, by Eq. (B), the value of N_0 is proportional to $\sin\theta$; i.e., the following proportion exists:

$$N_0 : \sin\theta = N_0|^{\beta} : \sin\beta$$

Therefore, Eq. (D) yields

$$N_0 = \frac{-M_{x0}\sin\theta}{r^2(\beta - \sin\beta\cos\beta + 2\lambda\sin^2\beta)} \qquad (E)$$

This is identical to Eqs. (9) and (10), which are a mathematical expression of the ratio of the bending moment to the section modulus.

Acknowledgment

This study was performed as part of a structural research program of the Consolidated Vultee Aircraft Corporation. The authors are indebted to the Consolidated Vultee Corporation for permitting the publication of this material. They particularly express their appreciation to Roy A. Miller, who initiated and directed the study.

References

[1] Beskin, L., *Stress Analysis of Open Cylindrical Membranes*, Journal of the Aeronautical Sciences, Vol. 11, No. 4, p. 343, October, 1944.

[2] Spaulding, I. E., *Torsion Analysis of Open Shell Structures*, Product Engineering, Vol. 13, No. 12, p. 718, December, 1942.

[3] Courant, R., and Hilbert, D., *Methoden der Mathematischen Physik*, Vol. 1, p. 104; Interscience Publishers, New York, 1931. Part 1, Isoperimetrische Probleme.

The Use of Damping Screens for the Reduction of Wind-Tunnel Turbulence

HUGH L. DRYDEN* AND G. B. SCHUBAUER†

National Bureau of Standards

SUMMARY

The effect of a damping screen in reducing the turbulence of an air stream is found to depend on the pressure-drop coefficient, k, of the screen. According to a plausible theory, which has been experimentally confirmed, the intensity of the turbulence is reduced in the ratio $1/\sqrt{1+k}$ by a single screen and in the ratio $1/(1+k)^{n/2}$ by n identical screens in series. These relations show that for the same power expenditure a greater turbulence reduction can be obtained with a number of screens of small k than with a single screen of coefficient nk. Factors that place a lower limit on velocity fluctuations are turbulence produced by the screens themselves and tunnel noise.

INTRODUCTION

IN ORDER THAT THE AIR STREAM in a wind tunnel may act on a body in the same way that it would if the body were moved through still air, it is necessary that the stream be uniform and steady in speed and direction. This ideal can never be perfectly attained. There are always present small eddies of varying size and intensity which are collectively described as the turbulence of the air stream. These eddies arise from the wind-tunnel fan, from the guide vanes at the corners and from the wind-tunnel walls upstream from the working section. In a satisfactory wind tunnel the turbulence conditions at any location are statistically constant, and it is possible to define the state of the turbulence in quantitative terms. The average intensity of the small eddies can be stated in terms of the root-mean-square values of the components of the velocity fluctuation. An average size of the eddies can be determined from measurements of the correlation of the velocities at neighboring points as a function of their distance apart.

Even though the turbulent fluctuations amount to less than 1 per cent of the mean speed, many aerodynamic measurements are greatly dependent on the exact values of the intensity and scale of the turbulence present. In free flight it has been found that there are no disturbances of sufficiently small scale to produce appreciable aerodynamic effects—i.e., the turbulence of the atmosphere may be regarded as zero. Hence, the designers of wind tunnels strive to reduce the intensity of the turbulence in wind tunnels as much as possible.

The design and construction of wind tunnels of low turbulence is a comparatively modern development for two reasons. First, the effect of increased turbulence in many aerodynamic measurements is qualitatively the same as an increase of Reynolds Number (i.e., in size of model or air speed). For a time, an increased turbulence was considered desirable as giving an increased "effective" Reynolds Number. Second, until recently no effective method was known of reducing the wind-tunnel turbulence to the point where there was no perceptible effect of turbulence on the measurements. About 10 years ago the intensity of the turbulence in the average wind tunnel was in the range 0.5 to 1.0 per cent of the mean speed. Today, there are several wind tunnels in which the intensity is of the order of 0.02 to 0.05 per cent.

During the period about 15 years ago, when increased turbulence was considered to be possibly advantageous, screens of coarse mesh were used for increasing the turbulence of the air stream. It may seem paradoxical to the uninitiated that now screens are used for decreasing the turbulence. At this point an analogy may be helpful, for the "smoothing" of an air stream has some features in common with the "smoothing" of a metal surface. Thus, to smooth a metal casting the machinist may begin with coarse file or rasp that takes out the gross irregularities and introduces a new roughness of finer scale. This process is repeated with finer files, coarse and fine emery cloth, etc., until the desired smoothness is obtained. In somewhat similar fashion a screen "smooths" an air stream to the extent of decreasing turbulent motions of larger scale than the mesh size while at the same time introducing turbulent motions of smaller scale. Fortunately, the small-scale turbulence decays much more rapidly than the large-scale turbulence, and, hence, at some distance from the screen the overall effect is a smoothing of the airflow in which both the intensity and the scale of the turbulence are reduced. Damping screens differ from turbulence-producing screens by being of finer mesh and by being located in the large cross section ahead of the entrance cone at a great distance from the working section rather than in the working section itself.

In the course of the investigations of turbulence and boundary-layer flow, carried out at the National Bureau

Presented at the Aerodynamics Session, Fifteenth Annual Meeting, I.A.S., New York, January 28–30, 1947.

* Associate Director.

† Chief, Aerodynamics Section, Division of Mechanics and Sound.

of Standards in 1940 with the cooperation and financial assistance of the National Advisory Committee for Aeronautics, considerable information was obtained on the use of damping screens for the reduction of wind-tunnel turbulence. A theory to explain the action of damping screens was formulated, and theory and experimental results were summarized in an N.B.S. Report dated August 1, 1940, to the N.A.C.A. Publication of the results has been delayed because of the need for wartime security; but even though the delay has been considerable, the work of 1940 is the only known systematic investigation of damping screens in which hot-wire measurements of turbulence were made. The results may therefore be of interest, since damping screens are widely used in wind tunnels of low turbulence.

The use of screens in wind tunnels to improve the flow dates from some of the earliest wind tunnels. Prandtl[1] called attention to the use of screens for improving the velocity distribution and gave a simple theory of the effect. The use of screens to reduce turbulence is, as already noted, of fairly recent origin. In 1934 a reduction in turbulence was noted behind a screen of 8 meshes per in. in the old N.B.S. 4½-ft. tunnel. In the N.A.C.A. smoke tunnel at Langley Field, cloth was used over the tunnel entrance to secure steady flow. Nevertheless, the possibilities of damping screens were not fully realized until 1938 when a 60-mesh screen was installed in the entrance cone of the old N.B.S. 4½-ft. tunnel and turbulence measurements made in the test section showed a reduction in turbulence from 0.54 to 0.19 per cent.

Various theories of the effect of screens have been proposed in addition to Prandtl's, among which are Collar's[2] regarding the effect of a screen on the velocity distribution and Batchelor's[3] regarding the effect of screens on both velocity distribution and turbulence. The relatively simple theory given herein is the only known one that agrees even approximately with the observed effect of screens on turbulence. Although the experiments antedated the successful theory, the theory is discussed first.

Symbols

A = cross-sectional area of wind stream, or duct
U = mean speed at any point
p = mean static pressure at any point
u = component of velocity fluctuations produced by turbulence, parallel to mean flow, measured with respect to mean speed
v, w = mutually perpendicular components of velocity fluctuations produced by turbulence, normal to mean flow
u', v', w' = root-mean-square values of u, v, w
U' = mean turbulence intensity defined by $U' = \sqrt{\frac{1}{3}(u'^2 + v'^2 + w'^2)}$
ρ = density of the air
E' = kinetic energy of turbulence $= \frac{1}{2}\rho(u'^2 + v'^2 + w'^2) = \frac{3}{2}\rho U'^2$
k = pressure-drop coefficient of a screen
n = number of screens
d = wire diameter of a damping screen or rod diameter of a turbulence-producing grid
L = scale of turbulence
x = distance downstream from a screen
t = time for a particle to travel from a screen to some point x
C = contraction ratio of a wind tunnel, A_s/A_t (see subscripts)

Subscripts

t = test section of a wind tunnel
s = settling chamber of a wind tunnel
1, 2, 3 = sections upstream, at a screen, and downstream from a screen, respectively, in a duct of constant cross section (see Fig. 1)
0 = conditions at a particular time—used in decay formulas

Theory of Effect of Screens on Turbulence

Consider a straight duct of constant cross section with a screen placed entirely across section 2 as shown in Fig. 1. Assume now that a turbulent air stream is flowing in the duct with constant mean speed U. One may regard the turbulence as motions of the air in all directions, with component velocities u, v, and w with respect to a coordinate system moving with the mean speed U. The mean kinetic energy per unit volume of the turbulence is then

$$E' = \tfrac{1}{2}\rho\,(\overline{u^2} + \overline{v^2} + \overline{w^2}) \qquad (1)$$

The energy per unit volume of the mean motion is

$$p + \tfrac{1}{2}\rho\,U^2$$

Let us consider for the present that the screen is so fine that it may be regarded simply as a plane of uniformly distributed resistance across which some of the energy of the flow is converted into heat. It is assumed that the speed is well down in the subsonic region where temperature changes across the screen are so small that they have a negligible effect on the properties of the air. The problem now is to find the dissipation of energy per unit volume across the screen.

The resistance of a screen is proportional to the density of the air and the square of the speed. The resistance per unit area may be written $k(\frac{1}{2})\rho V^2$, where k is commonly called the pressure-drop coefficient and V is the speed close to the screen but not within the pores. It is important to bear in mind that V may be different from the speed at a great distance from the screen if changes occur in the cross section of the stream as a whole or in the cross section of any elementary stream tube. Since the mean speed U is uniform and the duct has constant cross section, U cannot change anywhere in the duct. Hence, the resistance per unit area of screen to the mean flow is

$$k(\tfrac{1}{2})\rho U^2$$

and this is also the energy loss per unit volume. Therefore, in the terminology of Fig. 1

$$k(\tfrac{1}{2})\rho U^2 = p_1 + \tfrac{1}{2}\rho U_1^2 - p_3 - \tfrac{1}{2}\rho U_3^2$$

and since $U_1 = U_3$

$$k^1/_2\rho U^2 = p_1 - p_3 \qquad (2)$$

Since the turbulent velocities are correlated only over a small portion of the duct area, it is not required that E' remain constant. In this case changes may occur in the cross section of the stream tubes with which E' is associated. We therefore write the mean resistance per unit area of screen to the turbulence as kE_2' assuming that the value of k is the same as for the mean flow.

Since this is also the energy loss per unit volume

$$kE_2' = E_1' - E_3' \qquad (3)$$

The absence of pressure terms in Eq. (3) is the result of the concept that the turbulence pattern is carried along with the mean flow but is not forced through a resistance by it. In other words, there is no transfer of energy to the turbulence from the mean flow.

It will now be assumed that the changes in E' occur on the approach side of the screen and that the E' at the screen is different from E_1'. Since all of the dissipation is assumed to take place in the plane of the resistance, no further reduction of energy will occur after the flow has passed the resistance. Therefore $E_2' = E_3'$ and Eq. (3) reduces to

$$E_3'/E_1' = 1/(1 + k) \qquad (4)$$

Eq. (4) expresses the reduction of turbulent energy by a screen of coefficient k. As mentioned previously, k is usually termed a pressure-drop coefficient because of its role in Eq. (2). Eq. (2) is in fact the relation used to determine k from the measured pressure drop $p_1 - p_3$ and the measured speed U.

By experiment the root-mean-square components of the turbulence u', v', and w' are determined separately, and E' is given by $^1/_2\,\rho$ times the sum of their squares. It is convenient, however, to use the sum of the squares to derive a mean turbulence intensity U', defined by

$$U' = \sqrt{^1/_3(u'^2 + v'^2 + w'^2)}$$

so that if the turbulence is isotropic $u' = v' = w' = U'$. The relative intensity is then expressed as U'/U, where U is any convenient reference speed.

It will be seen that Eq. (4) applies also to U'^2, and the fractional reduction in U' produced by a screen is

$$U_3'/U_1' = 1/\sqrt{1 + k} \qquad (5)$$

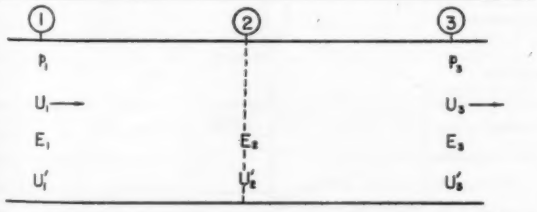

FIG. 1. Schematic diagram of a damping screen in a duct of constant cross section.

The simplifications and assumption involved in the foregoing development furnish ample grounds for questioning the validity of the answer. About all that can be said in defense of the methods is that the process can take place as assumed and that the assumption of different processes would generally lead to absurd results. For example, if E_2' is set equal to E_1' or to some value intermediate between E_1' and E_3', negative values are obtained for E_3'/E_1' for sufficiently large values of k.

The assumption that the energy lost at the screen goes directly into heat energy is known to be incorrect. The energy goes first into small jets through each pore, then into tiny eddies and heat, and finally into heat as the eddies decay. The eddies constitute high turbulence, and just back of a screen the turbulence may be extremely high, much higher in fact than it would generally be without a screen. However, if the screen is fine, the scale of the turbulence is small and the eddies decay rapidly.

A considerable amount of experimental and theoretical information exists[4] on the scale L and the intensity u' of the turbulence produced by square-mesh grids. The turbulence produced by grids is found to be isotropic, so that $u' = v' = w' = U'$. When lengths are expressed in terms of the rod diameter d of a grid, it is found that L/d and U'/U have approximately the same values for all grids at the same number of rod diameters downstream in a stream of constant mean speed. At 212.5 rod diameters, for example, L/d is about 1.5 and U'/U is about 0.02. This distance amounts to 1.5 in. for a screen with wires 0.0075 in. in diameter. It is only at distances of several feet that a net beneficial effect would be expected.

The experimental results for the decay of turbulence behind grids of wires 0.05 to 0.2 in. in diameter can be represented approximately by the relations

$$(U_0'/U')^2 = 1 + 0.58\,[U_0'(t - t_0)/L_0] \qquad (6)$$

$$(L/L_0)^2 = 1 + 0.58\,[U_0'(t - t_0)/L_0] \qquad (7)$$

where U_0' and L_0 are the values of the mean turbulent intensity and the scale at a time t_0 after a particle traveling with the mean motion passes the grid and where U' and L are the values at time t. It is not known how accurately these relations represent the decay behind screens of wire diameters 0.007 to 0.02 in. They probably give conservatively high values of U', for it is known that as the wire diameter decreases a Reynolds Number is eventually reached at which no eddies are shed from the wires. Thus a screen made up of sufficiently fine wires should create no turbulence of its own.

Returning to the consideration of Eq. (5), it may be noted that Prandtl,[1] in dealing with variations in mean speed over the cross section of a stream, obtained reductions in the differences from point to point in the ratio $1/(1 + k)$, which is the square of the value found for the reduction of turbulence. The difference in the

expressions arises from the fact that the average values of the velocity variations over a long time are zero for turbulence but not for differences of mean speed across the section.

The price paid for the reduction of turbulence by a damping screen is a loss of energy equal to the pressure drop $p_1 - p_3$ times the total volume of air moved through the screen. The pressure drop through a single screen is $k(1/2)\rho U_s^2$, where U_s is the speed at the screen. In a wind tunnel the speed at the screen can be diminished by locating the screen at the largest cross section of the entrance section. The speed can be reduced at will by increasing the contraction ratio; it is inversely proportional to the contraction ratio.

It is obviously advantageous to use a number of screens, say n, of coefficient k in series rather than a single screen of coefficient nk, both giving the same energy loss, since in the first case the reduction of turbulence is by a factor $1/(1+k)^{n/2}$ as compared with $1 \div (1+nk)^{1/2}$ in the second. Thus, if n is 5 and k is 2, the factor with five screens is 0.064 as compared to 0.301 for a single screen of the same total resistance.

The theoretical ratios of the turbulence behind the screens to that ahead of the screens for several values of n and k are given in Table 1.

It should be repeated that these relations take no account of turbulence set up by the screen itself, and they cannot be expected to hold unless the turbulence produced by the screen has decayed to insignificant proportions at the point where an observation is made. The lower limit of the turbulence level attainable by the use of damping screens is determined by the fineness and uniformity of the screen. Departures from theory are therefore to be expected when the turbulence is low and when large reductions are involved. There is also another factor affecting comparison with theory which becomes increasingly important as the turbulence is reduced—namely, the apparent turbulence due to sound in a wind tunnel.

TABLE 1

Theoretical Reduction of Turbulence by n Damping Screens of Pressure-Drop Coefficient k

n	$nk = 5$	$nk = 10$	$nk = 15$	$nk = 20$
	Ratio $= 1/(1+k)^{n/2}$			
1	0.400	0.301	0.250	0.218
2	0.286	0.167	0.118	0.091
3	0.230	0.111	0.068	0.047
4	0.197	0.082	0.044	0.0278
5	0.177	0.064	0.031	0.0178
6	0.162	0.052	0.0234	0.0123
10	0.132	0.031	0.0102	0.0041

EXPERIMENTAL RESULTS

The investigation was conducted in the rebuilt N.B.S. $4\frac{1}{2}$-foot wind tunnel shown in Fig. 2. The damping screens were installed in the settling chamber, not necessarily in the positions indicated in the figure, and turbulence measurements were made with the hot-wire turbulence-measuring equipment described in reference 5. Briefly, the method employs a single platinum wire 0.0002 in. in diameter about 0.2 in. long normal to the wind for the measurement of u' and a pair of such wires in the form of an X for the measurement of v' and w'. The plane of the X was horizontal for the measurement of the horizontal component v' and vertical for the measurement of the vertical component w'. Fluctuating voltages from the wires heated by a constant current were amplified and compensated for thermal lag, and the mean-square was then measured by a thermocouple-type milliammeter. Using calibration data for wires and amplifier, values of u', v', and w' were calculated. The bulk of the measurements were made at a single station in the test section about 6 ft. from the upstream end. Some measurements were also made in the settling chamber.

Data are available on four single screens, two screens in series, three screens in series, and six screens in series. Neither the position in the settling chamber nor the spacing between screens had a measurable effect on the results. The spacing was usually between 6 and 12 in., but to study the effect it was varied in one case from 2 to 28 in. The detailed results of the measurements in the test section are given in Table 2 and of the measurement in the settling chamber in Table 3. To facilitate com-

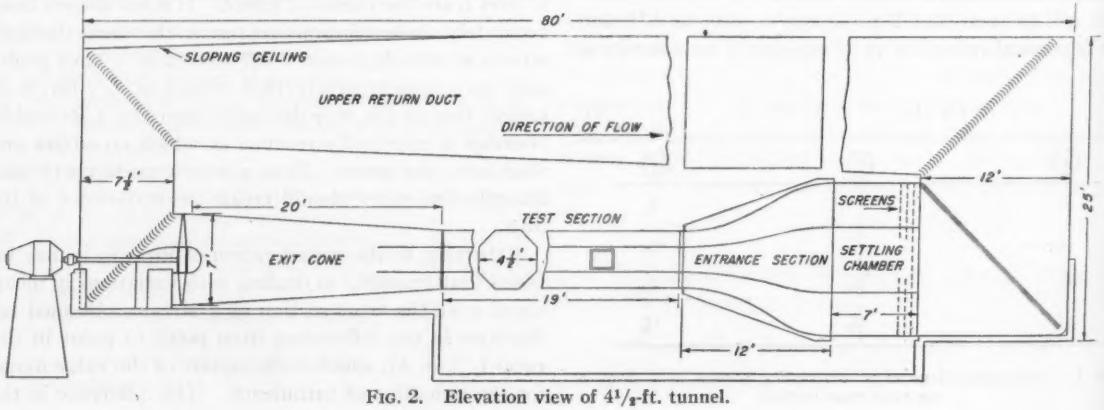

FIG. 2. Elevation view of $4\frac{1}{2}$-ft. tunnel.

TABLE 2

Turbulence of N.B.S. 4½-Ft. Wind Tunnel with Various Damping Screens
(Measurements at a Single Station in the Test Section)

I. No Damping Screens

U_t, Ft. per Sec.	$\frac{u'}{U_t}$, %	U_t, Ft. per Sec.	$\frac{v'}{U_t}$, %	U_t, Ft. per Sec.	$\frac{w'}{U_t}$, %
...	...	31.6	0.335	32.4	0.373
45.9	0.090	44.8	0.333	45.7	0.363
67.1	0.094	65.2	0.302	66.4	0.364
87.4	0.093	87.6	0.289	87.6	0.326
108.8	0.089	109.6	0.301	109.7	0.335
133.0	0.084	131.7	0.317	132.5	0.346

U_s, Ft. per Sec.	U_t, Ft. per Sec.	k	U_t, Ft. per Sec.	$\frac{u'}{U_t}$, %	U_t, Ft. per Sec.	$\frac{v'}{U_t}$, %	U_t, Ft. per Sec.	$\frac{w'}{U_t}$, %
			II. One 18-Mesh Screen, 0.011-In. Wire					
9.41	62.1	1.050	...	...	31.8	0.195	30.7	0.217
15.20	100.3	0.917	44.9	0.041	44.7	0.195	47.2	0.216
20.0	132.0	0.842	64.9	0.046	65.4	0.210	63.1	0.226
			87.0	0.048	88.5	0.201	88.3	0.208
			108.6	0.052	109.2	0.199	110.7	0.239
			136.1	0.054	136.5	0.198	132.8	0.235
			III. One 20-Mesh Screen, 0.017-In. Wire					
8.82	58.2	2.572	29.5	0.026	28.3	0.185	28.8	0.187
15.35	101.3	2.220	42.0	0.031	41.5	0.171	44.4	0.183
19.60	129.3	2.069	58.6	0.033	57.2	0.177	60.3	0.186
			81.6	0.039	83.0	0.162	80.8	0.185
			104.6	0.041	104.7	0.172	104.8	0.199
			127.0	0.051	127.0	0.163	125.7	0.199
			IV. One 24-Mesh Screen, 0.0075-In. Wire					
9.54	63.0	0.904	31.1	0.039	30.9	0.176	31.4	0.200
14.93	98.6	0.747	40.9	0.039	40.5	0.189	43.8	0.224
19.52	128.8	0.705	60.4	0.045	60.0	0.192	60.4	0.206
			83.4	0.047	84.0	0.194	83.6	0.219
			104.8	0.053	105.3	0.228	105.3	0.244
			130.5	0.058	131.1	0.245	132.8	0.259
			V. One 60-Mesh Screen, 0.007-In. Wire					
9.50	62.7	5.300	30.2	0.019	28.9	0.075	29.5	0.083
14.90	98.4	4.356	46.1	0.025	44.7	0.108	45.7	0.109
19.70	130.0	3.903	62.6	0.029	62.8	0.122	62.8	0.116
			88.4	0.033	89.0	0.134	88.0	0.129
			109.4	0.038	110.6	0.141	108.8	0.133

U_t, Ft. per Sec.	$\frac{u'}{U_t}$ %,	U_t, Ft. per Sec.	$\frac{v'}{U_t}$, %	U_t, Ft. per Sec.	$\frac{w'}{U_t}$, %
	VI. Two 18-Mesh Screens, 0.011-In. Wire. Spacing 6 In.				
30.7	0.022	28.9	0.117	30.3	0.125
46.8	0.026	45.1	0.125	46.2	0.130
63.2	0.031	61.4	0.136	63.2	0.147
86.4	0.034	87.1	0.144	86.6	0.155
108.6	0.041	109.0	0.166	110.0	0.155
		132.4	0.190	132.0	0.157
	VII. Three 18-Mesh Screens, 0.011-In. Wire. Spacing 6 In.				
30.0	0.016	30.4	0.071	28.1	0.077
42.3	0.020	45.0	0.092	43.5	0.087
62.4	0.026	61.1	0.112	61.0	0.099
87.6	0.032	87.2	0.111	87.8	0.118
108.2	0.037	109.1	0.114	109.7	0.123
131.2	0.043	129.3	0.119	130.0	0.121
VIII. Six Screens.	*(Three 20-Mesh, 0.017-In. Wire; Three 24-Mesh, 0.0075-In. Wire. Order of Screens, Upstream to Downstream, 20, 24, 24, 20, 20, 24. Spacing 4, 6, 8, 12, 23 In.)*				
28.8	0.019	27.5	0.009	28.5	0.011
41.7	0.021	40.4	0.020	41.9	0.020
60.2	0.027	60.6	0.026	61.6	0.021
84.0	0.034	84.5	0.037	86.2	0.036
107.4	0.039	108.1	0.044	109.2	0.045
123.1	0.046	124.0	0.047	124.0	0.048

parison with theory the results in the test section pertaining to a single speed (about 109 ft. per sec.) have been summarized in Table 4. The values shown in the seventh column of Table 4 agree with the predictions of the theory well within the precision of the experiments, except for the six-screen combination. It will be shown later that the lack of agreement for the six-screen combination may be attributed partly to incomplete decay of the turbulence produced by the last screen and partly to an effect of sound, discussed in the next section. It is known from a few traverses that there were small variations across most of the

TABLE 3
Turbulence in Settling Chamber of N.B.S. 4½-Ft. Wind Tunnel
(Measurements at a Single Station. Experimental Value of $U_t/U_s = 6.6$)

U_t, Ft. per Sec.	$\frac{u'}{U_s}$, %	$\frac{u'}{U_t}$, %	U_t, Ft. per Sec.	$\frac{v'}{U_s}$, %	$\frac{v'}{U_t}$, %	U_t, Ft. per Sec.	$\frac{w'}{U_s}$, %	$\frac{w'}{U_t}$, %
I. No Damping Screens								
33.0	1.51	0.229	31.9	1.57	0.238	33.4	1.67	0.253
44.6	1.69	0.256	45.5	1.58	0.239	45.5	1.62	0.245
62.3	1.69	0.256	66.8	1.47	0.223	64.6	1.58	0.239
84.1	1.94	0.294	86.6	1.49	0.226	85.8	1.52	0.230
105.0	1.97	0.299	107.2	1.51	0.229	107.2	1.56	0.236
127.9	2.31	0.350	131.3	1.47	0.223	131.3	1.65	0.250
II. Six Damping Screens. (Arrangement VIII in Table 2. Measurements 25½ In. from Downstream 24-Mesh Screen)								
28.9	0.051	0.008	29.1	0.036	0.005	29.3	0.037	0.006
39.1	0.090	0.014	39.7	0.040	0.006	39.7	0.041	0.006
58.2	0.139	0.021	58.2	0.126	0.019	58.2	0.130	0.020
81.1	0.148	0.022	80.0	0.131	0.020	79.7	0.180	0.027
103.7	0.175	0.027	104.0	0.146	0.022	104.0	0.222	0.034
119.3	0.207	0.031	118.7	0.144	0.022	118.4	0.247	0.037
			39.4	0.054	0.008			
			51.2	0.108	0.016			

TABLE 4
Comparison of Observed and Predicted Reduction of Turbulence by the Use of Damping Screens in N.B.S. 4½-Ft. Wind Tunnel

			U_t = 109 ft. per sec.				
						$\frac{U'}{U_t}$	
Screen	nk	$1/(1+k)^{n/2}$	$\frac{u'}{U_t}$, %	$\frac{v'}{U_t}$, %	$\frac{w'}{U_t}$, %	Observed, %	Predicted, %
None	...	...	0.089	0.301	0.335	0.265	...
18-mesh, 0.011-in. wire	0.895	0.726	0.052	0.199	0.239	0.182	0.192
20-mesh, 0.017-in. wire	2.18	0.561	0.041	0.163	0.199	0.150	0.149
24-mesh, 0.0075-in. wire	0.730	0.760	0.053	0.228	0.244	0.195	0.201
60-mesh, 0.007-in. wire	4.20	0.438	0.038	0.141	0.133	0.114	0.116
Two 18-mesh, 0.011-in. wire	1.790	0.527	0.041	0.166	0.155	0.133	0.140
Three 18-mesh, 0.011-in. wire	2.685	0.383	0.037	0.114	0.123	0.099	0.102
Six screens (three 20-mesh, 0.017-in. wire, three 24-mesh, 0.0075-in. wire)	8.7*	0.0776†	0.039	0.044	0.044	0.043	0.021

* $3k_{20} + 3k_{24}$, where k_{20} and k_{24} are the pressure-drop coefficients for the 20-mesh and the 24-mesh screens, respectively.
† $1/[(1+k_{20})^{3/2}(1+k_{24})^{3/2}]$.

test section with large increases in the wake of the seams of the screens. In a previous test with the same six screens, a 20-mesh screen with 0.017-in. diameter wires was tried as the final screen. There was considerable variation across the section in this case, which was taken to indicate that a measurable turbulence was produced by the final screen either because the mesh and wire size were too large or because the screen was not sufficiently uniform. It is well therefore to consider the decay of turbulence behind the last screen in greater detail.

As pointed out in the previous discussion, the decay formula, Eq. (6), probably predicts high values for the turbulence produced by grids of wires as small as those used in damping screens. Nevertheless, it is informative to calculate the decay by Eq. (6), using U_0' and L_0' for grids, and thus estimate the maximum turbulence produced by a damping screen. For grids the following values are assumed:

$$U_0' = 0.02^* U_s, \quad L_0 = 1.5d \text{ at } t_0 = 212.5/U_s$$

* For different grids U_0' at this location varied between 0.014 and 0.030 times U_s.

To obtain U' it is assumed that the acceleration of the stream through the contraction affects only the time for decay. The relative intensities may then be expressed in terms of the speed in the settling chamber U_s or the speed in the test section U_t. Taking t as the time of decay from a point 2 ft. upstream from the entrance section to a point 6 ft. into the test section, the relative intensities found for the several screens are shown in Table 5.

If the values in the last column of Table 5 are compared with those in the last column of Table 4, it is seen that the turbulence created by the last screen is considerably less than the turbulence passed by the

TABLE 5
Turbulence in Test Section Produced by Last Damping Screen as Computed from Eq. (6)

Screen		$\frac{U'}{U_s}$, %	$\frac{U'}{U_t}$, %
Meshes per in.	Wire diameter, in.		
18	0.011	0.228	0.035
20	0.017	0.282	0.043
24	0.0075	0.188	0.029
60	0.007	0.182	0.028

screen, except for the case of the six-screen combination. Here, the above value of U'/U_1 is comparable with the value actually measured. In the case of the six-screen combination, if the last 24-mesh screen produced 0.029 per cent and the predicted value of the turbulence passed by the screen were 0.021 per cent, the expected total intensity would be

$$\sqrt{(0.029)^2 + (0.021)^2} = 0.036\%$$

which stands in fair agreement with the 0.043 per cent observed.

The scanty observations made in the settling chamber demonstrate that Eq. (6) for the decay of turbulence does not apply too well to damping screens. Unfortunately, observations were not made of the scale of the turbulence in the settling chamber and in the test section for each combination. However, if the same assumptions are made as those used in computing Table 5, one finds that the turbulence produced by the 24-mesh screen at a distance of $25\frac{1}{2}$ in. is predicted to be 0.38 per cent as compared with observed values from 0.04 per cent at low speeds to 0.20 per cent at high speeds. The Reynolds Number of the screen wires ranges from about 35 to 140, which is in the range at which eddies first begin to form behind cylinders. The Reynolds Number of the turbulence itself is also low. At the highest speed the predicted turbulence passing through the screen is 0.20 per cent. It appears therefore that there is practically no turbulence produced by the damping screen itself in this case.

Effect of Sound

Assuming that the last screen of the six-screen combinations was producing a significant part of the turbulence measured, a seventh screen made of silk bolting cloth was installed as the final screen. Silk bolting cloth was used because it was finer than any wire screen commercially available. Some additional reduction was obtained, but the discrepancy between theory and experiment was even greater than before.

During the course of these experiments it was noted that the wave form of the velocity fluctuations did not have the randomness usually associated with turbulence. This led to the conclusion that something in the nature of a vibration was being picked up by the hot wire. Tests showed that vibration was not being transmitted to the wire itself, and the only other conceivable source was sound. Measurements with a sound meter connected to a crystal microphone showed the sound level to be between 105 and 110 db. at 100 ft. per sec, depending on where the microphone was placed. Since it was necessary to keep the microphone out of the wind, the sound level could not be measured at the position of the hot wire. Assuming plane waves, the root-mean-square particle velocity was calculated for 105 and 110 db. above a base level of 10^{-9} ergs per cm.^{3} per sec., giving the following results:

Db.	Particle Velocity, Ft. per Sec., or Apparent Percentage Turbulence Due to Sound at Wind Speed 100 Ft. per Sec.
105	0.028
110	0.051

The foregoing percentages are what might have been indicated by the hot wire because of sound alone; the actual value indicated, including sound and all components of real turbulence, was 0.043 per cent. Obviously, the sound measurements were not accurate enough to permit even an approximate correction for the sound. It is interesting to note, however, that the remaining discrepancy $[\sqrt{(0.043)^2 - (0.036)^2}]$ is 0.024, and this figure is of the same order as those estimated from sound measurements.

As a further test to determine whether particle velocity of sound was picked up by the hot wire, a frequency analysis was made of the output of the hot wire with the tunnel running at 80 ft. per sec. with the six-screen combination of Table 2—VIII and of the sound in the control room under the same conditions. The results are shown in Fig. 3. The similarity of the two curves leaves little doubt that a considerable part of the hot-wire output is derived from sound.

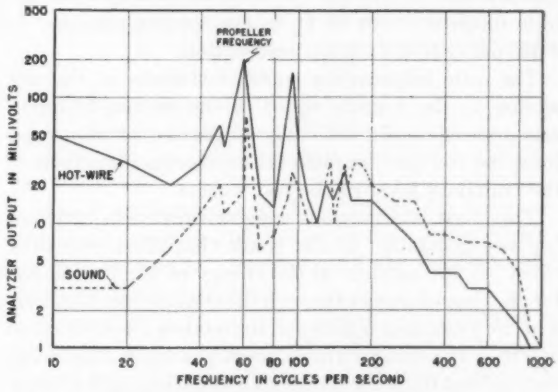

Fig. 3. Distribution with frequency of u-component of turbulence and sound. Wind speed—80 ft. per sec., u'/U_1 (total) = 0.033 per cent.

According to Batchelor,[6] noise in closed wind tunnels has many sources, two important ones being the propeller and the so-called drag noise produced by irregular eddy motion in the boundary layer at the tunnel walls. In the present tunnel propeller noise was evident in the measurements, and by ear the roar of the propeller seemed to be louder than all other sounds. In this tunnel therefore, the propeller is evidently the major source of sound, and being in the same arm as the test section, the sound is readily transmitted to the test section.

It should be pointed out that the screens are still partially responsible for the lower limit placed by sound.

In the present arrangement, for example, the propeller had to run faster and faster for a given wind speed in order to overcome the increasing pressure drop across the screens as more or denser screens were added. The net result was that the propeller noise increased with each addition of a screen.

Effect of Contraction

The application of the theory of the damping effect of screens located in the settling chamber to measurements made in the test section cannot be expected to be successful unless the effects of decay and contraction in the entrance cone are equivalent to multiplication by a constant factor. Measurements were made in the settling chamber for two conditions, first with no damping screens and again with the six-screen combination. Values of the turbulent fluctuations are given in Table 3, both as percentages of the local speed, U_s, and as percentages of the speed in the test section, U_t. At U_t equal to about 104 ft. per sec., for example, the average turbulence in the settling chamber at the point under consideration, without damping screens, is 0.257 per cent of U_t. That in the test chamber itself is 0.265 per cent of U_t, which is not significantly different from that in the settling chamber. With the six-screen combination the average turbulence appears to increase from 0.028 per cent of U_t in the settling chamber to 0.043 per cent of U_t in the test section.

The ratio between the speed of the core at the test section to the average speed in the settling chamber was approximately 6.6. The departure of this value from the contraction ratio 7.1 represents the effects of the boundary layer in the test section.

These few observations suggest caution in attributing any generality to the result that there was little effect of contraction on the energy of the turbulence, for the time of transit through the contraction is equivalent to a distance traveled at the settling chamber speed of 9 ft. The decay formula predicts a fairly large decay (ratio about 0.3 if the initial scale is 0.6 in.), and it therefore is obvious that the effect of the contraction is actually to increase the turbulent energy. In the case of the $4^1/_2$-ft. wind tunnel the effects happen to balance approximately.

With no screens present the contraction of the air stream does exert a selective effect on the three components u', v', and w', u' being reduced to about one-third of its initial value and v' and w' increased by about 40 per cent. Such selective effects of a contraction are discussed by Prandtl[1] and by Taylor.[7] Their theories neglect the decay of turbulence and are based on regular types of disturbances without statistical considerations. Prandtl predicts a decrease of u' in the ratio $1/C$ and an increase of v' and w' in the ratio $\sqrt{C}$, where C is the contraction ratio. This result corresponds to an increase of U' in the ratio $\sqrt{(2C/3) + (1/3C^2)}$, which equals 2.1 for a contraction ratio of 6.6. Taylor obtains a result dependent on the assumed form of the disturbance—in some cases a decrease in the turbulent energy, in others an increase. Neither theory is free from objection.

The principal advantage of a large contraction ratio has already been mentioned—namely, that of permitting the installation of damping screens without an excessive energy loss. Furthermore, if the turbulent energy remains constant or decreases, the ratio of the mean turbulent intensity U' to the mean speed decreases because of the increasing mean speed as the cross section contracts.

Conclusions

The experiments described in this paper show that damping screens materially reduce the turbulence of an air stream, and by their aid it is possible to obtain turbulence levels as low as 0.02 to 0.05 per cent. The action of the screens is interpreted in terms of a simple theory that assumes that the effect of a damping screen is partly to absorb the kinetic energy of the turbulence. The theory takes no account of any turbulence set up by the screen itself and therefore may predict values too low. This, of course, depends on the fineness and uniformity of the screen. The turbulence set up by the screens themselves may be the limiting factor in the attainment of low turbulence, but in the $4^1/_2$-ft. tunnel the principal limiting factor is probably the tunnel noise. While velocity fluctuations arising from a sound field should not be classed as turbulence, they, like turbulence, are generally an undesirable source of disturbance and should be reduced as much as possible.

The information available on the effect of a contraction on turbulence is not sufficient to permit the exact computation of the turbulence levels to be expected in wind tunnels of different contraction ratios.

References

[1] Prandtl, L., *Attaining a Steady Air Stream in Wind Tunnels*, N.A.C.A. T.M. No. 726, October, 1933.

[2] Collar, A. R., *The Effect of a Gauze on the Velocity Distribution in a Uniform Duct*, British A.R.C. Reports and Memoranda, No. 1867, February, 1939.

[3] Batchelor, G. K., *On the Hydrodynamic Resistance*, Australian Council for Scientific and Industrial Research, Division of Aeronautics, Report No. A. 27, October, 1944.

[4] Dryden, Hugh L., *A Review of the Statistical Theory of Turbulence*, Quarterly of Applied Mathematics, Vol. 1, No. 1, pp. 7–42, April, 1943.

[5] Schubauer, G. B., and Skramstad, H. K., *Laminar Boundary-Layer Oscillations and Transition on a Flat Plate*, N.A.C.A. Advance Confidential Report, April, 1943 (declassified).

[6] Batchelor, G. K., *Sound in Wind Tunnels*, Australian Council for Aeronautics, Report ACA-18, June, 1945.

[7] Taylor, G. I., *Turbulence in a Contracting Stream*, Zeit. für angew. Math. u. Mech., Vol. 15, pp. 91–96, February, 1935.

The Application of Basic Physiologic Data in the Design of Respiratory Equipment

LOREN D. CARLSON* AND VERNER J. WULFF†

University of Washington and State University of Iowa

ABSTRACT

Data on respiratory physiology are assembled and unified into general statements that may be of use to engineers in the design of respiratory equipment. The varied and apparently independent data concerned with partial pressures of oxygen required for adequate arterial blood saturation; pulmonary ventilation; respiratory rate; human tolerable resistance to flow; and gas exchange in the lungs are collected and presented in a generalized framework.

SYMBOLS

F	= flow of oxygen liters per minute S.T.P.D.
S.T.P.D.	= 760 mm. Hg, 0°C., dry
B.T.P.S.	= body temperature and pressure saturated with water vapor at 37°C.
M.I.F.	= maximum instantaneous rate of flow, liters per min. B.T.P.S.
V	= ventilation or minute volume in liters per min. B.T.P.S.
O_2	= fraction of oxygen required
P	= 760 mm. Hg
P_a	= ambient pressure, mm. Hg
T	= 273°K.
T_b	= body temperature, 310°K.
n	= number of breaths per min.
V_e	= volume economizer or rebreather in liters
pO_2	= partial pressure of oxygen in mm. Hg
pCO_2	= partial pressure of carbon dioxide in mm. Hg
R.Q.	= respiratory quotient
I.F.	= instantaneous rate of flow, liters per min. B.T.P.S.

INTRODUCTION

THE DESIGN OF CONTINUOUS FLOW or diluter demand oxygen equipment for use in combat or passenger aircraft requires the establishment and use of certain basic physiologic data. Design of more specialized equipment, such as pressure demand or pressure suit equipment, involves additional pertinent physiologic data. At present much of this basic physiologic and technical data has been accumulated by research divisions of the armed forces and under the auspices of the O.S.R.D. However, it has not been completely collated or organized, nor is it available for general use. The use of these data in formulating equipment design has necessitated an organization of the data for the specific purpose. It is the purpose of this paper to present and elaborate those data which are the bases for the design requirements of respiratory equipment. The amount of data in this field is large and a review of all work is not attempted. Only pertinent quantitative data will be reviewed.

The factors that the engineer must carefully evaluate are few in number but the volume of data is large and, at times, complexly interrelated. Factors to be considered are:

(1) The pressure of oxygen required to maintain adequate arterial oxygen.
(2) Pulmonary ventilation:
  (a) Effect of activity, cold, altitude, flight conditions.
  (b) Inspiratory instantaneous rates of flow.
  (c) Expiratory instantaneous rates of flow.
  (d) Maximum instantaneous rate of flow.
  (e) Mean instantaneous rate of flow.
  (f) Per cent of total volume drawn in at various rates of flow.
(3) Respiratory rate.
(4) Resistance to flow tolerable to humans.
(5) Gas exchange in lungs.

The data pertaining to these factors may have varying significance on the design of the various types of oxygen apparatus. Basically, all the data should be reviewed for any system.

Generally, data on any experimental subject are presented as an average with sufficient data being collected to insure significance. However, the average figure, if used in the design of respiratory equipment, can give an erroneous interpretation of equipment value. In no piece of equipment can the design be confined to the mean or average, for by definition that development excludes practically 50 per cent of the individual users from having adequate protection. A tenable thesis is proposed that the requirement for equipment should be so designated that 90 per cent of its users will be completely protected. Thus, in prediction of the duration of an oxygen supply, a value on the basis of average figures would give the flier an even chance of having sufficient oxygen; on the basis of the thesis just stated the chances would be 9 to 1. If the average figure and the standard deviation are known, then the value to be used is determined as:

$$\text{average} + (1.3 \times \text{standard deviation}) \qquad (1)$$

Received September 10, 1946.

* Formerly at the Aero Medical Laboratory, Wright Field. Now at Department of Physiology and Biophysics, University of Washington.

† Formerly at the Aero Medical Laboratory, Wright Field. Now at Department of Physiology, State University of Iowa.

In a few cases where necessary a minimum figure may be obtained by a corresponding subtraction.

Partial Pressure of Oxygen

The question of the partial pressure of oxygen necessary to maintain adequate arterial saturation has been extensively discussed and adequate basic data presented.[1, 2] Calculations to determine the necessary fraction of oxygen may be determined by:

$$fO_2 = [pO_2 + (pCO_2/\text{R.Q.})]/ [P_a - 47 - pCO_2 + (pCO_2/\text{R.Q.})] \quad (2)$$

or by a simpler formula

$$fO_2 = pO_2/(P_a - 47) \quad (3)$$

The desirability of using the latter formula in equipment has been ably presented by Boothby and Ferguson.[2, 3]

The minimum pO_2 that is desirable has been indicated to be that simulating 5,000-ft. breathing air.[1–4] This then is a minimum value for the equipment; the apparatus must deliver at least this quantity of oxygen at all conditions of flow and temperature. Alveolar pO_2 at 5,000 ft. is given at 81.6 mm. Hg by Boothby.[2] The standard deviation is 4.5 mm. Hg. To cover 90 per cent of the cases in maintaining a pO_2 (alveolar) at 81.6 mm. Hg, the pO_2 for tracheal air in Eq. (3) will be fixed at 134 mm. Hg.

Pulmonary Ventilation

Pulmonary ventilation or the amount of gas mixture breathed has significance in the design of respiratory equipment (mask and regulator) and in the amount of oxygen placed in the aircraft. The latter may be discussed briefly. The amount of oxygen to be carried in aircraft certainly cannot be based on an average nor entirely on experimental results. Reports on experimental flights[5] indicate that the average ventilation in flight expressed at B.T.P.S. is constant up to 33,000 ft. The average value is 14.2 liters per min. B.T.P.S. for normal flying conditions. Statistical analysis places the 90 per cent inclusive figure at 18.4 liters per min. Data from actual combat flights[6] present an average of 11.4 liters per min. B.T.P.S. and the 90 per cent inclusive figure is 18.2 liters per min. These values are for A.A.F. airplanes. For cargo or passenger aircraft, the value of 10 liters per min. given by Boothby[2] may be more nearly correct. Addition to this to cover 90 per cent of the cases would give a value of 12 liters per min. B.T.P.S.

An average active ventilation has also been determined experimentally. No combat data are now available. The average active figure is presented[5] as 23.2 liters per min. B.T.P.S. Ninety per cent of the cases are covered by a value of 37.1 liters per min. B.T.P.S. From these data it is interesting to note that to cover adequately approximately 100 per cent of the cases

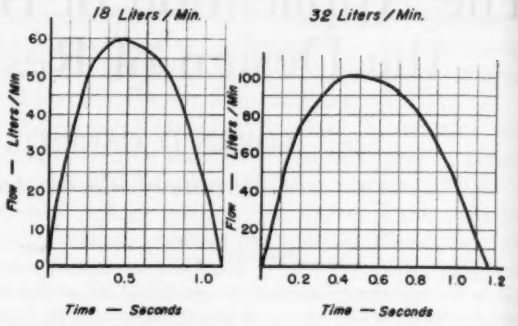

Fig. 1. Standard inspiratory flow-time curves for 18 and 32 liters per min. Ventilation reconstructed from data presented in this report. Inspiratory flow curves reconstructed from the generalized data presented in Figs. 3 and 5. These inspiratory curves will result in minute volumes of approximately 18 and 32 liters per min. Such curves may be used as a basis for design of cams for driving mechanical pumps. In order to obtain the data required for the construction of these curves, the minute volume must be predetermined.

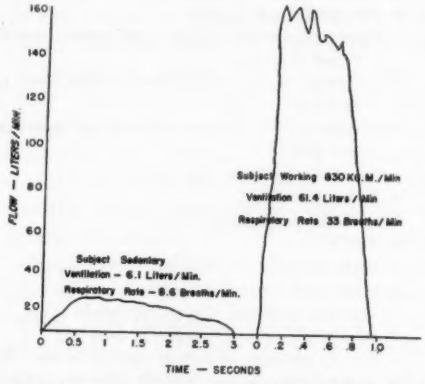
FLOW — LITERS / MIN
TIME — SECONDS
Subject Working 830 KG. M./Min
Ventilation 61.4 Liters / Min
Respiratory Rate 33 Breaths/ Min
Subject Sedentary
Ventilation — 6.1 Liters / Min.
Respiratory Rate — 8.6 Breaths/Min.

Fig. 2. Maximum and minimum inspiratory flow-time curves obtained by tracing of original records. The minimum flow-time curve pertains to a subject with the lowest ventilation and the lowest respiratory rate in a group of 27 sedentary subjects. These respiratory curves may also be used for the design of test equipment for respiratory apparatus.

under consideration, the value becomes 66.0 liters per min. B.T.P.S. The maximum figure actually observed in these flights was approximately 60 liters per min. B.T.P.S.

In the design of equipment the average figures for ventilation have value for use in design of mechanical lungs for fatigue testing, for varying degrees of work, and also are utilized for mechanical mask freezing tests, etc. The ventilation must be further analyzed to determine maximum, minimum, average, and instantaneous flow patterns (Figs. 1, 2). Data on these at present are taken from Silverman, *et al.*[7] (that data which involves no inspiratory resistance), since a complete study is available for 27 subjects. Studies of this nature have also been made by Hull, *et al.*[8] General deductions from these data have been transferred to data collected in aircraft. The minimum ventilation given is 6.1 liters per min. B.T.P.S.; the maximum is 90 liters per min. B.T.P.S. (Compare with minimum of 6.8 and maxi-

mum of 60 liters per min. in aircraft experiments.[5]) Average respiratory patterns in use for fatigue testing and mask freezing have been made as composites from the data of Lovelace, *et al.*,[5] and Silverman, *et al.*[7] (Fig. 1).

The effect of activity on ventilation has been well shown by Silverman, *et al.*,[7] and Wilson, *et al.*[9] Earlier work has been reported by Dill[10] and Penrod.[11] The effect of cold would seem to be negligible from data of Lovelace, *et al.*,[5] although other data indicate an increase in ventilation when subjects were exposed to the cold. Flight conditions seem to effect an increase in the ventilation of fighter personnel with increasing altitude and of bomber personnel at altitudes above 33,000 ft.[12] Altitude introduces a factor above 33,000 ft.[9, 12] The effect of clothing, tight-fitting parachutes, and position in the airplane on respiratory patterns has not been quantitatively defined. Dill has shown that protective clothing may add somewhat to the oxygen requirement for performing a task, particularly if the clothing is ill fitting, and that exposure to cold (to the point of shivering) may increase the oxygen requirement six times. The actual flight data of Carlson and Wulff[12] seem to indicate that the factor of clothing and cold is not evident or is a constant in their overall averages. More recently Ferguson has further evaluated this problem on a larger group of subjects and his results are shown in Table 1. Since it has been shown[7] that the inspiratory pattern changes with the type of exercise, further work is indicated.

Instantaneous rates of inspiratory gas flow are of interest from several points of view. The variation in flow during respiration must be used to duplicate respiratory patterns. Maximum instantaneous inspiratory flow indicates the maximum flow to be met by the respiratory equipment. The mean inspiratory flow has been used by Hart[13] in mask leakage considerations.

An analysis of the data of Silverman, *et al.*,[7] with the design of oxygen dispensing equipment specifically in mind discloses a number of relationships which may serve as a physiologic basis and form a framework which must be tested experimentally and upon which future data may be applied. These data furnish basic information about four important respiratory phenomena: minute volume, respiratory rate, maximum instantaneous flow, and portions of the respiratory cycle spent in inspiration and expiration. When the latter three are plotted against the minute volume certain regularities become apparent (Fig. 3). The relative time of inspiration is less than half at low ventilations and increases to one-half with increasing ventilation. The maximum instantaneous flow may be determined from these data as given in Fig. 3 as:

$$\text{M.I.F.} = 2.6V + 10 \qquad (4)$$

The 90 per cent inclusive maximum instantaneous flow may be calculated from:

$$\text{M.I.F. (90)} = 3.1V + 16 \qquad (5)$$

TABLE 1*

Effect of Temperature, Anoxia, and Work on Pulmonary Ventilation, measured by inhaling air through a dry gas meter wearing R.C.A.F. oxygen mask.

Number of subjects—66 (normal adult males).

Work—Standing up (on floor) and sitting down (on bench) 12 times per min. for 3 min. Volume measured for the third minute of exercise.

Seated—Sitting at ease but not absolutely quietly.

Cold—−25° to −40° with wind 10 m.p.h. Subjects sat 15 min. in cold before measurements taken, first seated then with exercise.

Clothing—Flying clothing in cold. Indoor clothing at room temperature.

G.L.—585 ft.

Temperature	Altitude in Ft.	Activity	Pulmonary Liters per Min. Range	Ventilation B.T.P.S. Average
Room temperature	G.L.	Seated	4.3–20.7	10.2
Room temperature	G.L.	Work	7.3–34.3	16.5
Room temperature	10,000	Seated	5.1–19.9	11.0
Room temperature	10,000	Work	9.5–33.3	19.5
Room temperature	15,000	Seated	6.4–19.1	11.9
Room temperature	15,000	Work	9.1–37.1	22.6
Cold	G.L.	Seated	8.6–31.1	17.1
Cold	G.L.	Work	7.7–54.6	28.3
Cold	10,000	Seated	4.0–34.6	17.8
Cold	10,000	Work	10.6–49.7	31.6
Cold	15,000	Seated	8.1–24.8	17.1
Cold	15,000	Work	13.0–58.6	33.2

Most obvious source of error is mask leakage which would tend to make results low.

* Data from No. 1 Clinical Investigation Unit R.C.A.F. to be published. Furnished through the courtesy of J. K. W. Ferguson, M.D.

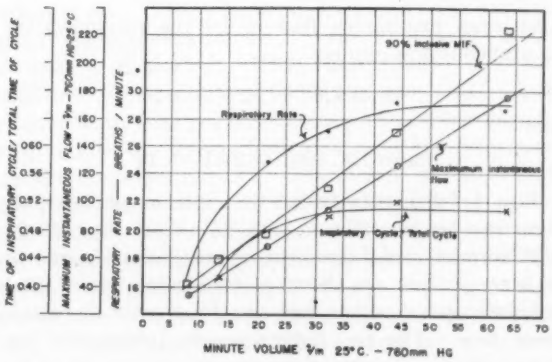
90% inclusive M.I.F.
Respiratory Rate
Maximum Instantaneous Flow
Inspiratory Cycle / Total Cycle
TIME OF INSPIRATORY CYCLE / TOTAL TIME OF CYCLE
MAXIMUM INSTANTANEOUS FLOW
RESPIRATORY RATE — BREATHS / MINUTE
MINUTE VOLUME

FIG. 3. Presentation of average respiratory data. This graph represents several factors in respiration plotted against the minute volume. The data used for all curves except 90 per cent inclusive maximum instantaneous flow (M.I.F.) curve are average data obtained from reference 7.

The 90% inclusive M.I.F. curve was calculated from the average minute volume data of reference 7. The standard error of the M.I.F. 90 per cent data, computed for the data series having the largest standard deviation, is ±0.63 liters per min., indicating that out of any number of future groups of data, 90 per cent of the M.I.F. 90 per cent figures will fall within ±2 liters per min. of the indicated values.

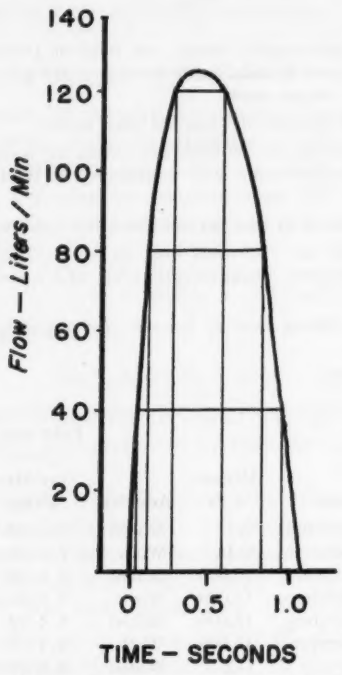

FIG. 4. Inspiratory flow-time pattern marked to obtain data for construction of curves on Fig. 5. An average inspiratory flow curve for a work load of 620 Kg. meter per min. obtained from reference 7. This curve is divided into seven parts by vertical lines which intersect the flow curve at 40, 80, and 120 liters per min. Relative flow is obtained from the ratio of fractional flow to maximum flow; relative volume from the ratio fractional time to total time. A plot of the latter two against relative flow is illustrated in Fig. 5.

The 90 per cent inclusive minute volume as taken from reference 7 may be determined by the equation:

$$V\,(90) = 1.4V - 2 \tag{6}$$

The mean inspiratory flow is 0.9 the maximum instantaneous flow and is:

$$\text{mean I.F.} = 2.3V + 9 \tag{7}$$

and

$$\text{mean I.F.}\,(90) = 2.8V + 14 \tag{8}$$

Figs. 4–7 demonstrate that the actual inspiratory patterns can be generalized. The data from Figs. 20–24 of Silverman, *et al.*,[7] representing ventilations from 8 to 40 liters per min. are shown plotted as fraction of tidal volume inspired versus flow as a fraction of the maximum flow. The two figures supply information for determining representative curves at any minute volume.

Expiratory rates of flow should be categorized similarly. Further data must be obtained. These data are important in design of expiratory valves. They cannot be transposed directly to intermittent or continuous pressure breathing equipment since the effects of the pressure alter the respiratory pattern.[14] Silverman's data (unpublished) indicate that the expiratory pattern will differ from the inspiratory pattern. Maximum expiratory rates of flow are found to be 2.8 times the ventilation.

The per cent of tidal volume drawn in at various rates of flow has proved significant in certain aspects of continuous flow equipment, in the design of demand equipment, and in the consideration of mask leakage. Hart[15] indicates that about 29 per cent of the inspired volume of air is inhaled at rates below 75 per cent of peak flow rates and about 60 per cent of the inspired volume

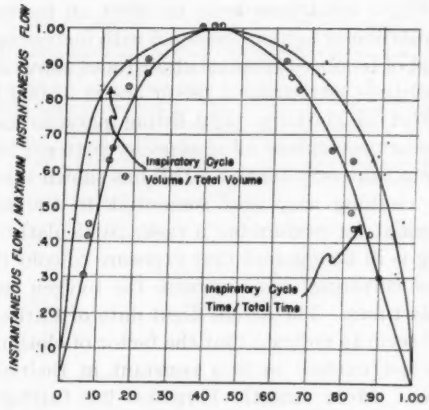

FIG. 5. Generalized relative volume—relative flow and relative time—relative flow curves obtained in the manner described in the explanation for Fig. 4. From these curves average data may be extracted for construction of inspiratory flow curves and for construction of curves in Fig. 7.

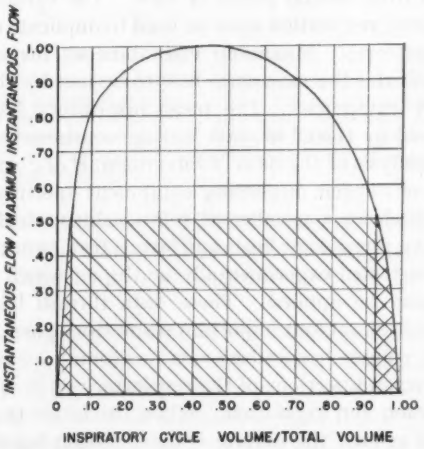

FIG. 6. Generalized relative volume-relative flow curve marked to illustrate extraction of data used to construct curves of Fig. 7. The flow ratio is arbitrarily selected, i.e., 0.50, and a horizontal line intersecting the relative volume curve is drawn. The ratio of the area below this horizontal line and bounded by the relative volume curve (hatched and cross-hatched region) and the total area is plotted against relative flow to obtain data for the construction of curve 2, Fig. 7, labeled "Total Volume at Fraction." Where the horizontal line, i.e., 0.50, intersects the relative volume curve, perpendicular lines are dropped to the abscissa. The ratio of the sum of areas between these perpendicular lines and the relative volume curve (cross-hatched lines) and the total area beneath the relative volume curve is plotted against relative flow to obtain curve 1 of Fig. 7, labeled "Total Volume at Fraction or Less."

is inhaled at rates below 95 per cent of the peak rate at rest and during exercise. This agrees with Fig. 7. The individual variation is great and the report states that during quiet breathing 1–14 per cent of the inspired volume is inhaled at rates below 10 liters per min.

Respiratory Rate

The general relationship of respiratory rate to ventilation is shown in Fig. 3. At low ventilations, between 5 and 20 liters per min., this curve may be sigmoid although a scatter diagram of the actual data indicates a straight line is more applicable. In this range the variation in respiratory rate is great. The data of Silverman[7] indicate that where the average minute volume is 16.6 the range is from 8 to 24 breaths per min. The extent of the range at any given average ventilation decreases with increasing ventilation.

Human Tolerable Resistance to Flow

Tolerable inspiratory and expiratory resistance to flow has been indicated[1] and the effect of resistance on flow rates studied.[7] Negative pressures less than 1 in. water column are unnoticed at 50 liters per min. flow (see Fig. 8). At 100 liters per min. flow suctions as high as 1.5 in. water column are unnoticed. Maximum instantaneous rates of flow decrease and the relative time of inspiration increases with increased inspiratory resistance. Increasing inspiratory resistance decreases the minute volume and the maximum instantaneous rate of flow, and the relative time of inspiration increases. At high work loads a resistance of 50 mm. (measured at 80 liters per min., 70°C. dry flow) causes a 7 per cent decrease in ventilation and approximately 15 per cent decrease in the maximum instantaneous flow. Demand and continuous flow equipment require low resistance or positive pressure and are well below tolerable limits generally. Expiratory resistance is necessary in pressure demand equipment.

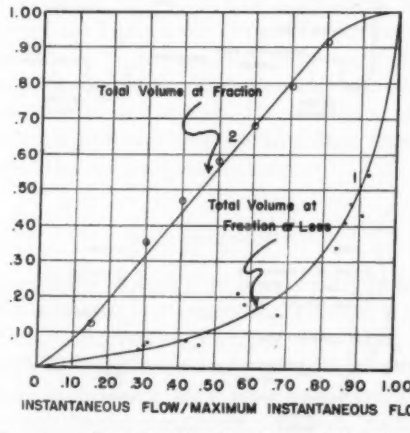

Fig. 7. Generalized fractional volume-relative flow curves. The curves in Fig. 7 present generalized inspiratory flow data obtained from curves in Fig. 6 as follows: (a) Curve 1 is a plot of the ratio of flow (instantaneous flow and maximum instantaneous flow) against the fraction of the volume inspired at a given instantaneous rate of flow. (b) Curve 2 is a plot of the ratio of the flow against total volume inspired at a given instantaneous rate of flow. These data are obtained from Fig. 6 in the manner described in that figure.

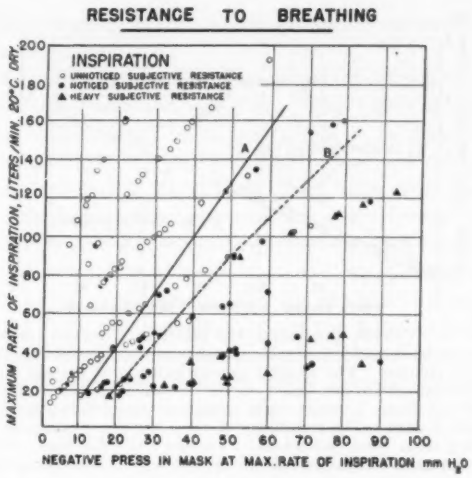

Fig. 8. Resistance to breathing. Data illustrating negative mask pressure in relation to maximum instantaneous rates of flow. The data were obtained by the instantaneous measurement and recording of pressure in a mask fitted with orifices of varying diameter. The open circles denote resistances which were not noticed by subjects. The closed circles denote resistances noticed by the subjects; the closed triangles denote resistance uncomfortable for short periods. Curve A represents the maximum allowable inspiratory resistance that is unnoticed by subjects; curve B represents the maximum allowable resistance that is noticed but not classified as uncomfortable by subjects. Data are from reference 1.

Gas Exchange in the Lungs

For the design of closed respiratory systems it is necessary to consider the magnitudes of the gas exchanges that take place in the lungs (Fig. 9). These changes are: (1) the removal of oxygen from inspired gas (oxygen consumption); (2) the addition of carbon dioxide to expired gas (CO_2 elimination); and the addition of water vapor to expired gas (H_2O vapor elimination). Oxygen consumption and carbon dioxide production vary among individuals and the respective curves are experimentally determined and represent the 90 per cent inclusive figures for oxygen consumption and carbon dioxide elimination. The data represent the volume of vapor in expired air saturated at 37°C. Seeley[16] has published data on the rate of saturation of expired air and indicates that it approaches 100 per cent. Burch[17] has reported that expired air is not and cannot be saturated with water. The average relative humidity of expired air in a comfortable environment is reported to be 88 per cent at a temperature of 33°C.

Application to Design

The application of these data can be sampled by reference to the schematic types of continuous flow systems in Fig. 10. In a straight continuous flow

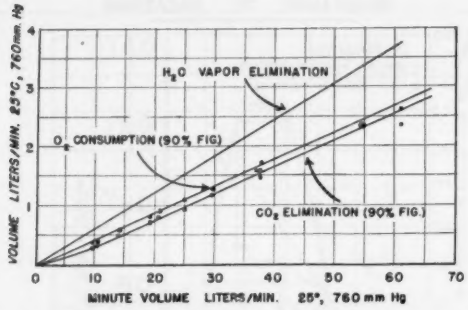
VOLUME LITERS/MIN. 25°C, 760mm Hg
H_2O VAPOR ELIMINATION
O_2 CONSUMPTION (90% FIG)
CO_2 ELIMINATION (90% FIG.)
0 10 20 30 40 50 60 70
MINUTE VOLUME LITERS/MIN. 25°, 760 mm Hg

FIG. 9. Curves illustrating the relation of oxygen consumption, carbon-dioxide elimination, and water-vapor elimination to minute volume. The oxygen consumption and carbon-dioxide elimination curves are based on the 90 per cent inclusive figure calculated from average data obtained from Silverman, unpublished data. The reliability of these curves was checked by plotting data from Schneider, *Physiology of Muscular Activity*. Open squares represent carbon-dioxide elimination and closed squares represent oxygen consumption. Notice that these values taken from Schneider fall on or below the 90 per cent inclusive curves. The standard error of the oxygen consumption and carbon-dioxide elimination 90 per cent inclusive values, computed for the data series having the largest standard deviation, is ±0.0047 liter per min., indicating that out of any number of future groups of data, 90 per cent of the oxygen consumption and carbon-dioxide 90 per cent inclusive values will fall within ±0.014 liter per min. of the indicated values. The curve for water vapor elimination is calculated, assuming the expired air is saturated with water vapor at 37 °C. See text for further discussion.

system (Fig. 10-1), such as the Japanese use, the continuous supply of oxygen must be carefully related to the volumes inspired under given instantaneous flows. A use of the data for straight continuous flow may be given. Since only that part of the flow is used which is flowing during inspiration, the flow required will be equal to the flow at which a fraction of the inspired volume equals the fraction of oxygen required. Thus,

F = M.I.F. × fraction of M.I.F. under which fraction of tidal volume taken in is equal to the fraction of added oxygen required. (See Fig. 7.)

since:

$$\text{M.I.F.} = 2.6V + 10 \tag{9}$$

$$\text{Fraction added oxygen required} = 1.27 \times (fO_2 - 0.21) \tag{10}$$

(converting oxygen required to fraction of oxygen added). Fraction of M.I.F. under which fraction of tidal volume is taken in is equal to the fraction of added oxygen required taken from Fig. 4, Curve 2 and between the fractions 0.1 and 0.9 is:

$$(8/9)[1.27(fO_2 - 0.21)] \tag{11}$$

The flow required for a continuous flow system without economizer systems is:

$$F = (2.6V + 10)\{(8/9)[1.27(fO_2 - 0.21)]\} \times \{[(P_a - 47)/P](T/T_b)\} \tag{12}$$

where the fraction $\{[(P_a - 47)/P](T/T_b)\}$ corrects the values to 760 mm. Hg and 0°C. This equation, because of the inadequacies of the fraction 8/9, is valid when fO_2 is greater than 0.10 and less than 0.90.

These equations may be simplified by the substitution of the actual fraction of oxygen desired.

Flows calculated from these data are in fair agreement with Swann.[18] When a reservoir or rebreather reservoir (Fig. 10-2 and -3) are used the relationship of the factors change. These systems are more complex to evaluate than the demand system. Making the assumption that the reservoir will save half the oxygen the above equation can be utilized. Values here are analogous to those reported by Swann.[18, 19] Further refinements of the formula to evaluate the effect of a rebreather reservoir can be made from the graphic data. Limitations of the rebreather economizer due to its volume can be further expressed by:

$$(V/n)/V_e \tag{13}$$

and the equation becomes:

$$2F = (2.6V + 10)\{(8/9)[1.27(fO_2 - 0.21)]\} \times [(P_a - 47)/(PT/T_b)][(V/n)/V_e] \tag{14}$$

This equation is in error by the amount of flow that occurs during the inspiratory cycle and can be further corrected with the use of:

$$\{[(V/n)/V_e] - (8/9)[1.27(fO_2 - 0.21)]\}/2 \tag{15}$$

An economizer without a rebreather will require the modification of the basic formula whenever $[(V/n)/V_e]$ is greater than one. With a 700-cc. economizer, $[(V/n)/V_e]$ becomes 1.0 at 15 liters per min. ventilation

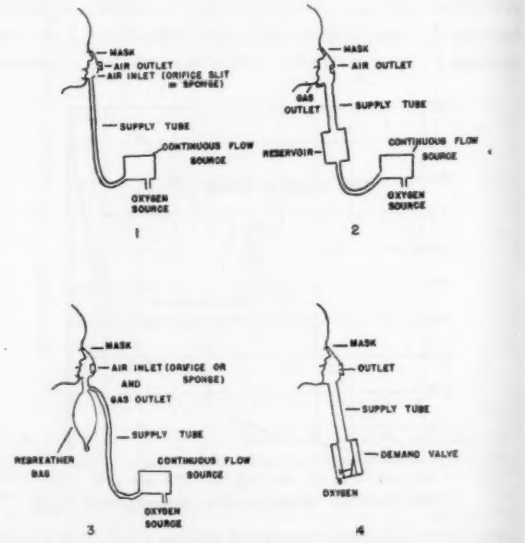

FIG. 10. Schematic sketches of oxygen supply systems are illustrated. Sketch 1 represents a constant flow system consisting only of regulator and mask. Sketch 2 represents a constant flow system consisting of a regulator, mask, and a reservoir volume. Sketch 3 represents a constant flow system consisting of a regulator, mask, and a rebreather bag. Sketch 4 represents a demand system consisting of a regulator and mask. Refer to text for further detail.

which may lead to the statement that little difference exists in the two systems.[20] Since these formulations incorporate the fraction of oxygen required they may be utilized to calculate flows necessary for oxygen therapy and such calculations show good agreement with Boothby[21] and unpublished data from the Aero Medical Laboratory.

In the demand system, requirements may be taken from the Figs. 3, 5, and 7 when the value of pulmonary ventilation is set. Army Air Forces' equipment is designed for an average inactive ventilation of 14 liters per min. B.T.P.S.; an average active ventilation of 24 liters per min. B.T.P.S.; and a maximal ventilation of 60 liters per min. B.T.P.S. Using Eq. (6) the 90 per cent inclusive ventilations are 18 and 32 liters per min. B.T.P.S., respectively. Using Eq. (4) the 90 per cent inclusive maximum instantaneous flows are 45, 93, and 166 liters per min., respectively. Oxygen regulators must be designed to deliver these inclusive flows within the minimum suction requirements.

In the testing of respiratory equipment, average data should be employed and corrected to the 90 per cent inclusive value. At the present time A.A.F. regulators are tested with a mechanical lung that duplicates the breathing pattern for 18 and 32 liters per min. ventilation, illustrated in Fig. 1. These flow-time curves were reconstructed from the curves in Figs. 3 and 5. In addition to testing with average +1.3 standard deviation data, extremes of the range encountered should also be used. Thus, in the inactive ventilation group[7] there is illustrated the flow-time pattern of the lowest ventilation (Fig. 2), that should be duplicated on the mechanical lung. A ventilation pattern for 70 liters per min. (Fig. 2) is used to test performance at maximum respiratory volumes.

The variables of respiratory phenomena discussed above have not been clearly defined for pressure breathing equipment.[14] Interrelated physiologic factors as well as characteristics of equipment complicate the problem but do not obscure the solution. A similar approach can and will be made to reduce these factors to generalities for equipment design.

Conclusion

The synthesis of varied and apparently independent data into a unified and generalized relation is desirable when large and diverse groups of data exist and this data is to be transferred from the field of physiologic investigation to serve as a basic requirement for an engineering development. In addition, such a synthesis has the advantage of establishing a measure for evaluation of such data, readily directs research into channels where sufficient data are lacking, and permits rapid and sufficiently accurate (i.e., 10 per cent) extraction of average data for practical application. The presentation of the general relations of respiratory data in the foregoing report embodies the characteristics of such a synthesis.

The construction of such a generalized framework is based upon experimental data. The value of such a framework depends upon the accuracy and validity of the data used. As an example, the average curve for respiratory rate in Fig. 3 embodies a large range among individual determinations which is not apparent upon inspection of the curve but is apparent when compared with other experimental data. Similarly, the curve for water vapor elimination in Fig. 9 is not based on experimental data but is calculated on the basis of certain assumptions (refer to text). Comparison of this curve with experimental data, as these become available, shows a discrepancy, since the values in Fig. 9 are probably too high.

In spite of the faults of the framework presented in this report, it is believed to be a worth-while approach to a synthesis of respiratory data which should not be considered a definitive attempt but rather a directional attempt to be modified and corrected by subsequent experimental data.

References

[1] U.S., Office of Scientific Research and Development, Committee on Medical Research, Committee on Aviation Medicine, *Handbook of Respiratory Data in Aviation;* 1944.

[2] Boothby, Walter M. (checked by E. J. Baldes), *Development of Oxygen Equipment; Physiologic Criteria to Be Considered by Engineers,* O.S.R.D., Committee on Medical Research, Mayo Aero Medical Unit, Special Report No. 3, August 20, 1942.

[3] Ferguson, J. K. W., *The Problem of Equivalent Altitudes,* R.C.A.F. No. 1 Clinical Investigation Unit, Report No. B-114, January, 1944.

[4] Wulff, Verner J., *Requirements and Design Characteristics of Regulators,* A.A.F. A.T.S.C., Engineering Div., Aero Medical Laboratory, Memorandum Report ENG-49-660-17-F-2, November 19, 1943.

[5] Lovelace, W. Randolph, II, Carlson, L. D., and Wulff, V. J., *Pulmonary Ventilation of Flyers,* A.A.F. A.T.S.C., Engineering Div., Aero Medical Laboratory, Memorandum Report ENG-49-660-50-H, March 11, 1944.

[6] Bennett, Mary, and Wulff, V. J., *Oxygen Consumption of Aircrew in Combat,* A.A.F. A.T.S.C., Engineering Div., Aero Medical Laboratory, Memorandum Report ENG-49-660-48-F, September 20, 1944.

[7] Silverman, Leslie, Lee, Robert C., Lee, George, Drinker, Dr. Katherine R., and Carpenter, Dr. Thorne M., *Fundamental Factors in the Design of Respiratory Equipment: Inspiratory Air Flow Measurements on Human Subjects With and Without Resistance,* O.S.R.D., National Defense Research Council, Div. 11, Sect. 11.2, Report No. 1222, January, 1943.

[8] Hull, W. E., and Hall, F. G., *Optical Flow Meter,* A.A.F. A.T.S.C., Engineering Div., Aero Medical Laboratory, Memorandum Report ENG-49-696-42.

[9] Wilson, John W., Bonner, John T., and Finkel, Asher J., *Oxygen Requirements as Affected by Physical Activity and Altitude,* A.A.F. A.T.S.C., Engineering Div., Aero Medical Laboratory, Memorandum Report ENG-49-696-7C, November 11, 1943.

[10] Dill, D. B., *Metabolic Effects of Low Temperature,* A.A.F. Matériel Division, Memorandum Report No. EXP-M-54-653-55 1941.

(Continued on page 236)

(*Continued from page 235*)

[11] Penrod, K. E., *Rates of Inspiration and Expiration under Various Conditions*, A.A.F. Matériel Division, Memorandum Report No. EXP-M-54-653-75, 1942.

[12] Carlson, Loren D., and Wulff, V. J., *Pulmonary Ventilation of Flyers at High Altitude*, A.A.F. A.T.S.C., Engineering Div., Aero Medical Laboratory, Memorandum Report ENG-49-660-48-G, October 9, 1944.

[13] Hart, J. S., *Theory of Inspiratory Mask Leakage*, R.C.A.F. No. 1 Clinical Investigation Unit, Report No. B-150, August 21, 1944.

[14] Barach, A. L., Fenn, W. O., Ferris, E. B., and Schmidt, C. F., *The Physiology of Pressure Breathing: A Brief Review of Its Present Status*, O.S.R.D., Committee on Medical Research, December, 1944.

[15] Hart, J. S., *Instantaneous Rates at Which Various Fractions of Inspired Air Are Inhaled*, R.C.A.F. No. 1 Clinical Investigation Unit, Report No. B-67, January, 1944.

[16] Seeley, L. E., *Study of the Changes in the Temperature and Water Vapor Content of Respired Air in the Nasal Cavity*, Heating, Piping and Air Conditioning, Vol. 51, p. 377, 1940.

[17] Burch, G. E., *The Rate of Water Loss from the Respiratory Tract of Man Living in a Sub-tropical Climate*, Science, Vol. 102, p. 619, 1945.

[18] Swann, Howard G., *Oxygen Requirements While Using the A-8B Mask without the Rebreather Bag*, A.A.F. A.T.S.C., Engineering Div., Aero Medical Laboratory, Memorandum Report No. TSEAL3-696-42I, February 20, 1945.

[19] Swann, Howard, *Oxygen Requirements with Constant Flow Equipment*, A.A.F. A.T.S.C., Engineering Div., Aero Medical Laboratory, Memorandum Report No. TSEAL3-696-42H, December 30, 1944.

[20] Ferguson, J. K. W., *Adequacy of Reservoir Delivery Oxygen Systems*, R.C.A.F. No. 1 Clinical Investigation Unit, Report No. B-117, February 8, 1944.

[21] Boothby, W. M., *The B.L.B. Oxygen Inhalation Apparatus: Improvement in Design and Efficiency by Studies on Oxygen Percentages in Alveolar Air*, Proc. Staff Meet., Mayo Clinic, Vol. 15, p. 194, 1940.

Letter to the Editor

Dear Sir:

As is pointed out in a Letter to the Editor in the JOURNAL OF THE AERONAUTICAL SCIENCES, Vol. 14, No. 1, p. 23, January, 1947, by Messrs. Krzywoblocki and McCloy, a considerable amount of confusion exists with regard to the concept of propulsive efficiency. This quantity, η_p, is defined as the ratio of "useful work" or product of thrust and air speed, to "energy input" to the gases ejected from the propulsor. For the conventional propeller, it reduces to

$$\eta_p = 2/[1 + (V_p/V)] \tag{1}$$

where V_p is the air speed in the slipstream and V is the aircraft speed. For a rocket with exhaust gas ejection velocity C, η_p reduces to

$$\eta_p = 2V/C \tag{2}$$

a quantity that varies from 0 to ∞ as V increases without limit.

The confusion that exists with regard to η_p is blamed by the authors of the previous letter, on the fact that this efficiency can have a value greater than 1. It would seem that there is more wrong with η_p than that. If, for example, the expression for V as reached by a rocket in empty space, is put into Eq. (2) above, the result is disturbing. For such a rocket,

$$V = c \log_e(m_0/m) \tag{3}$$

where c is the exhaust velocity of the combustion products, m_0 and m are masses of the craft when V is 0 and V, respectively. It follows from Eq. (3) that

$$\eta_p = 2 \log_e (m_0/m) \tag{4}$$

The "efficiency" is here independent of the fuel and even of the propulsive mechanism. The change in definition of η_p proposed by the authors mentioned does not improve its properties in this respect.

It is suggested that the whole basis of definition of η_p should be re-examined. The idea of an efficiency η is useful in certain fields of engineering. In particular, it characterizes a machine that does useful work. When η is 100 per cent, there are no friction losses; η cannot be greater than 100 per cent without violating the energy conservation law.

If a quantity η_p is applied to the flight process, a great difficulty is at once apparent: there is no standard "useful work" required to accomplish flight that cannot in principle be reduced toward 0 as a limit. If the thrust power necessary to be expended in steady flight is defined as "useful work," any value of $\eta_p > 100$ per cent does not indicate a failure of the conservation of energy; if anything, it simply indicates an error in definition of the "useful work" required to fly.

Furthermore, thrust power devoted to acceleration rather than overcoming drag, is not "expended" in the ordinary sense of the term as used in defining η_p. Such power is really stored in the form of kinetic energy of the craft. It can be applied to the overcoming of drag in flight at a later time. Therefore, the use of η_p to characterize accelerated flight in any sense at all—and this is especially true for the case of rockets—is bound to lead to confusion and is probably meaningless.

It is suggested that specific impulse in the form c, or $I = c/g$, where g is 32.2 ft. per sec.^{2}, is a proper performance criterion for rockets. The impulse per unit of fuel mass expended is proposed as preferable to η_p also in characterizing propeller-driven aircraft.

DAVID T. WILLIAMS
Associate Professor of Aeronautical Engineering
University of Michigan

Numerical-Graphical Methods of Characteristics for Plane Potential Shock-Free Flow Problems*

LESTER L. CRONVICH†

Applied Physics Laboratory, The Johns Hopkins University

SUMMARY

Two numerical-graphical methods of solution of supersonic flow problems are developed from the basic theory of characteristics. Both are restricted to plane potential shock-free flow. The "lattice-point" method, recommended for flows with given boundaries, is applied to flow in a hyperbolic channel. The "field" method, suitable for problems in which flow boundaries are to be determined, as in the case of supersonic nozzle design, is used for a problem of parallel routing of an initially expanded flow. Complete rules of procedure are presented for each method.

INTRODUCTION

IN 1929 PRANDTL AND BUSEMANN[1] presented a graphical scheme for determining two-dimensional supersonic flows, which has come to be known as the Prandtl-Busemann "method of characteristics." The essential features of the method are explained in Busemann's handbook article[2] and more recently in the book by Sauer.[3] A detailed exposition of the fundamental ideas and procedures is contained in a report by Heybey.[4]

The mathematical basis for the method may be found in the book *Methoden der Mathematischen Physik*, by Courant and Hilbert[5] or in a series of reports by Tollmien.[6] A brief discussion of the theory necessary for the methods of solution of this paper is given in the following section.

MATHEMATICAL THEORY

Consider a differential equation of the form

$$A\phi_{xx} + B\phi_{xy} + C\phi_{yy} + D = 0 \qquad (1)$$

where A, B, C, and D are functions of x, y, ϕ, ϕ_x, and ϕ_y and satisfy the relation

$$B^2 - 4AC > 0$$

The function $\phi(x, y)$ may be considered to define a surface in xyz-space. Certain space curves lying on this surface have projections in the xy-plane which satisfy the differential equation

$$Ady^2 - Bdydx + Cdx^2 = 0 \qquad (2)$$

These projections are usually referred to as "characteristics." The properties of these curves[5, 6] make possible the development of the approximate methods discussed here. From Eq. (2) it is found that there are two families of characteristics in the xy-plane given by

$$\left.\begin{aligned} dy/dx &= (B - \sqrt{B^2 - 4AC})/2A \\ dy/dx &= (B + \sqrt{B^2 - 4AC})/2A \end{aligned}\right\} \qquad (3)$$

One of the properties of the characteristics is that the differential equation, Eq. (1), can be satisfied *along* such a curve without having to depart from it obliquely. In other words, if initial values of ϕ, ϕ_x, and ϕ_y are given on a curve C which is intersected by characteristics, one may proceed *along* characteristics and determine the unknown values of ϕ, ϕ_x, and ϕ_y on the curves by a step-by-step process in the xy-plane. Since the region of definition of ϕ in the xy-plane can be covered by a mesh of characteristics of any desired fineness, it is evident that theoretically a solution may be obtained with any degree of approximation desired. In practice, however, the degree of approximation is limited by the amount of numerical or graphical work involved in obtaining such a solution. The idea of solving the differential equation by proceeding *along* characteristics is the basic idea in the development of the "lattice-point" method of solution.

Another property of characteristics is that they are curves across which the second derivatives of ϕ may experience discontinuities. Thus, solutions of differential equation, Eq. (1), in two regions separated by a characteristic may be patched together along this characteristic. This is the basic idea in the development of the "field" method of solution of this paper and also that of Prandtl and Busemann.

PLANE, SHOCK-FREE, POTENTIAL FLOW

For plane, shock-free, potential flow the differential equation of motion is

$$\left(1 - \frac{u^2}{a^2}\right)\phi_{xx} - \frac{2uv}{a^2}\phi_{xy} + \left(1 - \frac{v^2}{a^2}\right)\phi_{yy} = 0 \qquad (4)$$

where

ϕ = velocity potential
$u = \phi_x$ = x-component of velocity

Received October 8, 1946.

* Contribution No. 3 from Applied Physics Laboratory, The Johns Hopkins University, based on work done under Contract NOrd 7386 with the Bureau of Ordnance, U.S. Navy Department.

† Mathema ician

$v = \phi_y$ = y-component of velocity
$a = \sqrt{[(k-1)/2](q_m^2 - q^2)}$ = local velocity of sound
$q = \sqrt{u^2 + v^2}$ = velocity
q_m = maximum velocity, corresponding to $a = 0$
k = ratio of specific heats

Comparing this equation with Eq. (1) it is found that $D = 0$ and

$$B^2 - 4AC = 4[(q^2/a^2) - 1] > 0$$

for $q > a$, that is, for supersonic velocity.

The two families of characteristics are

$$\left.\begin{aligned} \frac{dy}{dx} &= \frac{uv + a\sqrt{q^2 - a^2}}{u^2 - a^2} \\ \frac{dy}{dx} &= \frac{uv - a\sqrt{q^2 - a^2}}{u^2 - a^2} \end{aligned}\right\} \tag{5}$$

Now let θ be the inclination of the velocity vector with the x-axis, so that

$$u = q\cos\theta, \quad v = q\sin\theta \tag{6}$$

By differentiating,

$$\left.\begin{aligned} du &= dq\cos\theta - qd\theta\sin\theta \\ dv &= dq\sin\theta + qd\theta\cos\theta \end{aligned}\right\} \tag{7}$$

Now at any point P let the x-axis coincide with the stream direction so that Eqs. (6) and (7) become

$$u = q, \quad v = 0 \tag{6a}$$

$$du = dq, \quad dv = qd\theta \tag{7a}$$

Using these transformations the differential equation, Eq. (4), may be written

$$[1 - (q^2/a^2)]dq(dy/dx) + qd\theta = 0 \tag{8}$$

Furthermore, the equations of the characteristics become

$$\left.\begin{aligned} \frac{dy}{dx} &= \frac{a}{\sqrt{q^2 - a^2}} = \tan\alpha \\ \frac{dy}{dx} &= \frac{-a}{\sqrt{q^2 - a^2}} = \tan(-\alpha) \end{aligned}\right\} \tag{9}$$

where α is the well-known Mach angle usually defined by the relation

$$\sin\alpha = a/q = 1/M \tag{10}$$

M being the Mach Number.

Thus one family of characteristics forms the Mach angle α with the tangents to the streamlines and is referred to as "left-running" characteristics or Mach lines, since any one of them is on the left as one faces in the downstream direction; the other family forms the angle $-\alpha$ with the tangents to the streamlines and is referred to as "right-running" characteristics or Mach lines.

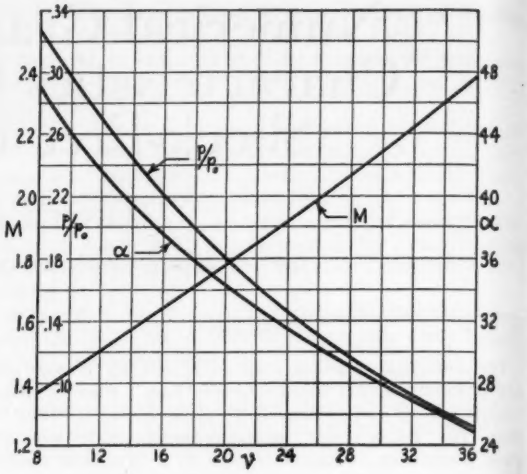

FIG. 1. Pressure ratio p/p_0, Mach Number M, and Mach angle α vs. ν for plane potential flow.

The differential equation, Eq. (8), can now be written with the aid of Eqs. (9) in the form

$$\left.\begin{aligned} dq - (a/\sqrt{q^2 - a^2})qd\theta &= 0 \\ dq + (a/\sqrt{q^2 - a^2})qd\theta &= 0 \end{aligned}\right\} \tag{11}$$

along the left-running and right-running Mach lines, respectively. These equations can be integrated to yield

$$\left.\begin{aligned} \theta &= \nu(q/a) + K_L \\ \theta &= -\nu(q/a) + K_R \end{aligned}\right\} \tag{12}$$

where

$$\nu\left(\frac{q}{a}\right) = \sqrt{\frac{k+1}{k-1}}\arctan\sqrt{\left(\frac{k-1}{k+1}\right)\left(\frac{q^2}{a^2} - 1\right)} - \arctan\sqrt{\frac{q^2}{a^2} - 1} \tag{13}$$

K_L, K_R = constants of integration. One method for carrying out this integration is indicated on p. 56 of reference 3. The results presented there can be transformed to Eqs. (12) above.

By application of Bernoulli's equation it is possible to express the pressure ratio p/p_0, where p_0 is the pressure corresponding to zero velocity, as a function of q/a. Thus

$$\frac{p}{p_0} = \left(1 + \frac{k-1}{2}\frac{q^2}{a^2}\right)^{-k/(k-1)} \tag{14}$$

The Mach angle α may likewise be expressed as a function of q/a by the equation

$$\alpha = \arcsin(a/q) \tag{10a}$$

In view of Eq. (13), therefore, Mach Number $M = q/a$, Mach angle α, and pressure ratio p/p_0 may be regarded as functions of ν. For convenience in application these quantities are plotted against ν. A

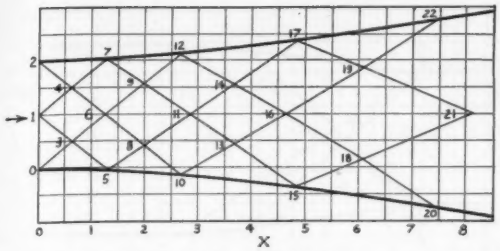

FIG. 2. Construction of characteristics for flow in a hyperbolic channel, $M = 1.6$.

sample of such curves for air ($k = 1.405$) is given in Fig. 1.

"LATTICE-POINT" METHOD OF SOLUTION

In the preceding section the characteristics were identified with the familiar Mach lines in the flow plane. These characteristics form a mesh covering the flow region, and their points of intersection give a system of "lattice points." In the "lattice-point" method of solution one proceeds along the characteristics from lattice-point to lattice-point (the characteristics being made up of straight-line segments for this approximation). All calculations along left-running characteristics are governed by the equations

$$\left.\begin{aligned} dy/dx &= \tan \alpha \\ \theta &= \nu(q/a) + K_L \end{aligned}\right\}. \qquad (15)$$

and along the right-running characteristics by the equations

$$\left.\begin{aligned} dy/dx &= \tan(-\alpha) \\ \theta &= -\nu(q/a) + K_R \end{aligned}\right\} \qquad (16)$$

The method is to be used for flows with *given boundaries*

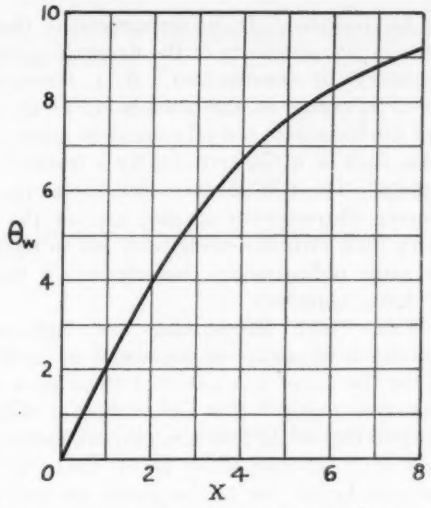

FIG. 3. Angle of inclination of channel wall of Fig. 2 in degrees.

for which the Prandtl-Busemann method and the "field" method of this paper are not always suitable.

The general procedure of this method can be given by the following set of rules which are applied to flow in a hyperbolic channel with initially uniform flow at a Mach Number of 1.6 (see Figs. 2 and 3 and Table 1).

(1) Construct a scale drawing of the flow boundaries (as in Fig. 2).

(2) Plot θ_w, angle of inclination of the wall to the initial flow direction. This is illustrated in Fig. 3.

(3) Choose a suitable set of points on the initial curve (points 0, 1, and 2 in Fig. 2), and from the given initial conditions determine ν for each of the points from Fig. 1. (These are recorded in Table 1.) Points of intersection of the initial curve and the boundaries

TABLE 1
Calculated Data for Hyperbolic Channel of Fig. 2

			R	L		L	R			
Pt	$\theta°$	$\nu°$	$(\theta+\nu)°$	$(\theta-\nu)°$	$\alpha°$	$(\theta+\alpha)°$	$(\theta-\alpha)°$	M	p/p_0	x
0	0	14.9	14.9	−14.9	38.6	38.6	−38.6	1.6	0.234	0
1	0	14.9	14.9	−14.9	38.6	38.6	−38.6	1.6	0.234	0
2	0	14.9	14.9	−14.9	38.6	38.6	−38.6	1.6	0.234	0
3	0	14.9	14.9	−14.9	38.6	38.6	−38.6	1.6	0.234	0.63
4	0	14.9	14.9	−14.9	38.6	38.6	−38.6	1.6	0.234	0.63
5	−2.6	17.5	14.9	−20.1	36.2	33.6	−38.8	1.69	0.205	1.31
6	0	14.9	14.9	−14.9	38.6	38.6	−38.6	1.6	0.234	1.26
7	2.6	17.5	20.1	−14.9	36.2	38.8	−33.6	1.69	0.205	1.31
8	−2.6	17.5	14.9	−20.1	36.2	33.6	−38.8	1.69	0.205	1.98
9	2.6	17.5	20.1	−14.9	36.2	38.6	−33.6	1.69	0.205	1.98
10	−5.0	19.9	14.9	−24.9	34.3	29.3	−39.3	1.775	0.181	2.67
11	0	20.1	20.1	−20.1	34.1	34.1	−34.1	1.78	0.179	2.87
12	5.0	19.9	24.9	−14.9	34.3	39.3	−29.3	1.775	0.181	2.67
13	−2.4	22.5	20.1	−24.9	32.4	30.0	−34.8	1.825	0.157	3.67
14	2.4	22.5	24.9	−20.1	32.4	34.8	−30.0	1.825	0.157	3.67
15	−7.5	27.6	20.1	−35.1	29.2	21.7	−36.7	2.05	0.1185	4.85
16	0	24.9	24.9	−24.9	30.8	30.8	−30.8	1.95	0.138	4.65
17	7.5	27.6	35.1	−20.1	29.2	36.7	−21.7	2.05	0.1185	4.85
18	−5.1	30.0	24.9	−35.1	27.9	22.8	−33.0	2.135	0.103	6.10
19	5.1	30.0	35.1	−24.9	27.9	33.0	−22.8	2.135	0.103	6.10
20	−9.0	33.9	24.9	−42.9	25.9	16.9	−34.9	2.29	0.081	7.45
21	0	35.1	35.1	−35.1	25.3	25.3	−25.3	2.34	0.075	8.16
22	9.0	33.9	42.9	−24.9	25.9	34.9	−16.9	2.29	0.081	7.45

should be included. It is recommended that one make use of the symmetry of the figure as a check on the accuracy of construction. If a discontinuous change of θ_w occurs at the intersection of the initial line and the boundary, several coincident points should be taken, each of which accounts for a fraction of the total jump. The coincident points lie on the same left-running characteristic if they are on the upper boundary (flow direction being from left to right) and on the same right-running characteristic if they are on the lower boundary.

(4) Draw both left-running and right-running characteristics (straight-line segments) at each point chosen on the initial line provided these lines extend into the flow region. The inclinations of these line segments to the initial flow direction are given by the columns $(\theta + \alpha)$ and $(\theta - \alpha)$ of Table 1. Their intersections locate new lattice points on the characteristics.

(5) Values of θ and ν for each new point are obtained by simultaneous solution of Eqs. (12). For example, for point 3

$$\theta_3 - \nu_3 = \theta_0 - \nu_0$$

since points 0 and 3 lie on a left-running characteristic and

$$\theta_3 + \nu_3 = \theta_1 + \nu_1$$

since points 1 and 3 lie on a right-running characteristic. Thus we have

$$\theta_3 = [(\theta_1 + \nu_1) + (\theta_0 - \nu_0)]/2$$

$$\nu_3 = [(\theta_1 + \nu_1) - (\theta_0 - \nu_0)]/2$$

(6) From Fig. 1 read off the value of α corresponding to ν at the newly found point. Calculate angles $\theta + \alpha$ and $\theta - \alpha$ and draw the characteristics as indicated in Step 4.

(7) The procedure is modified in case one of the new points lies on the boundary (such as points 5, 7, 10, etc., of Fig. 2). In such a case, the value of θ is read from the curve constructed in Step 2 (that is, Fig. 3 for this illustration). And ν is then obtained from whichever of Eqs. (12) applies.

(8) Values of Mach Number and pressure ratio p/p_0 at any point can be read from Fig. 1 after the value of ν has been determined for that point.

"Field" Method of Solution

As pointed out in the preceding section, the characteristics form a mesh covering the flow region, so that the region is broken up into small fields. In the field method of solution the characteristics are used for patching together the flows in two adjacent fields, throughout each of which the flow variables are assumed constant. Thus the crossing of a characteristic must account for a discontinuity or jump in certain flow variables. It is found convenient in each problem

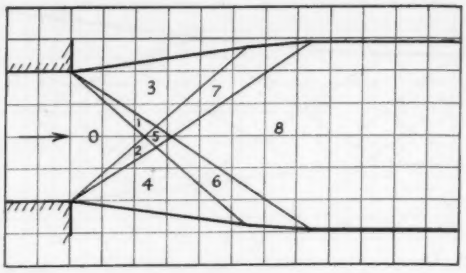

Fig. 4. Construction of characteristics and boundary for parallel routing of an initially expanded flow, $M = 1.4$.

to assign a standard jump to the quantities $\theta + \nu$ and $\theta - \nu$. The jump used for both quantities is numerically the same but opposite in sign. In advancing from one field to the next a characteristic is crossed, thereby resulting in a jump in $\theta + \nu$ if a right-running characteristic is crossed or in $\theta - \nu$ if a left-running characteristic is crossed. However, it is considered that the crossing of a right-running characteristic takes place by proceeding *along* an intersecting left-running characteristic (usually not drawn) along which the first of Eqs. (12) must be satisfied. Similarly, the crossing of a left-running characteristic takes place by proceeding *along* an intersecting right-running characteristic along which the second of Eqs. (12) must be satisfied.

The slope of the boundary between two fields is determined from the values of θ and ν in each of them in such a way as to satisfy approximately Eqs. (9). For example, if the boundary separating fields 1 and 3 is a right-running characteristic, it is drawn so as to make an angle $\theta_{av} - \alpha$ with the x-axis where

$$\theta_{av} = (\theta_1 + \theta_3)/2$$

and α is the Mach angle corresponding to ν_{av} where

$$\nu_{av} = (\nu_1 + \nu_3)/2$$

Since this method, like that of Prandtl and Busemann, is suitable for problems in which flow boundaries are to be determined (such as free jets, nozzle design, etc.), the rules of procedure are laid down with this type of problem in mind. An application of the method is given in Fig. 4 and in Tables 2a and 2b. A steady flow at Mach Number 1.4, corresponding to $\nu = 9°$, enters a channel that initially turns the flow through 8°, making $\nu = 17°$, which corresponds to a Mach Number of 1.675. A channel must be so constructed as to again direct the flow parallel to its original direction.

The general procedure is as follows:

(1) At the point of intersection of the initial line and the boundary (unknown beyond this point), determine ν *before* and *after* the flow has been turned, from Fig. 1. The difference gives the total bend of the flow direction, $\nu_F - \nu_0$, which is equivalent to $\theta_F - \theta_0$ of the upper boundary (the flow being from

TABLE 2a
Field Data for Fig. 4

Field	$\theta°$	$\nu°$	$(\theta+\nu)°$	$(\theta-\nu)°$	M	p/p_0
0	0	9	9	−9	1.4	0.313
1	4	13	17	−9	1.535	0.257
3	8	17	25	−9	1.675	0.210
2	−4	13	9	−17	1.535	0.257
4	−8	17	9	−25	1.675	0.210
5	0	17	17	−17	1.675	0.210
6	−4	21	17	−25	1.815	0.170
7	4	21	25	−17	1.815	0.170
8	0	25	25	−25	1.955	0.137

TABLE 2b
Boundary Data for Fig. 4

Boundary	$\theta_{av}°$	$\nu_{av}°$	$\alpha°$	$(\theta_{av}+\alpha)°$	$(\theta_{av}-\alpha)°$
0–1	2	11	42.9		−40.9
0–2	−2	11	42.9	40.9	
1–3	6	15	38.5		−32.5
2–4	−6	15	38.5	32.5	
1–5	2	15	38.5	40.5	
2–5	−2	15	38.5		−40.5
4–6	−6	19	35.0		−41.0
3–7	6	19	35.0	41.0	
5–6	−2	19	35.0	33.0	
5–7	2	19	35.0		−33.0
6–8	−2	23	32.1		−34.1
7 8	2	23	32.1	34.1	

left to right). The subscript 0 refers to initial values and F to values after the flow has been turned. In the illustration this angle is 8°.

(2) Let n be the number of right-running characteristics to be crossed in changing from $\theta_0 + \nu_0$ to $\theta_F + \nu_F$ along the upper boundary. The choice will depend on the accuracy desired. In Fig. 4, $n = 2$. The standard jumps are given by

$$\Delta_R = [\theta_F + \nu_F - (\theta_0 + \nu_0)]/n$$

and

$$\Delta_L = -\Delta_R$$

for the right-running and left-running characteristics, respectively. In the illustration the corresponding jumps are 8° and −8°. For a free jet the reflection of a characteristic in a boundary reverses the sign of the jump. Thus a reflected right-running characteristic with an original jump Δ_R becomes a left-running characteristic with a jump $-\Delta_L = \Delta_R$. In other words, for a free jet each characteristic retains its original jump throughout the flow even though its direction is changed as a result of reflections. On the other hand, no change is encountered when a characteristic is reflected in a straight boundary. The reflected characteristic may be omitted provided the boundary is bent sufficiently to compensate for the omitted jump. This property is essential for the solution of the problem illustrated by Fig. 4.

(3) Set up a table of values of θ, ν, $\theta + \nu$, and $\theta - \nu$ for the various fields, starting with the initial values of θ_0 and ν_0. To proceed to an adjoining field determine the *type* of characteristic that must be crossed. If it is a right-running characteristic, then in the new field

$$\theta + \nu = \theta_0 + \nu_0 + \Delta_R$$

and

$$\theta - \nu = \theta_0 - \nu_0$$

If it is a left-running characteristic, then

$$\theta + \nu = \theta_0 + \nu_0$$

and

$$\theta - \nu = \theta_0 - \nu_0 + \Delta_L$$

From these pairs of formulas θ and ν can be found. The same procedure is followed in progressing from any known field to an adjacent unknown field. (See Table 2a.)

(4) Set up a table of values of θ_{av}, ν_{av}, α, $\theta_{av} + \alpha$, and $\theta_{av} - \alpha$ for the field boundaries as in Table 2b, using the procedure outlined earlier in this section.

(5) All graphical construction can be given in this step since it amounts merely to the drawing of the boundaries between fields which make angles $\theta_{av} + \alpha$ and $\theta_{av} - \alpha$ with the original flow direction. Steps 3, 4, and 5 are carried out simultaneously.

COMMENTS ON THE METHODS

The "Lattice-Point" Method

Since the method is approximate, the effect of a change of slope of the boundary is carried along the flow only by the Mach lines being reflected from the walls. Consequently, the more Mach lines used, the greater is the possibility of showing the effects of the true contour. If the slope of the boundary is discontinuous, a judicious selection of points along the initial line is needed so that the reflections of the Mach lines will occur as near to the points of discontinuity as possible. Brief preliminary estimates should be made to insure this behavior in the final solution.

Theoretically the method is adaptable to problems in which flow boundaries are to be determined, as well as those with given boundaries. However, it is found in the case of the problem of a free jet expanding into air at lower pressure that the method of approximation is such that the theoretical periodicity of such solutions is not obtained except in the limit—i.e., when infinitely many characteristics are used. This periodicity is obtained, however, in the solution by the field method of this paper.

One of the errors of approximation appears in the procedure of locating new points by drawing characteristics from known points with slopes given by data at these points rather than at some intermediate points. An iterative procedure may be employed if it is felt that the added computations are not prohibitive. Some improvement may be obtained in this

way for flow regions in which the Mach Number is near unity.

The "Field" Method

The field method of this paper, although theoretically equivalent to the Prandtl-Busemann method, has an advantage over the latter in that jumps of *any* magnitude (fractional or integral) may be used. The Prandtl-Busemann method uses integral jumps necessitating the approximation of the problem itself as well as the solution.

A disadvantage of both field methods is that they have not yet been suitably adapted to problems with arbitrarily given boundaries, such as in Fig. 2. The reason for this is basic. Standard jumps in $\theta + \nu$ and $\theta - \nu$ are selected and must not be changed throughout the problem. Having chosen the jumps the directions of the Mach lines are then governed by the initial Mach Number. Thus one has no control over the locations of points of intersection of one boundary with Mach lines reflected from the opposite boundary. Consequently, it is highly improbable that any fields adjacent to the boundary would have a direction θ equivalent to the average direction of the section of the boundary forming one side of the field.

The curves of Fig. 1 may be extended to higher Mach Numbers by use of Eqs. (13), (10a), and (14). Likewise, they may be extended in the other direction to $q/a = 1$. For higher Mach Numbers greater care must be exercised in the graphical construction because of the low values of $\theta + \alpha$ and $\theta - \alpha$. Furthermore, a different set of curves must be prepared for each value of k. The use of these curves rather than a table of pressure numbers is one of the principal advantages of the method.

References

[1] Prandtl, L., and Busemann, A., *Näherungsverfahren zur zeichnerischen Ermittlung von ebenen Strömungen mit Überschallgeschwindigkeit*, Stodola Festschrift, pp. 499–509; Orell Füssli, Zurich, 1929.

[2] Busemann, A., *Gas Dynamics, Handbuch der Experimentalphysik*, Vol. 4, Part 1, Sec. 26; Wien-Harms, Leipzig, 1931.

[3] Sauer, R., *Theoretische Einführung in die Gasdynamik*, Chap. 18; Edwards Brothers, Inc., Ann Arbor, Mich., 1945.

[4] Heybey, W., *Das Prandtl-Busemannsche Näherungsverfahren zur zeichnerischen Verfolgung ebener Überschallströmungen*, Archiv. Nr. 66/31 and 66/32, Heeres-Versuchsstelle Peenemünde, 1940.

[5] Courant, R., and Hilbert, D., *Methoden der Mathematischen Physik*, Vol. 2, Chap. V, Art. 1; Julius Springer, Berlin, 1937.

[6] Tollmien, W., *Characteristikentheorie*, Archiv. Nr. 44/2 and *Ebene Potentialströmungen*, Archiv. Nr. 44/3, Technische Hochschule Dresden, 1941.

Changes of Address

Since the Post Office Department does not as a rule forward magazines to forwarding addresses, it is important that the Institute be notified of changes in address 30 days in advance of publishing date to ensure receipt of every issue of the JOURNAL and REVIEW.

Notices should be sent directly to:

Institute of the Aeronautical Sciences, Inc.
2 East 64th Street, New York 21, New York

A Method of Airplane Performance Calculation Applicable to Any Polar

R. E. WENDT*
Western Air Lines

SUMMARY

A method is presented for the determination of airplane performance by use of formulas and charts. The conventional method of approximating a polar by expressing the effective induced drag as C_L^2/πA.R.$_e$ is often inadequate because of the fact that many polars are not symmetrical about zero lift. A mathematical expression for the airplane polar is determined here by expressing the effective induced drag as a parabola symmetrical about the lift coefficient at which the minimum drag coefficient occurs. This coefficient is defined as $C_{L_{min}}$. The minimum drag coefficient is defined as $C_{D_{min}}$. Hence, the airplane drag coefficient is

$$C_D = C_{D_{min.}} + [(C_L - C_{L_{min.}})^2/\pi\text{A.R.}_e]$$

Performance is determined by use of the fundamental loading parameters in common use, λ_p, λ_s, and λ_t.

The velocity at maximum lift drag ratio is used throughout as the basic velocity. All other velocities are expressed in terms of the basic velocity by use of the nondimensional velocity ratio, R_v.

Three basic parameters are introduced: basic performance parameter,

$$\psi' = \lambda_t\lambda_s^{3/4}/\lambda_p^{1/4}$$

coefficient of asymmetry,

$$C_\alpha = C_{L_{min.}}/\sqrt{\text{A.R.}_e C_{D_f}}$$

performance parameter ratio,

$$R_\psi = \frac{R_v^2}{2} + \frac{1}{2R_v} - \frac{C_\alpha R_v}{\sqrt{\pi}}$$

C_{D_f} is the equivalent parasite drag coefficient. The basic performance equation based on the usual assumption that lift = weight is

$$\lambda_t(dh/dt) = 1 - \psi' R_\psi$$

When the effective induced drag term of the drag equation is expanded, a linear function of C_L appears. This term is accounted for by the coefficient of asymmetry. This coefficient has a constant value for any given polar. Rate of climb may be determined at any speed by use of the performance parameter R_ψ, which is a function of R_v. Level flight velocity is determined in terms of R_v for a given value of ψ and C_α.

Because of the ability to approximate any polar with negligible error and the rigorous analysis used thereafter, the results obtained have a high degree of accuracy and are easily determined.

NOMENCLATURE

A = constant to convert horsepower to desired physical units
A.R. = aspect ratio
A.R.$_e$ = effective aspect ratio = (A.R.)$_e$
b = span
b.hp. = brake horsepower
e = airplane efficiency factor
f = equivalent parasite area = $C_{D_f}S$
dh/dt = rate of climb
dh/dt_i = indicated rate of climb
L/D = lift-drag ratio
T = thrust
T_c = time required to climb
V = velocity
V_b = basic velocity or speed at maximum L/D
W = airplane weight
R_v = ratio of velocity to basic velocity
R_ψ = performance parameter ratio = $(R_v^2/2) + (1/2R_v) - (C_\alpha R_v/\sqrt{\pi})$
R_w = weight ratio = ratio of any weight to originally assumed weight
λ_p = parasite loading = $2W/\rho_0 f$
λ_s = span loading = $2W/\pi\rho_0 b^2 e$
λ_t = thrust power loading = W/Ab.hp.η_0
} loading parameters, physical units
l_p = parasite loading W/f
l_s = span loading W/b^2e
l_t = thrust power loading W/b.hp.η_0
} loading parameters, engineering units
$C_{D_{min.}}$ = minimum drag coefficient
C_α = coefficient of asymmetry = $C_{L_{min.}}/\sqrt{\text{A.R.}_e C_{D_f}} = C_{D_\alpha}\sqrt{\pi\lambda_p/\lambda_s}$
C_{D_α} = asymmetrical drag coefficient = $C_{L_{min.}}/\pi$A.R.$_e$
$C_{D_{imin.}}$ = minimum induced drag coefficient
$C_{L_{min.}}{}^2 = C_{L_{min.}}/\pi\text{A.R.}_e = C_{D_\alpha} C_{L_{min.}}$
C_{D_f} = equivalent parasite drag coefficient = $C_{D_{min.}} + C_{D_{imin.}}$
$C_{L_{min.}}$ = lift coefficient at minimum drag coefficient
ψ' = basic performance parameter = $\lambda_t\lambda_s^{3/4}/\lambda_p^{1/4} = \lambda_t\lambda_s/(\lambda_p\lambda_s)^{1/4}$
ψ = basic performance parameter (engineering units) = $l_t l_s^{3/4}/l_p^{1/4} = l_t l_s/(l_p l_s)^{1/4}$
ψ_i = indicated performance parameter = $\psi\sqrt{\rho_0/\rho}$
ψ_R = basic climb performance parameter = ψR_ψ
Υ' = basic velocity parameter = $\lambda_p\lambda_s$
Υ = basic velocity parameter (engineering units) = $(l_s l_p)$
Λ' = fundamental performance parameter = $\lambda_s\lambda_t/(\lambda_p/\lambda_t)^{1/3}$
Λ = fundamental performance parameter (engineering units) = $l_s l_t/(l_p/l_t)^{1/3}$
η = propeller efficiency
θ = angle between flight path and horizon
ρ = mass density of air
ρ_0 = mass density of air at sea level
σ = ρ/ρ_0
λ_{sp} = span-parasite loading = $2W_s/[\rho_0{}^{1/3}A^{2/3}(\pi b^2 e)^{1/3}/f^{1/6}]$ (physical units)
l_{sp} = span-parasite loading = $W_s/(b\sqrt{e}/f^{1/6})$ (engineering units)
P_{iw} = b.hp.$\eta\sqrt{\sigma}/(W/W_s)^{3/2}$
V_{Biw} = $V_B/(W/W_s)^{1/2}$
C_{iw} = $(dh/dt)\sqrt{\sigma}/(W/W_s)^{1/2}$
W_s = standard weight or an assumed weight

Received July 24, 1946.
* Senior Aerodynamicist.

R_{piw} = P_{iw} ratio = $P_{iw}/\lambda_p{}^{3/2}$
ΔP = power in excess of power required for level flight

Introduction

An analytical method is presented here for the determination of airplane performance from test data or an estimated polar. The method is particularly applicable to polars determined from wind tunnel or flight test. Analytical methods of performance determination in common use express the effective induced drag simply as a function of $C_L{}^2$. It has been found that many test polars are not symmetrical about zero lift. Therefore, an algebraic expression of the drag coefficient in terms of $C_L{}^2$ is not valid. This is particularly true of polars of airplanes with deflected flaps. In order to have a general expression applicable to any polar, the effective induced drag coefficient is expressed as $(C_L - C_{L_{min.}})^2/\pi$A.R.$_e$ in the method presented here. This furnishes an easy means of approximating any polar with a negligible error.

The assumption of constant parasite drag coefficient and the use of the airplane efficiency factor used in references 1, 2, and 3 are incorporated in the method shown here. However, the constant drag consists of the minimum drag plus the minimum induced drag. Because of the fact that the minimum drag does not necessarily occur at zero lift, the minimum induced drag is the induced drag resulting from the lift at minimum drag. When $(C_L - C_{L_{min.}})^2$ is expanded, a linear function of C_L also appears in the expression for the drag coefficient. In the final performance equation this term is accounted for by use of the coefficient of asymmetry.

The basic performance equation is developed by use of the loading parameters λ_s, λ_p, and λ_f used in references 1, 2, and 3. The velocity at maximum lift-drag ratio is used herein as the basic velocity. It is expressed in terms of the loading parameters λ_s and λ_p. Hence, it is independent of the power and propeller efficiency. Velocity is expressed in terms of the basic velocity by use of the nondimensional velocity ratio. The rate of climb is found at a predetermined velocity. This eliminates the necessity of assuming a propeller efficiency. However, determination of level flight velocities requires an assumed propeller efficiency, and two or three trials may be necessary in order to obtain an exact speed.

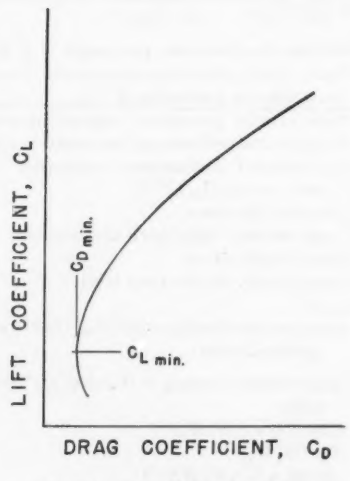

Fig. 1. Typical airplane polar.

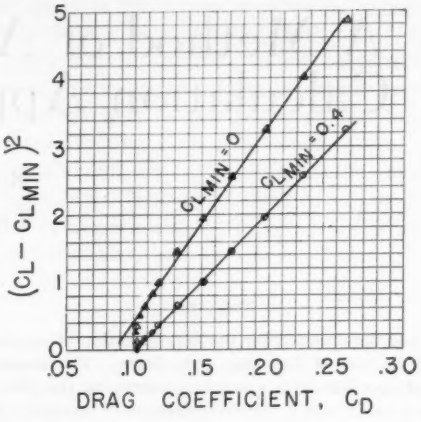

Fig. 2. Drag coefficient of a typical airplane as a function of $(C_L - C_{L_{min.}})^2$ for $C_{L_{min.}} = 0$ and $C_{L_{min.}} = 0.4$.

Because of the various types of power plants, the complex nature of propeller efficiencies, and the use of exhaust jet thrust on modern airplanes, no attempt is made to obtain an analytical expression for power in terms of velocity.

It is believed that a rapid performance evaluation with a high degree of accuracy may be achieved by the use of this method.

Discussion of Polar

According to the Prandtl wing theory, the induced drag of an elliptical wing is proportional to the square of the lift coefficient. However, because of the lift and drag contributed by the tail plane and the variation of profile drag with angle of attack, the effective induced drag, including the variation of profile drag with angle of attack, is more closely approximated as a linear function of $(C_L - C_{L_{min.}})^2$. Essentially, the polar is a parabola that is asymmetrical with respect to the lift coefficient. A typical polar is shown in Fig. 1. It can be seen that the minimum drag does not occur at zero lift. Therefore, the approximating parabola is not symmetrical about zero lift. The drag coefficient is expressed as:

$$C_D = C_{D_{min.}} + [(C_L - C_{L_{min.}})^2/\pi\text{A.R.}_e] \quad (1)$$

By expanding $(C_L - C_{L_{min.}})^2$ and substituting $C_{D_\alpha} = C_{L_{min.}}/\pi$A.R.$_e$ and $C_{D_f} = C_{D_{min.}} + C_{D_{i_{min.}}}$, Eq. (1) reduces to

$$C_D = C_{D_f} + (C_L{}^2/\pi\text{A.R.}_e) - 2C_{D_\alpha}C_L \quad (2)$$

Hence, the polar for any airplane may be defined by $C_{D_{min.}}$ and $C_{L_{min.}}$ and the airplane efficiency factor e if the geometry of the airplane is known. The value of e is easily determined by plotting the drag coefficient obtained from test data against $(C_L - C_{L_{min.}})^2$. $C_{L_{min.}}$ and $C_{D_{min.}}$ are easily determined from observation of the polar. $C_{L_{min.}}$ is the value of lift coefficient at minimum drag coefficient. A plot of drag coefficient versus $(C_L - C_{L_{min.}})^2$ for a typical airplane with flaps deflected is shown in Fig. 2. The flapped configuration is used because it best illustrates this method. The drag coefficient is plotted against $(C_L - C_{L_{min.}})^2$ for $C_{L_{min.}} = 0$ and $C_{L_{min.}} = 0.4$. It is readily seen that a close approximation of the test polar is obtained by using $C_{L_{min.}} = 0.4$ for this particular airplane. Observation of the curve for $C_{L_{min.}} = 0$ shows that the analytical expression of the drag coefficient in terms of C_L^2 does not approximate the polar so accurately as the curve for $C_{L_{min.}} = 0.4$.

Derivation

The determination of performance, regardless of the method, originates with the energy equation parallel to the flight path.

$$WV \sin \theta = W(dh/dt) = TV - DV \tag{3}$$

Consider the drag term first. From Eq. (2)

$$C_D = (f/s) + (C_L^2/\pi \text{A.R.}_e) \tag{4}$$

Therefore,

$$D = \frac{f\rho V^2}{2} + \frac{2W^2}{\rho V^2 \pi b^2 e} - 2C_{D_\alpha} W \tag{5}$$

$$DV = \frac{f\rho V^2}{2} + \frac{2W^2}{\pi \rho V b^2 e} - 2C_{D_\alpha} WV \tag{6}$$

The term TV is obviously (b.hp.)(ηA). Hence, the energy equation becomes

$$W(dh/dt) = (\text{b.hp.})\eta - \frac{f\rho V^3}{2} - \frac{2W^2}{\pi \rho V b^2 e} + 2C_{D_\alpha} WV \tag{7}$$

and the expression for rate of climb is

$$dh/dt = \frac{(\text{b.hp.})\eta}{W} - \frac{f\rho V^3}{2W} - \frac{2W}{\pi \rho V b^2 e} + 2C_{D_\alpha} V \tag{8}$$

In Eq. (8) ρ is replaced by $\rho_0 \sigma$ and V is replaced by $V_i/\sqrt{\sigma}$.

$$\frac{dh}{dt}\sqrt{\sigma} = \frac{(\text{b.hp.})\eta \sqrt{\rho}}{W} - \frac{f\rho_0 V_i^3}{2W} - \frac{2W}{\pi \rho_0 V_i b^2 e} + 2C_{D_\alpha} V_i \tag{9}$$

Basic Speed

The speed at the maximum value of L/D is now determined. D/L is expressed in terms of C_L.

$$\frac{D}{L} = \frac{C_D}{C_L} = \frac{C_{D_f}}{C_L} + \frac{C_L}{\pi \text{A.R.}_e} - 2C_{D_\alpha} \tag{10}$$

D/L is differentiated with respect to C_L and equated to zero. The lift coefficient at minimum D/L is determined by solving for C_L. This obviously equals the lift coefficient at maximum L/D. Therefore, at the maximum value of L/D,

$$C_L = \sqrt{\pi \text{A.R.}_e C_{D_f}} \tag{11}$$

Hence, the indicated velocity at maximum L/D is

$$V_B = \sqrt{2W/\rho S C_L} = \sqrt{2W/\rho_0 \sqrt{\pi b^2 e f}} \tag{12}$$

Substituting the loading parameters in Eq. (12),

$$V_B = \lambda_s^{1/4} \lambda_p^{1/4} = \left(\frac{4}{\rho_0^2 \pi}\right)^{1/4} l_s^{1/4} l_p^{1/4} \tag{13}$$

Hence, $V_B = \Upsilon'^{1/4}$. In order to express any velocity in terms of Υ', the parameter R_v is introduced.

$$V_B = R_v \Upsilon'^{1/4}$$

If the loading parameters λ_{t_i}, λ_s, and λ_p are substituted into Eq. (9), the equation for the rate of climb becomes

$$\frac{dh}{dt_i} = \frac{1}{\lambda_{T_i}} - \frac{V_i^3}{\lambda_p} - \frac{\lambda_s}{V_i} + 2C_{D_\alpha} V_i \tag{14}$$

Since any velocity may be represented by the basic speed, $V_B = \lambda_s^{1/4} \lambda_p^{1/4}$ and a velocity ratio R_v,

$$\frac{dh}{dt}\lambda_t = 1 - \frac{\lambda_{t_i} \lambda_s^{3/4}}{\lambda_p^{1/4}} R_v^3 - \frac{\lambda_{t_i} \lambda_s^{3/4}}{\lambda_p^{1/4}}\left(\frac{1}{R_v}\right) + 2C_{D_\alpha} \lambda_{t_i} \lambda_s^{1/4} \lambda_p^{1/4} R_v \tag{15}$$

From the definition of C_α it can be seen that

$$C_\alpha \psi' / \sqrt{\pi} = C_{D_\alpha} \lambda_t \lambda_s^{1/4} \lambda_p^{1/4}$$

Therefore,

$$\lambda_t \frac{dh}{dt} = 1 - \psi_i'(R_v^3 + \frac{1}{R_v} - \frac{2C_\alpha}{\sqrt{\pi}} R_v = 1 - 2\psi_i' R_\psi = 1 - 2\psi_R' \tag{16}$$

Level Flight Velocity

The required condition for level flight velocity is zero rate of climb. The relationship between the basic performance parameter and the velocity ratio is obtained by setting $dh/dt = 0$ in Eq. (16). Therefore, in level flight, the relationship between the basic performance parameter and the velocity ratio is

$$\psi_i' = 1/[R_v^3 + (1/R_v) - (2C_\alpha/\sqrt{\pi})R_v] \tag{17}$$

Time to Climb

The time required to climb to any altitude with constant power is determined by integrating the reciprocal of the rate of climb with respect to altitude as shown below. It is shown in Eq. (16) that the product of the rate of climb times the power loading is $(1 - \psi_i' R_\psi)$. Therefore, the reciprocal of the rate of climb is

$$1/(dh/dt) = \lambda_t/(1 - 2\psi_i' R_\psi) \tag{18}$$

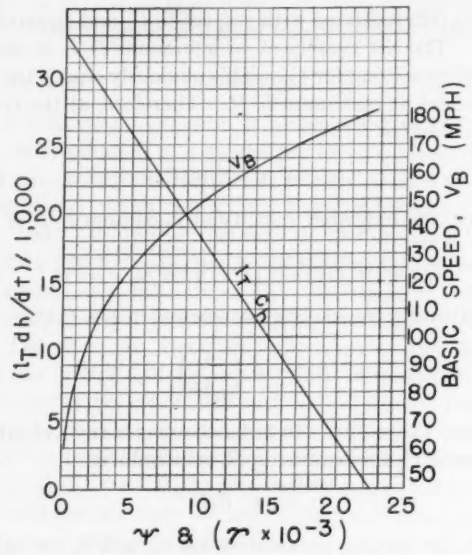

FIG. 3. Chart for determination of basic velocity and rate of climb.

The integral of the rate of climb with respect to altitude is

$$T_c = \lambda_t \int_{h_1}^{h_2} [1/(1 - 2\psi_i' R_\psi)]dh \qquad (19)$$

ψ_i' is replaced by $\psi'/\sqrt{\sigma}$ in Eq. (19). Hence, the value T_c/λ_t may be expressed as

$$\frac{T_c}{\lambda_t} = \int_{h_1}^{h_2} \frac{dh}{1 - (2\psi'/\sqrt{\sigma})} = \int_{h_1}^{h_2} \frac{\sqrt{\sigma}}{\sqrt{\sigma} - 2\psi'} dh \qquad (20)$$

Effect of Gross Weight on Climb

Since λ_t is a linear function of weight and ψ is a function of $W^{3/2}$, the general energy equation may be written in terms of an assumed weight and the weight ratio R_w as shown below:

$$R_w(dh/dt) = 1 - 2\psi_i' R_\psi R_w^{3/2} \qquad (21)$$

SIGNIFICANCE OF PARAMETERS

Basic Performance Parameter

The dimensionless parameter ψ_i' is indicative of the airplane performance. However, the parameter ψ_R' is the true index of climb performance at a specified velocity. A perfect airplane is represented when the basic performance parameter is zero. Although this value may only be achieved by infinite power, infinite span, or zero parasite drag, it shows that the airplane climb performance improves as ψ_R becomes smaller. The value $\lambda_t(dh/dt) = 0$ and the absolute ceiling of an airplane occur when ψ_R' equals 0.5. An airplane with ψ_R' equals 0.5 at sea level will not fly. If the performance parameter is expressed in terms of feet, pounds, and horsepower, ψ_R will equal 22.37 when ψ_R' equals 0.5.

Concerning the level flight speed, the value ψ_i' is the index of performance as R_ψ is a function of the independent variable R_v. The velocity in level flight increases as the basic performance parameter becomes smaller. A theoretically perfect airplane with infinite velocity is represented by the value of ψ being zero.

The basic performance parameter ψ has a definite relationship to the fundamental performance parameter Λ used in references 1, 2, and 3. From the definitions of ψ and Λ it is readily seen that $\psi = \Lambda^{3/4}$. There are several reasons for the use of ψ in preference to Λ in the method presented here. The derivation of the formulas evolves into a final expression that is a linear function of ψ. The relationship of R_v to R_ψ is proportional to the relationship of speed to power. Hence, observation of Fig. 4 permits visual determination of the position on the power required curve and R_ψ has a definite physical significance.

Observation of Fig. 3 shows that $l_t(dh/dt)$ is a linear function of ψ. Therefore, the value of dh/dt may be readily determined from ψ_R without the use of charts if desired.

Basic Speed Parameter

The basic speed parameter T furnishes a useful tool in performance determination. It is numerically equal to the fourth power of the velocity for maximum L/D. In terms of the known airplane parameters, it is $\lambda_s\lambda_p$. It is the only parameter used herein that is dimensional. It has the dimensions of (length/time)^4. The actual units depend, of course, on what units the performance is expressed in.

The Parameters R_v and R_ψ

The relationship between R_v and R_ψ is obviously the relationship between speed and power. The velocity ratio, R_v is the ratio between any desired speed and the speed at which maximum L/D occurs. R_ψ is the ratio between the basic performance parameter based on any desired speed and the basic performance parameter based on the speed for maximum L/D. Inasmuch as plot of R_v vs. R_ψ is a nondimensional speed power curve, a desirable climb speed may be determined from observation of the curve. This may be seen from observation of Fig. 4.

The Coefficient of Asymmetry

The coefficient of asymmetry is indicative of the symmetry of the polar. At C_α equals zero, the polar is symmetrical about zero lift. For any asymmetrical polar C_α has a finite value. This coefficient is incorporated in the parameter R_ψ as shown in Eq. (16). It should be noted that the asymmetry of the polar is accounted for in two ways. The constant term $C_{D_{min}}$ is added to the minimum drag coefficient to give a fictitious equivalent minimum drag. The linear function of lift coefficient is accounted for by use of the nondimensional coefficient C_α.

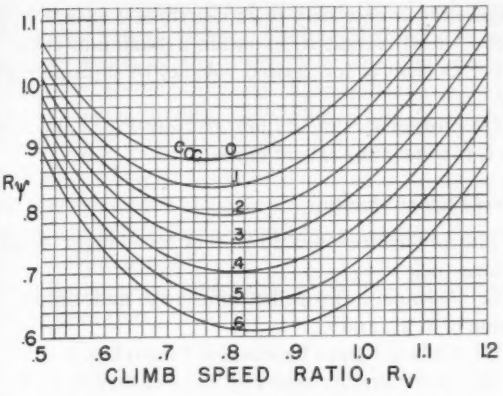

FIG. 4. Performance parameter ratio as a function of climb speed ratio and C_α.

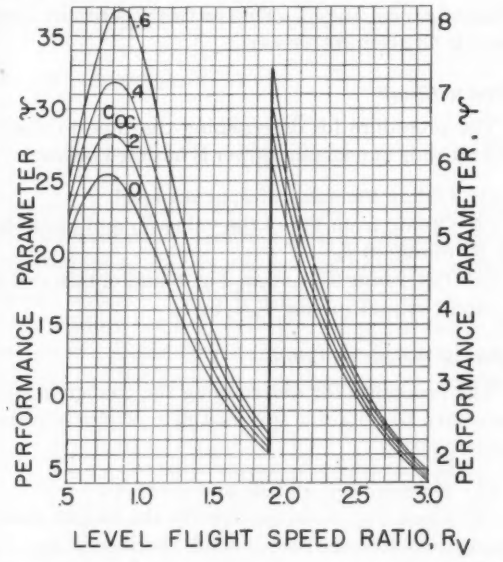

FIG. 5. Level flight velocity ratio as a function of ψ and C_α.

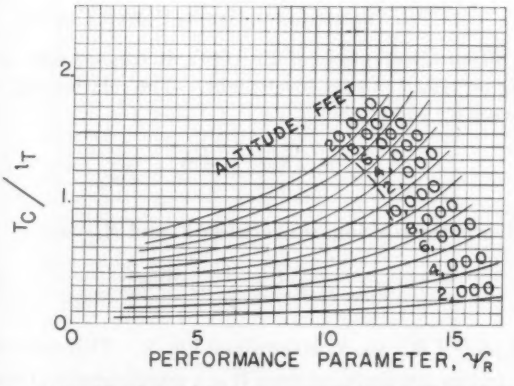

FIG. 6. Chart for determining time required for a constant power climb.

DISCUSSION OF CHARTS

Charts for Determining Rate of Climb

In order to determine rate of climb, it is necessary to use the chart showing the performance parameter ratio as a function of the climb-speed ratio shown in Fig. 4. This chart consists of a family of curves for various values of C_α. It should be noted that $l_t(dh/dt)$ may be easily calculated for any values of ψ, C_α, and R_v. Inasmuch as no charts are required for the determination of the climb-speed ratio and the determination of the rate of climb, the charts shown in Figs. 2 and 3 are not essential for determination of rate of climb. Algebraic solution of Eq. (16) is advocated if an exact value of rate of climb is desired. However, the charts furnish a reasonably accurate method to determine rate of climb.

Charts for Determining Velocity

Because of the relationship between R_v and R_ψ being a fourth degree equation, the complexity of an algebraic solution is prohibitive. Therefore, it is desirable to determine velocity by use of the charts. By assuming values of R_v, a family of curves with various values of C_α may be plotted as shown in Fig. 5. This furnishes a convenient manner of obtaining level flight velocity. An interesting characteristic of this chart is that it may be used in reverse. If a specified speed is desired, the chart may be used to determine the required power by determining from the chart the value of ψ required for the specified value of R_v and solving for the required thrust horsepower.

Charts for Determination of Time to Climb

It is difficult to establish a general chart to determine the time required to climb because of the infinite possibilities of application of power. However, with the advent of torquemeters in modern airplanes, climbs at constant power are now of practical significance. Fig. 6 shows T_c/l_t plotted vs. ψ for various altitudes. This chart furnishes a convenient means of obtaining time to climb to any specified altitude at a constant power.

Effect of Gross Weight on Climb

Heretofore, the performance has been considered at a constant assumed weight. In determining rate of climb, it is often necessary to know the weight that will allow a specified climb for a given airplane configuration. For transport operation, this is particularly important, since the Civil Aeronautics Administration specifies certain rates of climb for various airplane configurations. For military operation, it is important to know at what weight the absolute ceiling or the service ceiling will occur at a specified altitude. Fig. 7 shows the weight ratio plotted versus the performance parameter for various values of $l_t(dh/dt)$. From this chart it is easy to determine the change in weight from an initially assumed weight required to attain a specified

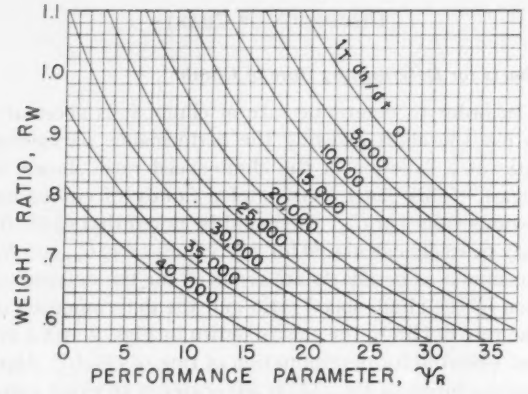

FIG. 7. Weight ratio for a specified climb as a function of basic performance parameter.

rate of climb. By using the curve for $l_t(dh/dt)$ equals zero, the change in weight required for absolute ceiling is obtained.

APPLICATION OF METHOD

In applying this method to actual use it is necessary to determine Υ, ψ_t, and C_α for a basic weight at sea level. The parameter ψ_t may be determined at any weight by multiplying by the factor $(W/W_{\text{basic}})^{1/2}$, and it may be determined at any altitude by multiplying by the factor $\sqrt{\rho_0/\rho}$. In order to determine ψ_t at some power other than the assumed power, ψ_t is multiplied by the ratio of the new power to the original assumed power. The parameter Υ is independent of both power and altitude and is directly proportional to W^2. The parameter C_α is a function of the polar and, once established, does not change unless the airplane configuration is altered. In actual application, the engineering units are used and the necessary conversion factors are used in determining the formulas and charts. The following units are used to determine the parameters in the charts shown herein:

l_s = lbs. per sq.ft.
l_p = lbs. per sq.ft.
l_t = lbs. per t.hp.

Determination of Rate of Climb

The rate of climb may be determined by use of formulas or by use of charts. The procedure with charts is outlined below:

(1) Determine the value of Υ, ψ_t, and C_α for a specified configuration and altitude.
(2) Obtain the basic speed from Fig. 3.
(3) Obtain the value of R_ψ from Fig. 4 as a function of R_σ and C_α. If the maximum rate of climb is desired, a value of R_σ equals 0.9 will closely approximate this for a conventional constant speed propeller and a reciprocating engine. If the exact maximum value is required, it is necessary to choose three values of R_σ and plot $l_t(dh/dt)$ versus R_σ to obtain a maximum value.
(4) Correct ψ_t for desired velocity by multiplying by R_ψ.
(5) Obtain a value of $l_t(dh/dt)$ from Fig. 3 and divide by l_t to obtain the rate of climb.

Level Flight Velocity

The procedure used to obtain level flight speed is shown below.

(1) Assume a propeller efficiency and obtain the value of Υ, ψ_t, and C_α.
(2) Obtain V_B as a function of Υ from Fig. 3.
(3) Determine R_σ from Fig. 5. Velocity is $R_\sigma(V_B) \times (\sqrt{\rho_0/\rho})$.

If the assumed propeller efficiency is incorrect for the velocity found in step 3, determine a new propeller efficiency and a new ψ_t by multiplying original ψ_t by η/η_0 and repeat step 3. One or two repetitions usually provide an accurate answer.

Time to Climb

The procedure for determining the time to climb to any altitude at constant power is outlined below:

(1) Obtain the value of ψ_t at sea level.
(2) Obtain from Fig. 4 the value R_ψ and multiply ψ_t by R_ψ to obtain ψ_R.
(3) Determine T_c/l_t from Fig. 6 and obtain the time to climb by multiplying T_c/l_t by l_t.

Effect of Weight on Climb

The procedure for determining the change in weight necessary to obtain a specified rate of climb is shown below:

(1) Determine ψ_t and R_ψ and $l_t(dh/dt)$.
(2) From Fig. 7 obtain directly the weight ratio required to obtain the rate of climb specified in step 1 and multiply the assumed weight by the weight ratio to determine the weight that permits the specified rate of climb.

NONDIMENSIONAL SPEED POWER CURVE

From observation of Eq. (16), it can be seen that $R_\psi = 1/2\psi_t'$ during level flight. The relationship between ψ_t' and P_{tw} is:

$$\frac{1}{2\psi_t'} = \frac{\lambda_p^{1/4}\sqrt{\sigma}}{\lambda_s^{3/4}\lambda_t} = \frac{P_{tw}}{\lambda_{sp}^{3/2}} = R_{p_{tw}} \tag{22}$$

Hence, the relationship between R_σ and $R_{p_{tw}}$ is:

$$R_{p_{tw}} = R_\sigma^3 + \frac{1}{R_\sigma} - \frac{2C_\alpha R_\sigma}{\sqrt{\pi}} \tag{23}$$

A plot of $R_{p_{tw}}$ vs. R_σ is shown on Fig. 8. This curve has a unique application, since it is a nondimensional speed power curve and furnishes a means of determining a

graphical or trial-and-error solution for level flight velocity and rate of climb. The use of this curve permits observation of the position on the power curve without the laborious process of computing power required versus velocity for various altitudes and weights.

Since $R_{p_{tw}}$ is equal to R_ψ, Fig. 4 differs from Fig. 8 only in that the former is plotted only over the range of climb speeds and the latter is plotted over the range of speeds from 80 per cent of speed for maximum L/D to high level flight speeds.

From the energy equations shown in Eqs. (7) and (8), it can be seen that

$$dh/dt = \Delta P/W = \frac{\Delta P}{W_s(W/W_s)} \tag{24}$$

From the definition of P_{tw}, dh/dt may be expressed as shown below:

$$\frac{dh}{dt} = \frac{\Delta P_{tw}(W/W_s)^{1/2}A}{W_s\sqrt{\sigma}} = \frac{\Delta R_{p_{tw}}\lambda_{sp}^{3/2}(W/W_s)^{1/2}A}{W_s\sqrt{\sigma}} \tag{25}$$

Hence, the value of C_{tw} is:

$$C_{tw} = \frac{\Delta R_{p_{tw}}\lambda_{sp}^{3/2}A}{W_s} \tag{26}$$

From the above relationships, it can be seen that the rate of climb is readily determined from Fig. 8 by plotting the values of $R_{p_{tw}}$ vs. R_τ for any specified values power and altitude.

The procedure for determination of performance is shown below. A standard weight, W_s, is first assumed. Preliminary to determining performance for specific altitudes, weight, and powers, it is necessary to determine the following values:

(1) Determine Υ and V_{Btw} for a standard weight, W_s.

(2) Obtain the value of C_α and $\lambda_{sp}^{3/2}$ for a standard weight, W_s,

$$\lambda_{sp}^{3/2} = 0.0447(W_s/b\sqrt{e})^{3/2}f^{1/4}$$

The following shows the procedure for determining level flight speed for any condition:

(1) Assume a velocity, V.

(2) Determine $R_\tau = V/V_{Btw}\sqrt{(W/W_s)\sigma}$.

(3) Determine η as a function of power, engine speed, velocity, and propeller diameter.

(4) Determine R_{ptw} = (b.hp.)$\eta\sqrt{\sigma}/[\lambda_{sp}(W/W_s)]^{3/2}$ and plot vs. R_τ on Fig. 8.

(5) Repeat above procedure if the point obtained in step 4 does not fall on the curve for the value of C_α determined above. Two repetitions of the above procedure furnish enough points to plot a curve of R_{ptw} vs. R_τ on Fig. 8. The value of R_τ for level flight is determined from the intersection of the calculated curve and the curve for the correct value of C_α on Fig. 8.

(6) Determine $V = R_\tau V_{Btw}\sqrt{(W/W_s)}/\sqrt{\sigma}$ for level flight.

The procedure for determination of maximum rate of climb for any condition is shown below:

(1) Assume several values of velocity and compute η as a function of power, engine speed, velocity, and propeller diameter.

(2) Determine the values of R_τ for the values of velocity shown above.

(3) Compute R_{ptw} for the values of η and V in step 1 and plot R_{ptw} vs. R_τ.

(4) Measure the maximum value of $\Delta R_{p_{tw}}$ for the previously determined value of C_α and compute $C_{tw} = (\Delta R_{p_{tw}}\lambda_{sp}^{3/2}/W_s)$ 33,000.

(5) Compute $dh/dt = C_{tw}\sqrt{W/W_s}/\sqrt{\sigma}$ ft. per min.

It should be noted that the above procedure must be completed for any weight. The value of $\Delta R_{p_{tw}}$ and C_{tw} in steps 4 and 5 are for a specific weight, and dh/dt may not be determined for other weights without determining a new value of P_{tw}.

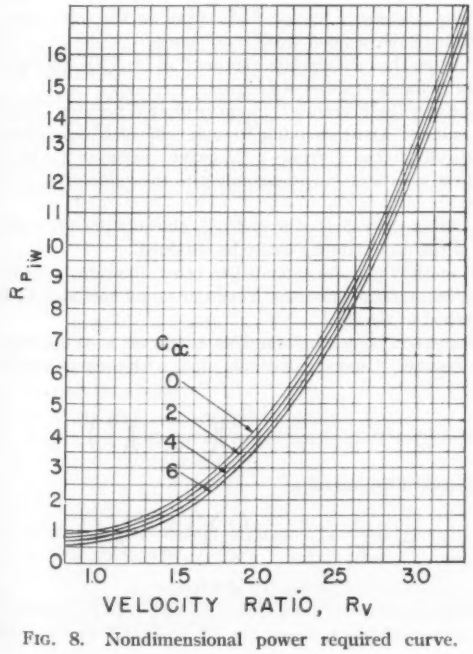

FIG. 8. Nondimensional power required curve.

CONCLUSIONS

By mathematically expressing the airplane polar about an axis of symmetry that coincides with the minimum drag coefficient, taken from wind tunnel or flight data, airplane performance may be determined analytically with negligible error.

The method of performance presented above furnishes a convenient manner to determine rate of climb, level flight speed, and time to climb. The rate of climb is obtained for a predetermined velocity, eliminating the necessity of assuming a speed and a propeller efficiency.

Changes in performance due to changes in weight or power are easily determined. The change in weight from an assumed weight to obtain a specified rate of climb may be determined directly from a chart.

A performance parameter is presented which is indicative of the performance of an airplane and furnishes a qualitative comparison of airplanes without a detailed analysis.

Although an assumed propeller efficiency is necessary to determine level flight velocities, a trial-and-error procedure is simple because of the basic performance parameter being directly proportional to the propeller efficiency.

A nondimensional power required curve is presented for graphical performance determination without the laborious process of computing power required curves for various weights and altitudes.

References

[1] Millikan, Clark B., *Aerodynamics of the Airplane*, 1st ed., pp. 99–130; John Wiley & Sons, Inc., New York, 1941.

[2] Oswald, W. Bailey, *General Formulas and Charts for the Calculation of Airplane Performance*, N.A.C.A. T.R. No. 408, 1932.

[3] Rockefeller, W. C., *General Airplane Performance*, N.A.C.A. T.R. No. 654, 1939.

Letters to the Editor

Dear Sir:

Starting with the general stress-strain curve equation given by Ramberg and Osgood[1]

$$\epsilon = \frac{s}{E} + K\left(\frac{s}{E}\right)^n \tag{1}$$

and using as parameters the basic modulus of the material (E) and two points not on the straight line portion of the actual stress-strain curve, (ϵ_1, F_1) and (ϵ_2, F_2) rather than the Ramberg-Osgood stresses $F_{0.7}$ and $F_{0.85}$ (where the subscript denotes stress at a secant modulus to tangent modulus ratio of 0.70 and 0.85, respectively), the following equation is obtained for the stress-strain curve:

$$\epsilon = (F/E) + [\epsilon_1 - (F_1/E)](F/F_1)^n \tag{2}$$

where ϵ is the desired strain at stress F, and n is obtained from

$$n = \frac{\log\,(E\epsilon_2 - F_2)/(E\epsilon_1 - F_1)}{\log\,F_2/F_1} \tag{3}$$

where ϵ_1 = strain at stress F_1, ϵ_2 = strain at stress F_2, and $F_2 > F_1$.

Continuing in this fashion, the equation of the (stress) versus (stress/tangent modulus) ratio curve becomes:

$$\frac{F}{E_t} = \frac{F}{E} + n\left(\epsilon_1 - \frac{F_1}{E}\right)\left(\frac{F}{F_1}\right)^n \tag{4}$$

Now, since

$$\epsilon = F/E_s \tag{5}$$

where E_s = secant modulus.

The substitution of Eq. (5) in Eq. (2) results in:

$$\frac{F}{E_s} = \frac{F}{E} + \left(\epsilon_1 - \frac{F_1}{E}\right)\left(\frac{F}{F_1}\right)^n \tag{6}$$

Comparison of Eqs. (4) and (6) shows that the (F/E_t) versus (F) curve may be obtained directly from the material stress-strain curve by the simple method of multiplying the offsets of the original stress-strain curve from the basic straight modulus line by the coefficient n and plotting through the points thus obtained.

Cozzone and Melcon in their paper[2] point out that equations of the form

$$F_c = \pi^2 E_t/(L'/\rho)^2 \tag{7}$$

can be rearranged so that

$$E_t/F_c = (L'/\rho)^2/\pi^2 \tag{8}$$

If we now invert Eq. (8), we obtain

$$F/E_t = \pi^2/(L'/\rho)^2 = c\pi^2/(L/\rho)^2 \tag{9}$$

where c = column end fixity coefficient.

If we let

$$\Delta = \frac{F}{E_t} = \frac{c\pi^2}{(L/\rho)^2} = \frac{F}{E} + n\left(\epsilon_1 - \frac{F_1}{E}\right)\left(\frac{F}{F_1}\right)^n \tag{10}$$

then the term Δ takes on the significance of a strain.

Now, since every value of Δ corresponds to a particular value of $c\pi^2/(L/\rho)^2$, it is possible to determine the column curve of the material from the stress-strain curve of that material by means of the following steps:

(1) From a conventional stress-strain curve of the material determine n from Eq. (3) by measuring the strains ϵ_1 and ϵ_2 at stresses F_1 and F_2, respectively, and the basic slope of the stress-strain curve. Note that F_2 must be greater than F_1.

(2) Multiply the offsets of the stress-strain curve from the basic modulus line by the coefficient n determined in step (1) above and plot the F versus F/E_t curve on the same sheet (if desired) with the original stress-strain curve.

(3) From the relationships expressed in Eq. (10) compute the value of Δ for each value of L'/ρ.

(4) Enter the F versus F/E_t curve plotted per step (2) above at the value of Δ corresponding to each value of L'/ρ and proceed up vertically to the F versus F/E_t curve, thence to the left and obtain the values of F_c corresponding to the value of $\Delta = c\pi^2/(L/\rho)^2$.

(5) From the values of F_c and L'/ρ thus obtained the column curve of the material may easily be obtained.

This method may be extended to other allowable stresses involving the tangent modulus E_t or the secant modulus E_s after the method of Gerard.[3]

This method of determining column curves is also applicable to the Ramberg-Osgood equations,[1] since with their general notation

$$\epsilon = \frac{s}{E_s} = \frac{s}{E} + \left(\frac{s_1}{E}\right)\left(\frac{1 - m_1}{m_1}\right)\left(\frac{s}{s_1}\right)^n \tag{11}$$

after proper differentiation

$$\Delta = \frac{s}{E_t} = \frac{s}{E} + n\left(\frac{s_1}{E}\right)\left(\frac{1 - m_1}{m_1}\right)\left(\frac{s}{s_1}\right)^n \tag{12}$$

where n is evaluated by Fig. 10 of reference 1.

The relationship between Eqs. (11) and (12) is precisely the same as that existing between Eqs. (2) and (4). The only differ-

ence exists in terminology and in the fact that with Eq. (2) any two points on the stress-strain curve not on the straight-line portion thereof may be used to determine the coefficient n, rather than stresses at specific values of the E_s/E ratio.

Other relationships which result from operating upon Eq. (2) are:

$$E_t = \frac{EF_1^n}{F_1^n + nF^{n-1}(E\epsilon_1 - F_1)} \tag{13}$$

$$\frac{E_t}{E} = \frac{1}{\left[1 + (E\epsilon_1 - F_1)\frac{n}{F}\left(\frac{F}{F_1}\right)^n\right]} \tag{14}$$

$$E_s = EF_1^n/[F_1^n + F^{n-1}(E\epsilon_1 - F_1)] \tag{15}$$

$$\frac{E_s}{E} = \frac{1}{\left[1 + \frac{(E\epsilon_1 - F_1)}{F}\left(\frac{F}{F_1}\right)^n\right]} \tag{16}$$

If the proportional limit stress $F_{p.l.}$ at a particular value of permanent set or deviation from the straight-line portion of the stress-strain curve is desired, then

$$F_{p.l.} = F_1\sqrt[n]{E(\Delta_{p.l.})/(E\epsilon_1 - F_1)} \tag{17}$$

where $\Delta_{p.l.}$ is the desired limit for deviation from the straight line stress-strain curve.

References

[1] Ramberg, Walter, and Osgood, Wm. R., *Determination of Stress-Strain Curves by Three Parameters*, N.A.C.A. T.N. No. 902, 1943.

[2] Cozzone, F. P., and Melcon, M. A., *Nondimensional Buckling Curves—Their Development and Application*, Journal of the Aeronautical Sciences, Vol. 13, No. 10, p. 511, October, 1946.

[3] Gerard, George, *Secant Modulus Method for Determining Plate Instability Above the Proportional Limit*, Journal of the Aeronautical Sciences, Vol. 13, No. 1, p. 38, January, 1946.

William Lee Gray
Stress Project Engineer
Wichita Division
Boeing Airplane Company

Dear Sir:

The paper by A. H. Flax appearing in the January, 1947, issue of the Journal presented an excellent summary of blade stress analysis procedures but seems to have neglected several significant factors that might well have been considered.

(1) The writer has shown[1,2] that the basic equation governing blade bending is reducible to a linear second order equation with variable coefficients, the equation being as follows:[2]

$$\overline{EI}'\varphi' + EI\varphi'' = S^3\int_1^x f(x)dx - B_w S^4(\sin\vartheta + \varphi\cos\vartheta)\int_1^x A_w x dx$$

where

- EI = product of modulus of elasticity times moment of inertia (variable)
- A_w = product of cross-sectional area times unit weight (variable)
- S = rotor semispan
- B_w = $\omega^2\cos\vartheta/g$; ω = rotational velocity
- ϑ = precone angle or angle between undeflected blade axis and plane of rotation
- φ = $d\zeta/d\xi$; $\varphi' = S(d\varphi/d\xi) = d\varphi/dx$; $\varphi'' = S^2(d^2\varphi/d\xi^2) = d^2\varphi/dx^2$
- ξ = undeflected blade axis
- ζ = axis normal to
- x = ξ/S
- $f(x)$ = arbitrary load distribution which need not be analytically definable

The boundary condition being $\varphi(0) = \varphi'(1) = 0$ for blades fixed at the root or continuous across the rotor mast, $\varphi'(0) = \varphi'(1) = 0$ for hinged blades without dampeners, and $\varphi'(0) = SM_h/EI_r$, $\varphi'(1) = 0$ for hinged blades with dampeners, where M_h = hinge moment and I_r = root moment of inertia.

The two additional available boundary conditions—namely, $\zeta(0) = 0$ and shear at tip = 0—have already been used in the definite integrals used to define the shear and deflection. Note that ζ = deflection = $S\int_0^x \varphi dx$ (since φ is defined by the basic equation this latter integral is not used to determine φ).

It should be noted that the above equation is readily modified to include effects of items such as an offset hinge axis.

(2) Depending on what set of boundary conditions are involved, the above equation may or may not be soluble by the various methods outlined in Mr. Flax's paper. Experience tends to indicate that the hinged rotor case is by far the easiest to handle, and perhaps that is why considerable literature is available on the subject. When dealing with rotors with fixed ends or rotors continuous across the mast (such as found on Bell, Bendix, Hiller, and other machines), it appears that only one of the methods mentioned in Mr. Flax's paper will work. This is the Stuart method.[3] In addition to the Stuart method, the other available means for solving the equations of blade bending is the one utilizing finite differences as outlined in the writer's papers.[1,2]

(3) The particular advantage of the finite difference method is that under no circumstances are any guesses necessary as to what the root moments should be, etc. The method is direct and leads at once to the complete determination of blade loads in one operation. Furthermore, like the Stuart method, it is applicable to any type of rotor blade subjected to any type of loading, since a semigraphical solution is readily obtained.

It is regrettable that all methods of blade analysis today present a rather terrifying appearance to all but those familiar with mathematical procedures. Invariably one gets a first impression of tremendous complication and of a tremendous amount of work involved. Perhaps more time should be spent in discussing physical principles in an attempt to remove the terrifying aspects of Greek letters and mathematical notations. Then, too, more time should be spent in describing the actual operations involved in actually obtaining numerical results. In this regard the writer has been asked a number of times how, in a reasonable length of time, is it possible to solve the five, ten, or 20 simultaneous equations involved in the finite difference solution for blade bending? When one is familiar with the equations involved it is clear that, because of the nature of the equations, even 20 of them can be solved in less than 8 man-hours. When only five are involved, work of solution is almost insignificant compared with the effort expended in computing the blade section properties. This rapid and simple solution is, of course, not a characteristic of simultaneous equations in general, and, unless the particular equations are examined in detail, it is not at all obvious that little work is involved in their solution. The reason for simple solution in the case under discussion is simply that none of the equations contains more than three of the unknowns and that these unknowns are grouped ascendingly. In addition, the boundary conditions remove an unknown from the first and last equations so that a system is obtained as follows:

If $\varphi_n = \varphi$ at any point, then, if a fixed blade be considered, $\varphi_0 = 0$ and the following typical system results:

$$\begin{aligned}
\varphi_2 &= k_1\varphi_1 - \epsilon_1 \\
\varphi_3 &= k_2\varphi_1 - \epsilon_2 \\
\varphi_4 &= k_3\varphi_1 - \epsilon_3 \\
&\vdots \quad\quad \vdots \quad\quad \vdots \\
\varphi_{19} &= k_{18}\varphi_1 - \epsilon_{19} \\
\varphi_{20} &= k_{19}\varphi_1 - \epsilon_{19}
\end{aligned}$$

with $C_1\varphi_{21} + C_2\varphi_{19} - C_3\varphi_{20} = 0$, where C_1, C_2, and C_3 are constants

But $\varphi_{19} = \varphi_{21}$ from the boundary conditions, so that

$$\varphi_1 = \frac{(C_1 + C_2)\epsilon_{18} - C_3\epsilon_{19}}{(C_1 + C_2)k_{18} - C_3k_{19}}$$

where the k and ϵ terms are constants depending on blade properties, loading and so forth. Most engineers have solved systems of equations almost identical to the above in connection with bolt pattern analysis, yet experience has shown that unless the similarity is pointed out, it will not be recognized.

Summary

(1) In addition to the blade analysis methods discussed in Mr. Flax's paper, the method of finite differences is available as a general rapid means to solve the blade bending equations. Finite differences have the advantage that they may be applied to any known type of rotor system and do not demand that blade shape or loading be definable analytically.

(2) The basic equation governing rotor bending moments is a second order differential equation with the slope rather than the deflection as the dependent variable.

(3) Only the Stuart method in addition to finite difference methods has been shown to yield solutions for the structurally continuous or the fixed end blade system.

(4) Although this is not intended to apply particularly to Mr. Flax's paper, since the writer himself is far from blameless, it is felt that authors of technical papers in general could ensure far greater utility of their products by endeavoring to show clearly the advantages of any new procedure, not only from the point of view of brilliant technical discovery but also from an application standpoint. Since the most popular procedures are the ones that we understand best and which we can apply easily, it would seem that more emphasis should be placed on giving the reader a good physical picture of the method, as well as an understanding of how the numerical drudgery can be minimized.

References

[1] Dommasch, Daniel O., *A Method for the Stress Analysis of Helicopter Blades*, Journal of the Aeronautical Sciences, Vol. 13, No. 4, pp. 195–203, April, 1946.

[2] Dommasch, Daniel O., *The General Equations for the Analysis of Rotor or Propeller Blades*, presented at the Fourteenth Annual Meeting of the Institute of the Aeronautical Sciences, New York, January 28–31, 1946.

[3] Stuart, J. A., *A Tabular Method of Propeller Blade Stress Analysis*, Journal of the Aeronautical Sciences, Vol. 10, No. 4, pp. 115–118, April, 1943.

Daniel O. Dommasch
Engineering Coordinator
Bell Aircraft Corporation

Library Facilities of the
Institute of the Aeronautical Sciences

To serve Institute members and others in the aeronautical industry, the Institute of the Aeronautical Sciences offers the facilities of:

The W. A. M. Burden Library
2 East 64th Street
New York 21, N.Y.

The facilities of this library are available for reference study at the Institute.

The Paul Kollsman Lending Library
2 East 64th Street
New York 21, N.Y.

This library loans books without charge to members and others in the United States over eighteen years of age. Full information will be sent on request.

The Pacific Aeronautical Library
6715 Hollywood Boulevard
Los Angeles 28, Calif.

This is a service and reference library for West Coast members and organizations. Full information as to its facilities will be sent on request.

Shear Distribution Due to Twist in a Cylindrical Fuselage with a Cutout

M. M. GOLOLOBOV*
Letov, Prague

SUMMARY

A general method is given by which the shear distribution due to twist in a cylindrical fuselage with a cutout can be obtained. In addition, a simple example is solved to illustrate the shear distribution.

INTRODUCTION

EVERY FUSELAGE has several cutouts, the largest, of course, being those for cabin doors. These cutouts cause considerable changes in the distribution of shear stresses due to torsion and additional axial forces in the stringers. This paper presents a method of solving the stated problem.

In order to obtain a simple solution of this statically indeterminate problem, the following assumptions are made:† (a) the stringers plus effective width of skin carry only axial forces; and (b) the skin between the stringers is subjected to shear stresses only.

GENERAL METHOD

Let us consider a cylindrical fuselage of circular cross section with a rectangular cutout (see Fig. 1). On both sides of the cutout are reinforcing rings. In the following it is assumed that the changes in the shear distribution caused by the cutout are confined to the length shown in Fig. 1, i.e., that they do not reach farther than the two adjacent bays of the fuselage.

First of all, let us determine the shear distribution in the section through the middle of the cutout (section *D-D* in Fig. 1). This can be done in the following manner: a shear q_b per unit length is applied along the whole perimeter of the circle (see Fig. 2); then a force $q_b b$ (equal to the resultant of a shear $-q_b$ acting along the cutaway perimeter) is applied to cancel the shear along the cutout, distance h being $h = 2S_b/b$. As the resultant shear distribution must give only a torque, it is further necessary to apply a force of the same magnitude but in the opposite direction at the shear center C of the section with the cutout.

The shear q_b is found from the equation $T = 2Sq_b - q_b bc$ so that

$$q_b = T/(2S - bc) \qquad (1)$$

where $S = \pi D^2/4$.

The shear distribution in the middle section is given by the algebraic sum of the uniform shear q_b and the shear distribution due to the shear force $q_b b$ acting at the shear center C, it is therefore necessary to determine this shear distribution.

The shape of the middle section is shown in Fig. 3. The two stringers at the edge of the cutout are stronger

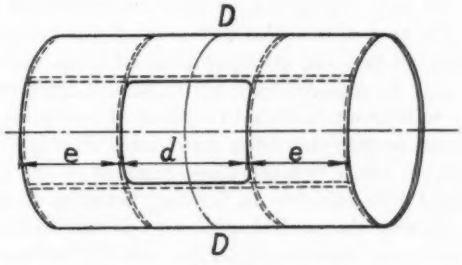

FIG. 1.

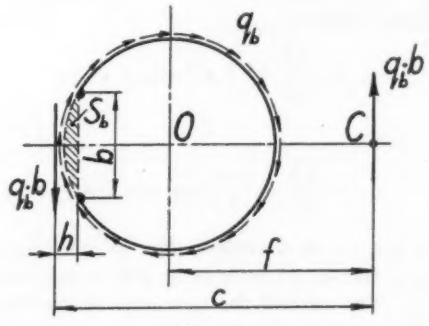

FIG. 2.

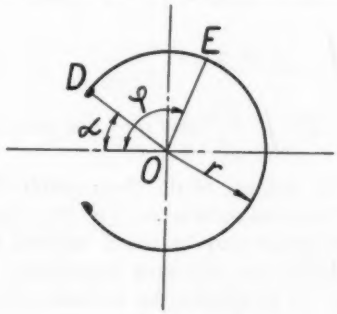

FIG. 3.

Received June 11, 1946.

* Chief Stress Analyst.

† These assumptions are usually made when solving statically indeterminate structures. The real stress distribution differs from this idealized one in that the skin is subjected not only to shear but also to direct stresses.

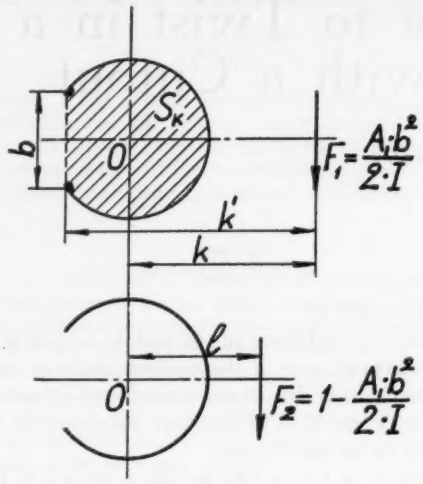

FIG. 4.

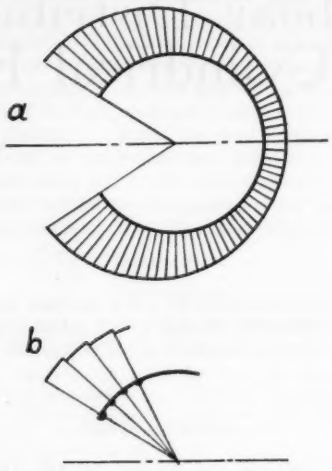

FIG. 5.

than the rest; let us denote their cross-sectional area A_1. The area of the cross section of all other members effective in bending stringers plus effective width of skin, may be replaced by a fictive skin of thickness s_r. It is a well-known fact that the shear at any point E of the cross section due to a shear force F is given by $q = FQ/I$, where Q is the static moment of the cross-sectional area effective in bending between points D and E about the neutral axis and I is the moment of inertia of the whole cross section effective in bending. The shear per unit length at point E defined by angle φ (see Fig. 3) due to a shear force $F = 1$ lb. applied at the shear center C is

$$q_\varphi = \frac{A_1 b}{2I} + \frac{1}{I}\int_a^\varphi r d\varphi s_r r \sin \varphi$$

or

$$q_\varphi = \frac{A_1 b}{2I} + \frac{r^2 s_r}{I}(\cos \alpha - \cos \varphi) \qquad (2)$$

From Eq. (1) it is evident that we must know the location of the shear center to be able to determine the shear q_b. The sum of the moments of the shears q_φ about the center of the section O is given by:

$$M_1 = \int q_\varphi r d\varphi \, r = \int r^2 q_\varphi d\varphi$$

$$M_1 = 2r^2 \int_a^\pi \frac{A_1 b}{2I} d\varphi +$$

$$2r^2 \int_a^\pi \frac{r^2 s_r}{I}(\cos \alpha - \cos \varphi) d\varphi = 1f \qquad (3)$$

where f is the distance of the shear center C from the center O of the cross section (see Fig. 2). The location of the shear center may be found without evaluating the integrals by the following reasoning: The first term of Eq. (3) represents the moment of a constant shear $A_1 b/2I$ the resultant of which is $F_1 = A_1 b^2/2I$ and acts at a distance $k' = 2S_k/b$ from the edges of the cut-out (see Fig. 4). The remaining shear force is $F_2 = 1 - A_1 b^2/2I = I_2/I$ where I_2 is the moment of inertia of the cross section without the edge stiffeners. The second term of Eq. (3) may therefore be represented as:

$$2r^2 \int_a^\pi \frac{r^2 s_r}{I}(\cos \alpha - \cos \varphi) d\varphi = \left(1 - \frac{A_1 b^2}{2I}\right) l$$

where l is the distance of the shear center of the circular arc from point O.

This distance is given by the expression

$$l = 2r[(\sin \beta - \beta \cos \beta)/(\beta - {}^1/_2 \sin 2\beta)] \qquad (4)$$

The distance f is then

$$1f = (A_1 b^2/2I)k + [1 - (A_1 b^2/2I)]l$$

or

$$f = l + (A_1 b^2/2I)(k - l) \qquad (5)$$

Now we can determine the shear q_b from Eq. (1). The resultant shear will be given by the expression (see also Eq. (2)):

$$q_2 = q_b - q_b b\left[\frac{A_1 b}{2I} + \frac{r^2 s_r}{I}(\cos \alpha - \cos \varphi)\right]$$

or

$$q_2 = q_b\left[1 - \frac{A_1 b^2}{2I} - \frac{b r^2 s_r}{I}(\cos \alpha - \cos \varphi)\right]$$

Substituting for q_b from Eq. (1) we get, finally:

$$q_2 = \frac{T}{2S - bc}\left[1 - \frac{A_1 b^2}{2I} - \frac{b r^2 s_r}{I}(\cos \alpha - \cos \varphi)\right] \qquad (6)$$

The resultant shear distribution is shown in Fig. 5a. As we have replaced the stringers by a skin of thickness s_r we have got a smooth curve. The real shear distribution differs somewhat from this idealized one:

between two neighboring stringers the shear remains constant and there is a sudden change of shear at every stringer. This shear distribution is shown in Fig. 5b. The difference of shears to the left and to the right of every stringer sets up an axial force in it. The diagram of the axial force in a stringer is shown in Fig. 6. The axial force at the middle section is zero; it increases linearly up to its maximum value at the section at the edge of the cutout, and then diminishes linearly to zero.

The shear distribution in the part of the fuselage adjacent to the cutout can be determined in the following manner. The difference Δq_1 of shears to the left and to the right of a certain stringer in bay I (see Fig. 1) can be found from the difference Δq_2 of shears to the left and to the right of the same stringer in bay II from the equation

$$P_0 = \Delta q_1 e = \Delta q_2 (d/2)$$

so that

$$\Delta q_1 = (d/2e)\,\Delta q_2$$

It follows, therefore, that the shear distribution in bay I is obtained by multiplying the shear distribution in bay II (with the cutout) by $d/2e$ and adding a constant shear Δq of such magnitude that the resultant torque at this section becomes equal to T. This constant shear Δq is given by: $\Delta q = [1 - (d/2e)](T/2S)$.

The resultant shear distribution in bay I is therefore

$$q_1 = \frac{d}{2e}\,q_2 + \left(1 - \frac{d}{2e}\right)\frac{T}{2S} \tag{7}$$

or

$$q_1 = \frac{d}{2e}\frac{T}{2S - bc}\left[1 - \frac{A_1 b^2}{2I} - \frac{br^2 s_r}{I}(\cos\alpha - \cos\varphi)\right] + \left(1 - \frac{d}{2e}\right)\frac{T}{2S}$$

The resultant shear distribution in bay I is shown in Fig. 7 for the case that $d/2e < 1$.

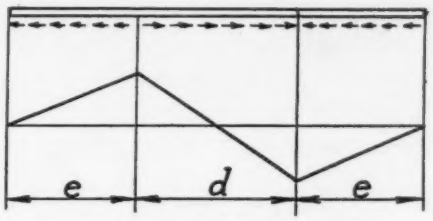

FIG. 6.

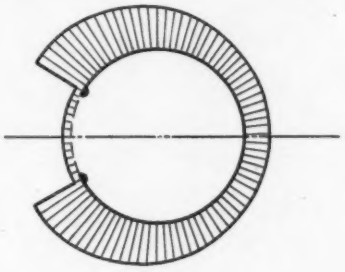

FIG. 7.

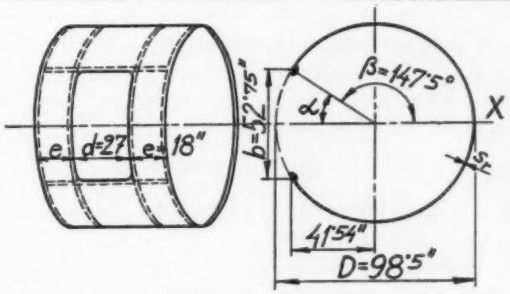

FIG. 8.

NUMERICAL EXAMPLE

As an illustration of the method let us determine the shear distribution due to torsion in the part of the fuselage shown in Fig. 8. The fuselage has a diameter of 98.5 in.; the rectangular cutout is 52.75 in. by 27 in. The edge stiffeners have a cross-sectional area $A_1 = 0.93$ sq.in.; stringers (inclusive of effective width of skin), $A_s = 0.194$ sq.in. Stringer spacing is 6.18 so that s_r becomes $s_r = 0.194/6.18 = 0.0314$. The moment of inertia of the fuselage cross section (with the cutout) about the axis X-X is $I = 12{,}380$ in.^{4}

First of all we must find the location of the shear center of the section with the cutout (see Figs. 2 and 4).

$S = \pi D^2/4 = 7{,}620$ sq.in.
$S_b = 270$ sq.in.

$$h = 2S_b/b = 2 \times \frac{270}{52.75} = 10.23 \text{ in.}$$

$S_K = S - S_b = 7{,}350$ sq.in.

Distance k' (see Fig. 4)

$$k' = 2S_K/b = \frac{2 \times 7{,}350}{52.75} = 279 \text{ in.}$$

$k = k' - (98.5/2 - 7.67)$
$k = 237.4$ in.
$\beta = 180 - \alpha = 147.5°$

$$l = 2r\,\frac{\sin\beta - \beta\cos\beta}{\beta - {}^1/_2\sin 2\beta} = 98.5 \times \frac{0.536 + 2.574 \times 0.844}{2.574 + {}^1/_2(0.906)} = 88.2 \text{ in.}$$

$l = 88.2$ in.

From Eq. (5)

$$f = l + \frac{A_1 b^2}{2I}(k - l) = 88.2 + \frac{0.93 \times 52.75^2}{2 \times 12{,}380} \times (237.4 - 88.2)$$

f = 103.8 in.

Distance c (see Fig. 2)

$c = 103.8 + 41.54 + 10.23$

$c = 155.6$ in.

Now we can determine the shear q_b (see Eq. (1))

$$q_b = \frac{T}{2S - bc} = \frac{T}{2 \times 7{,}620 - 52.75 \times 155.6}$$

$$q_b = 0.0001422 \times T \text{ lbs. per in.}$$

The resultant shear q_2 in the middle section is given by Eq. (6)

$$q_2 = \frac{T}{2S - bc}\left[1 - \frac{A_1 b^2}{2I} - \frac{br^2 s_r}{I}(\cos\alpha - \cos\varphi)\right] =$$

$$0.0001422\,T\left[1 - 0.1044 - \frac{52.75 \times 49.25^2 \times 0.0314}{12{,}380}(0.844 - \cos\varphi)\right]$$

$$q_2 = 0.0000885T + 0.0000461T\cos\varphi$$

(see Table 1).

The shear distribution in the middle section is shown in Fig. 5. The shear has its maximum value at the edge of the cutout. If the fuselage had no cutout the shear would be:

$$T/2 \times 7{,}620 = 0.0000657 \times T$$

The maximum shear at the edge of the cutout is twice as great.

Now we can determine the shear distribution in the adjacent parts of the fuselage (see Eq. (7)):

$$q_1 = \frac{d}{2e}q_2 + \left(1 - \frac{d}{2e}\right)\frac{T}{2S}$$

In our example $d = 27$ in.; $e = 18$ in.; $d/2e = 0.75$; hence,

$$q_1 = 0.75 \times q_2 + 0.25 \times 0.0000657T = 0.75q_2 + 0.0000164T$$

(see Table 2).

The shear distribution in the parts of the fuselage adjacent to the cutout is shown in Fig. 7.

Having determined the shear distribution, it is now an easy matter to calculate the axial force in each stringer from the difference of shears to both sides of it. The axial forces of all stringers at the middle section are equal to zero. The largest axial forces are, of course, in the edge stiffeners. The diagram of the axial force in one of the edge stiffeners is shown in Fig. 9.

$$P_0 = 0.0001274T(13.5) = (0.0001120T - 0.0000164T)18 = 0.00172T$$

TABLE 1

$\varphi°$	q_2
32.5	0.0001274 T
60	0.0001115 T
90	0.0000885 T
120	0.0000655 T
150	0.0000486 T
180	0.0000424 T

TABLE 2

$\varphi°$	q_1
0	0.0000164 T
32.5	0.0000164 T
32.5	0.0001120 T
60	0.0001001 T
90	0.0000828 T
120	0.0000655 T
150	0.0000529 T
180	0.0000482 T

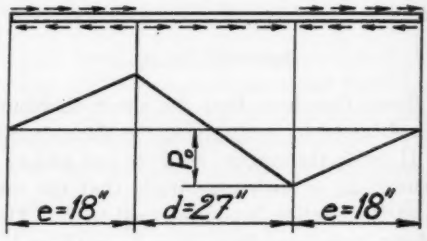

FIG. 9.

CONCLUSIONS

The method shown is general in nature and can be applied with small modifications to fuselages of every cross section. It is extremely suitable for fuselages having cross sections with two axes of symmetry. If, however, the fuselage has a cross section with only one axis of symmetry the calculations become complicated.